NATIONAL ADVISORY COMMITTEE FOR AERONAUTICS

WARTIME REPORT

ORIGINALLY ISSUED

July 1944 as
Advance Confidential Report L4G12

EFFECT OF COMPRESSIBILITY ON PRESSURE DISTRIBUTION OVER AN AIRFOIL WITH A SLOTTED FRISE AILERON

By Arvo A. Luoma

Langley Memorial Aeronautical Laboratory
Langley Field, Va.

WASHINGTON

NACA ACR No. L4G12

NATIONAL ADVISORY COMMITTEE FOR AERONAUTICS

ADVANCE CONFIDENTIAL REPORT

EFFECT OF COMPRESSIBILITY ON PRESSURE DISTRIBUTION OVER AN AIRFOIL WITH A SLOTTED FRISE AILERON

By Arvo A. Luoma

SUMMARY

Complete pressure-distribution measurements were made over an airfoil with a slotted Frise aileron for Mach numbers from 0.25 to approximately 0.76 for various airfoil angles of attack and aileron deflections. Section characteristics were determined from these pressure data.

The tests showed a loss in aileron rolling power for aileron deflections from -12° to -19°. At high diving speeds, a decrease in the rate of roll can be expected because of a loss in aileron effectiveness $\Delta\alpha/\Delta\delta_a$ at these speeds. High stick forces for non-differential aileron deflections at high speeds were indicated; and, owing to a tendency of the upgoing aileron to overbalance, serious control difficulties at high diving speeds may be expected. As a result of the present data, the Air Force specifications for the calculation of aileron loads have been revised to take into account the actual loads at high speeds as shown by these data.

INTRODUCTION

Flight tests to improve the aileron characteristics of the P-47B airplane had already been started by the NACA when serious structural difficulties of the ailerons were encountered by the Republic Aviation Corporation in the flight tests of a P-47B airplane. The present tests

in the NACA 8-foot high-speed tunnel were then inaugurated to determine, specifically, the loads on the ailerons of the P-47B airplane and, generally, the effects of compressibility on the aileron characteristics. An aileron model based on the wing of the XP-47B airplane was tested and the aerodynamic characteristics of the airfoil and the aileron were determined from complete pressure distributions over the main portion of the airfoil and the aileron. The tests were made for Mach numbers from 0.25 to approximately 0.76 and included various wing angles of attack and aileron deflections.

SYMBOLS

The term "airfoil" is herein used to mean the combination of aileron and the main portion of the airfoil. The term "aileron alone" refers to the characteristics of the aileron in the presence of the main portion of the airfoil. Aerodynamic coefficients and other symbols are defined as follows:

α	angle of attack
V	velocity in undisturbed stream
p	local static pressure at a point on airfoil section
p_o	static pressure in undisturbed stream
ρ	mass density in undisturbed stream
a	speed of sound in undisturbed stream
q	dynamic pressure in undisturbed stream $\left(\frac{1}{2}\rho V^2\right)$
P	pressure coefficient $\left(\frac{p - p_o}{q}\right)$
M	Mach number (V/a)
δ_a	aileron deflection; positive for down deflection
c_a	total chord of aileron (see fig. 1)
c_M	chord of main portion of airfoil (without aileron)
c_w	chord of airfoil (with aileron)

x distance along chord from leading edge of airfoil or aileron

x_{h_a} hinge-axis location along chord from leading edge of aileron

x_{h_w} hinge-axis location along chord from leading edge of airfoil

y distance normal to chord

y_h hinge-axis location normal to chord

Subscripts:

cr when local speed of sound has been reached on some point on airfoil section

U upper surface of airfoil section

L lower surface of airfoil section

ah ahead of maximum ordinates of aileron

r to the rear of maximum ordinates of aileron

max maximum

min minimum

c_{n_a} section normal-force coefficient of aileron alone from pressure-distribution data

$$c_{n_a} = \frac{1}{c_a}\int_0^{c_a} (P_L - P_U)\, dx$$

c_{n_M} section normal-force coefficient of main portion of airfoil (without aileron) from pressure-distribution data

$$c_{n_M} = \frac{1}{c_M}\int_0^{c_M} (P_L - P_U)\, dx$$

c_{n_w} section normal-force coefficient of airfoil (with aileron) from pressure-distribution data; component of total normal-force coefficient due

to aileron chord force neglected; maximum absolute error thus introduced only about 0.01

$$c_{n_w} = \frac{1}{c_w}\left(c_{l'}c_{n_{l'}} + c_a c_{n_a} \cos \delta_a\right)$$

c_{c_a} section chord-force coefficient of aileron alone from pressure-distribution data

$$c_{c_a} = \frac{1}{c_a}\int_{y_{min}}^{y_{max}} \left(P_{ah} - P_r\right) dy$$

c_{h_a} section hinge-moment coefficient of aileron alone about aileron hinge axis from pressure-distribution data

$$c_{h_a} = \left(\frac{1}{c_a}\right)^2\left[\int_0^{c_a} \left(P_U - P_L\right)\left(x - x_{h_a}\right) dx + \int_{y_{min}}^{y_{max}} \left(P_{ah} - P_r\right)\left(y - y_h\right) dy\right]$$

c_m section pitching-moment coefficient of airfoil (with aileron) about quarter-chord point of airfoil due to normal force on main portion of airfoil and aileron; pitching moment due to chord force of main portion of airfoil and aileron not included

$$c_m = \left(\frac{1}{c_w}\right)^2\left[\int_0^{c_M} \left(P_U - P_L\right)\left(x - \frac{c_w}{4}\right) dx + \int_0^{c_a} \left(P_U - P_L\right)\left(x - x_{h_a}\right) dx - c_{n_a} c_a \cos \delta_a\left(x_{l_w} - \frac{c_w}{4}\right) + c_{n_a} c_a \sin \delta_a\, y_h\right]$$

c_{p_a} section center-of-pressure coefficient of aileron alone (ratio of distance of c.p. of aileron from L.E. of aileron to total chord of aileron)

APPARATUS AND TESTS

The tests were made in the NACA 8-foot high-speed tunnel, which is a single-return, circular-section, closed-throat wind tunnel with the airspeed continuously controllable in an approximate Mach number range of 0.15 to 0.75.

The model used in these tests was a 24-inch-chord 10.5-percent-thick airfoil with a slotted Frise aileron, was of uniform section, and spanned the tunnel. The main portion of the airfoil passed through the walls of the tunnel in a manner typical of model installation in the NACA 8-foot high-speed tunnel and, to permit deflection of the aileron, a gap of 1/16 inch was included between the ends of the aileron and the tunnel walls.

The dimensions of the model section were obtained by reducing scaled dimensions of the wing of the P-47B-3 airplane at the midsection of the aileron. (See fig. 1 and tables I and II.) Sufficient static-pressure orifices were located on the main portion of the model and on the aileron to determine the complete pressure distribution over the airfoil.

Static-pressure measurements were made for Mach numbers from 0.25 to approximately 0.76 for various airfoil angles of attack and aileron deflections. At the higher speeds, the range of angle of attack was limited by structural load considerations. The tests were made with aileron deflections from -19° to 16°. Simultaneous observations of the static pressures acting over the airfoil were obtained by photographing a multiple-tube liquid (tetrabromethane) manometer.

RESULTS

The aerodynamic force and moment data presented herein were determined from mechanical integration of diagrams of pressure coefficient P plotted against

chord for pressures over the upper and lower surfaces of the main portion of the airfoil and of the aileron. At the highest speeds, some of the peak negative pressures exceeded the range of the manometer board and consequently were not obtained; in these cases, however, the faired pressure-distribution plots with the peaks estimated are believed to yield data sufficiently accurate for engineering purposes. In order to illustrate graphically the nature of the pressure distribution over the airfoil, a few of the pressure diagrams are included in figure 2.

The wing angle of attack α has been corrected for model twist and most of the aerodynamic coefficients are plotted against this corrected angle of attack with aileron deflection δ_a as a parameter. Cross plots of the aerodynamic coefficients against aileron deflection δ_a have been made from the basic data for several values of Mach number. In this report the aerodynamic coefficients, which are derived from pressure-distribution data, can be taken as section characteristics.

Airfoil section normal-force coefficient c_{n_w} is plotted against angle of attack α at various aileron deflections in figure 3. Other airfoil characteristics (slope of normal-force curve $\partial c_{n_w}/\partial\alpha$ and $\partial c_{n_w}/\partial\delta_a$, angle of attack for normal-force coefficient of 0, and aileron effectiveness $\Delta\alpha/\Delta\delta_a$), based on the data of figure 3, are given in figures 4 to 6. It is to be noted that the effectiveness ratio $\Delta\alpha/\Delta\delta_a$ is directly proportional to the value of $pb/2V$ at unit aileron deflection for a rigid wing in pure roll, where p is the rate of roll in radian per second and $b/2$ is the semispan in feet. Reference 1 shows that, for usual rates of aileron application on current fighter-type airplanes, the rate of roll of the airplane while the ailerons are being deflected nearly attains the full value of the steady rate of roll corresponding to any given aileron deflection. Figure 7 shows the section steady rate of roll per degree deflection of single aileron $p'/\Delta\delta_a$ against Mach number at two altitudes. The section steady rate of roll is calculated on the basis that the section rolling moment resulting from deflection of the aileron is simply balanced by the section damping moment due to roll and, based on this assumption, the following equation is used:

$$\frac{p'}{\Delta\delta_a} = \frac{\Delta\alpha}{\Delta\delta_a}\frac{V}{b'/2}$$

where

p' section steady rate of roll, degrees per second

$b'/2$ distance from plane of symmetry of airplane to midspan of aileron (taken as 15 ft)

$\Delta\delta_a$ deflection of single aileron, degrees

$\Delta\alpha/\Delta\delta_a$ aileron effectiveness

The curve of section steady rate of roll is included (fig. 7) to show the nature of the compressibility effects on the rate of roll. For the actual airplane, the rate of roll would be appreciably less than the section values shown because damping moments are developed by the entire wing and wing twist is present.

Aileron section hinge-moment-coefficient data are included in figures 8 to 10. Figure 11 has data for aileron section center-of-pressure coefficient. Illustrative stick-force data based on nondifferential aileron deflections and hinge-moment coefficients at airfoil section lift coefficients corresponding to those of the P-47B airplane in level flight are given in figure 12. These data were calculated for an aileron linkage of 1.7° aileron deflection per inch of stick movement, an area for the single aileron of 13 square feet, an aileron mean chord of 18.75 inches, and a hinge-axis location 25.7 percent back from the leading edge of the aileron. No account has been taken of variation of the section aileron balance along the aileron span or of the effect of three-dimensional flow on actual stick forces.

Data on peak negative pressure coefficient and section critical Mach number for the aileron are given in figures 13 and 14, respectively. Figures 15 and 16 contain aileron section normal-force-coefficient data, and figure 17 shows the average aileron section loading against Mach number at two altitudes for steady rate of roll.

Figures 18 to 20 have data on peak negative pressure coefficient and section critical Mach number for the main portion of the airfoil. Airfoil section pitching-moment-coefficient data appear in figures 21 and 22. Figure 23 has aileron section chord-force-coefficient data

DISCUSSION

Control Characteristics

For a given Mach number, a decrease in aileron deflection generally results in only a small decrease in the slope of the normal-force curve $\partial c_{n_w}/\partial \alpha$ (fig. 3) and the effect of this decrease is to make the ailerons somewhat more effective at the higher airfoil normal-force coefficients. The rapid rise in slope at supercritical speeds (fig. 4) has been shown by plain airfoils that have the maximum thickness well forward (reference 2). At Mach numbers beyond the range of the present tests, the typical fall in slope shown by plain airfoils (reference 2) and attributable to flow changes associated with the formation of severe compression shocks can be expected. Also included in figure 4 is the slope of the normal-force curve $\partial c_{n_w}/\partial \delta_a$ for moderate aileron deflection, and the similarity between the compressibility effects and those shown by the slope $\partial c_{n_w}/\partial \alpha$ is evident.

Frise ailerons are characteristically inefficient at large up deflections. The data of these tests indicate an actual decrease in rolling-moment coefficient, as shown by an increase in airfoil normal-force coefficient (fig. 3) when the aileron deflection is changed from -12° to -19°. This reduction in rolling efficiency can be explained by a consideration of the static pressures acting over the airfoil. For a given angle of attack, the aileron normal-force coefficient decreases as δ_a changes from -12° to -19° (fig. 15). The normal-force coefficient on the main portion of the airfoil, however, increases for the -19° deflection since the slot pressures, which are more positive for the -19° deflection, cause an increase in the pressures on the lower surface of the main portion of the airfoil forward of the slot to about the 25-percent-chord location. The upper-surface pressures over the main portion of the airfoil, in addition, are somewhat more negative for the -19° deflection and this condition further increases the normal force of the airfoil main portion. For the airfoil tested, the net effect of changing the aileron deflection from -12° to -19° is to cause an increase in airfoil normal force since the increase in normal force over the main portion of the airfoil is greater than the decrease in normal force

over the aileron. This increase in airfoil normal-force coefficient results in a decrease in rolling-moment coefficient which, in terms of airplane control characteristics, means a reversal in control effectiveness.

The effectiveness of the aileron as a means of changing the angle of attack for an airfoil normal-force coefficient of 0 is illustrated by figure 5; and it is to be noted that the greater the negative slope of the curves, the more effective the ailerons are for producing a high rate of roll. The effect of compressibility on the slope is more clearly brought out in figure 6, in which the aileron effectiveness or proportionality factor $\Delta\alpha/\Delta\delta_a$ is taken as the average value for aileron deflections from -6° to 6°. For a constant airfoil normal-force coefficient of 0, $\Delta\alpha/\Delta\delta_a$ decreases from 0.435 (the minus sign is omitted) to 0.32, or 26 percent, as the Mach number is increased from 0.25 to 0.76. Most of the decrease results at Mach numbers above 0.70, which is approximately the critical Mach number of the main portion of the airfoil. The data show some increase in $\Delta\alpha/\Delta\delta_a$ with increase in airfoil normal-force coefficient; at a Mach number of 0.70, $\Delta\alpha/\Delta\delta_a$ increases 5 percent as the normal-force coefficient increases from 0 to 0.2. The significance of $\Delta\alpha/\Delta\delta_a$ is brought out in figure 7, which shows the variation with Mach number of the section steady rate of roll per degree aileron deflection. For Mach numbers up to 0.4, the rate of roll per degree aileron deflection $p'/\Delta\delta_a$ is nearly a linear function of Mach number since the aileron effectiveness $\Delta\alpha/\Delta\delta_a$ is essentially constant. At Mach numbers above 0.4, however, the rate of roll increases less rapidly with Mach number owing to the decrease in aileron effectiveness until, at the critical Mach number of 0.70, there is actually a decrease in rate of roll. As was brought out previously, the rate of roll of the actual airplane for rigid-wing conditions would be proportionately smaller than the section rate of roll since damping moments in roll are developed by the entire wing. Wing twist would modify further the rate of roll shown.

The inefficiency of Frise ailerons at large up deflections is borne out by these tests, which show a loss in rolling power as the deflection changes from -12° to -19°. The shift in the angle of attack for zero normal force with Mach number decreases the aileron effectiveness $\Delta\alpha/\Delta\delta_a$ at high speeds; and this decrease may be sufficient, as in these tests, to cause an actual decrease in the

section steady rate of roll per degree aileron deflection. The aileron effectiveness increases somewhat with airfoil normal-force coefficient.

Aileron Hinge-Moment Coefficient

The hinge-moment coefficient for moderate positive aileron deflections is essentially insensitive to small changes in angle of attack in the vicinity of an angle of attack of 0°, whereas the hinge-moment coefficient for negative aileron deflections decreases with increasing angle of attack (fig. 8). In other words, the rate of change of hinge-moment coefficient with angle of attack $\Delta c_{h_a}/\Delta\alpha$ is practically zero for moderate positive deflections and is negative for negative deflections. A negative value of $\Delta c_{h_a}/\Delta\alpha$ during roll introduces a hinge-moment component that tends to increase the total aileron deflection and, for an underbalanced hinge-moment component due to aileron deflection, will decrease the stick force. The reduction in stick force due to roll of the airplane is a desirable feature but, for a closely balanced aileron, the possibilities of overbalance must be considered. In figure 9, $\Delta c_{h_a}/\Delta\alpha$ is taken as the average of the slopes for equal up and down aileron deflections and applies for airfoil normal-force coefficients from 0 to 0.2. It is seen that $\Delta c_{h_a}/\Delta\alpha$ becomes more negative with (1) increasing aileron deflection and (2) increasing Mach number for the larger moderate deflections ($\pm 6°$). The decrease in average slope is mainly due to the decrease with Mach number of the slope of the upgoing aileron.

The typical rapid increase in the hinge-moment coefficient of Frise ailerons at the larger up deflections due to flow separation off the lower surface is shown in figure 10. The pressure distributions over the aileron indicate that, for the -19° aileron deflection, the flow over the lower surface has completely separated right from the sharp nose of the aileron, with a consequent shift in center of pressure back to about 39 percent of the aileron chord (fig. 11). The pressure data for the -12° aileron deflection also show separation off the lower surface of the aileron but, in this case, the separation is less drastic than with the -19° deflection. Compressibility effects aggravate

the separated flow of the -12° deflection. Even for the -6° aileron deflection, incipient separation is indicated with decreasing angle of attack at the highest Mach numbers. This separation off the lower surface of the aileron at the larger negative deflections with the consequent rearward shift in center of pressure causes the large increase in hinge-moment coefficient c_{h_a} at these deflections.

For aileron deflections of -4° and -6°, the center of pressure moves forward as the Mach number increases (fig. 11) owing to the building up of the negative pressures about the nose and the forward portion of the ailerons. For some of the airfoil normal-force coefficients, an overbalance of the individual aileron exists, particularly at the highest Mach numbers (fig. 10(c)). For positive aileron deflections, there is a general rearward movement of the center of pressure (fig. 11) and consequently a more negative hinge-moment coefficient with both increasing aileron deflection and Mach number. For aileron deflections of 12° and 16°, the pressure plots indicate some separation off the rearward portion of the upper surface of the aileron; this separation is much less severe, however, than the separation off the lower surface at large negative deflections.

At high Mach numbers, the ailerons are limited to small deflections, particularly at low altitudes, because of large stick forces (fig. 12). At a Mach number of 0.525 (400 mph for sea-level conditions) and an aileron deflection of ±4°, the calculated stick force is 55 pounds. As has been pointed out previously, the calculations were made by assuming the same hinge-moment coefficient for all sections of the aileron, and no correction was made for three-dimensional effects on stick forces. The calculated section steady rate of roll for these conditions is 66° per second; the rate of roll would be less for the actual airplane, since the entire wing in roll contributes to damping and the wing is not rigid. Tests of the Spitfire have shown that wing twist at 400 miles per hour decreased the steady rate of roll 65 percent (reference 1). Airplane speeds in dives approach a Mach number of 0.88 (610 mph at 25,000 ft), and figure 12 shows that aileron difficulties can be expected at such high speeds.

At an altitude of 25,000 feet and a Mach number of 0.76 (525 mph), for example, the data show a region of aileron deflection that is unstable since the stick force decreases with increasing aileron deflection. Besides being unsuitable for well-controlled maneuvers, this region of unstable aileron characteristics can well lead to structural difficulties of the ailerons from vibration and shake. At speeds beyond those of the test data, control difficulties may be even worse.

Frise Aileron Difficulties

For moderate negative Frise aileron deflections, there is a typical abrupt increase of the aileron peak negative pressure coefficient in the supercritical region and then a collapse at still higher Mach numbers as illustrated by figure 13, which is for an aileron deflection of -4°. Even at these higher Mach numbers, however, a general increase of the air loads occurs on the forward portion of the aileron with a resulting increased tendency toward overbalance. Although there may be no net overbalance of the combined ailerons, the tendency of the upgoing aileron to overbalance produces an unstable stick-force variation that can well lead to further control difficulties. The high peak negative pressures and the steep adverse pressure gradient about the nose of a Frise aileron at up deflections are in themselves undesirable, but equally significant is the fact that the air flow, and hence the pressure distribution, about the aileron nose may be very sensitive to nose shape. Small nose-shape differences resulting from manufacturing irregularities or mishandling in aileron assembly or in subsequent operations can give rise to appreciable changes in aileron behavior, particularly hinge-moment characteristics. Variations in aileron rigging may also have an appreciable effect on the aerodynamic characteristics of the aileron.

Figure 14 clearly illustrates the basic characteristic of a Frise aileron for deflections with the nose protruding into the air stream, namely, low aileron critical Mach numbers due to high negative pressures about the aileron nose. A knowledge of the critical speeds of ailerons of this type is important in determining speeds at which aileron difficulties can be expected.

For high-speed aircraft, any type of aileron balance that depends for its operation and balance on the air loads acting about an aileron nose which protrudes into the air stream is undesirable because of its aerodynamic drawbacks.

Aileron Section Loads

The present tests bring out the fact that, in the structural design of slotted frise ailerons, equal consideration must be given the magnitude of the downloads and the uploads on the aileron. (See figs. 15 and 16.) Compressibility has a greater effect on aileron loading for negative deflections than for positive deflections. For an airfoil normal-force coefficient of 0, the value of aileron normal-force coefficient c_{n_a} at an aileron deflection of -6° changes from -0.30 to -0.42 with increase in Mach number from 0.25 to 0.76; whereas, for an aileron deflection of 6°, the change is from 0.23 to 0.29 for the same increase in Mach number. For an airfoil normal-force coefficient of 0.2 and the same Mach numbers, the value of aileron normal-force coefficient varies from -0.24 to -0.34 for a deflection of -6° but, for a deflection of 6°, it remains essentially constant at 0.30. The inadequacy of the Air Corps specifications of reference 3 for the structural design of ailerons is brought out in figure 17, which shows the actual average aileron section loading at two altitudes for airfoil section lift coefficients corresponding to those of the P-47B airplane in level flight. By using the Air Corps specifications to calculate aileron average design loads (these specifications include a factor of safety of 1.5), values of 112 pounds per square foot for uploads and 56 pounds per square foot for downloads are obtained. It is quite evident that the actual loads in high-speed flight can well exceed the calculated values, particularly for downloads.

As a result of the present data, specifications for the calculation of aileron loads as given in reference 3 have been revised so that due account is taken of the actual aileron loads attained in the normal operation of the airplane at high speeds.

Other Airfoil Characteristics

An example of the usual type of plot of peak negative pressure coefficient of the main portion of the airfoil

against Mach number is included in figure 18 for an aileron deflection of 0°. For the airfoil tested, the maximum critical Mach number of the main portion of the airfoil for moderate aileron deflections is approximately constant at 0.70, and this maximum Mach number is of course for the values of angle of attack at which both upper and lower surfaces become critical simultaneously (fig. 19). For airfoil normal-force coefficients from 0 to 0.2, the upper surface of the main portion of the airfoil is critical for negative aileron deflections and either the lower surface or the upper surface is critical for positive aileron deflections (fig. 20). The difference in critical speeds - hence, difference in drags - of an airfoil with upgoing and downgoing ailerons of course affects the yawing tendencies of an airplane.

Characteristic of ailerons which have a nose protruding into the air stream on up deflections, it is to be noted that the critical speed of the aileron may be reached at speeds lower than the critical speed of the main portion of the airfoil; for example, with an aileron deflection of -6° and at an airfoil normal-force coefficient of 0, the aileron tested (lower surface) becomes critical at a Mach number of 0.545 whereas the main portion of the airfoil (upper surface) becomes critical at a Mach number of 0.66. For high-speed airplanes, the adverse aerodynamic effects due to the development of compression shock on ailerons of this type cannot be overlooked.

The rate of change of pitching-moment coefficient with angle of attack $\partial c_m/\partial \alpha$ generally is positive for all aileron deflections except at the highest Mach numbers at which the slope becomes negative for negative aileron deflections (fig. 21). This change in slope in the supercritical region is due to the rearward shift of the center of pressure of the uploads on the main portion of the airfoil with increase in angle of attack. Compressibility has a greater effect on the airfoil pitching-moment coefficient at moderate positive aileron deflections than at moderate negative deflections (fig. 22). For the positive deflections, the pitching-moment coefficient consistently decreases with Mach number and, for the negative deflections, the pitching-moment coefficient generally increases with Mach number except at the highest speeds, at which the pitching-moment coefficient decreases.

For ailerons that have the hinge axis located well below the chord line, the hinge-moment component due to the chord force may be appreciable. In the present tests, this component amounted to about 8 percent for the largest aileron deflections. Figure 23 is included to show the magnitude and variation of the aileron chord-force coefficient with aileron deflection. These data are based on pressure forces and of course do not include skin-friction forces.

CONCLUDING REMARKS

Complete pressure-distribution measurements were made over an airfoil with a slotted Frise aileron for Mach numbers from 0.25 to approximately 0.76 for various airfoil angles of attack and aileron deflections. Section characteristics determined from these pressure-distribution measurements indicated the following conclusions:

1. A loss in aileron rolling power was found for aileron deflections from -12° to -19°.

2. A 26-percent decrease in aileron effectiveness $\Delta\alpha/\Delta\delta_a$ occurred between Mach numbers of 0.25 and 0.76 and, even without wing twist, this decrease would cause an actual decrease in the rate of roll at high diving speeds.

3. High stick forces for nondifferential aileron deflections at high speeds were indicated.

4. Control difficulties at high diving speeds can be expected because of a tendency of the upgoing aileron to overbalance.

5. As a result of the present data, the Air Force specifications for the calculation of aileron loads have been revised to take into account the actual loads at high speeds as shown by these data.

Langley Memorial Aeronautical Laboratory
National Advisory Committee for Aeronautics
Langley Field, Va.

REFERENCES

1. Morris, D. E., and Morgan, M. B.: Aileron Tests on Spitfire K.9944. 5057, S. & C. 1219, Rep. No. B.A. 1667, R.A.E., April 1941.

2. Stack, John, and von Doenhoff, Albert E.: Tests of 16 Related Airfoils at High Speeds. NACA Rep. No. 492, 1934.

3. Anon.: Stress Analysis Criteria. Air Corps Specification No. C-1803-A (formerly X-1803-A), Nov. 15, 1938, appendix D, p. 8.

TABLE I

ORDINATES FOR MAIN PORTION OF AIRFOIL (WITHOUT AILERON)

[24-in.-chord model of section of P-47B-3 wing taken through midsection of slotted Frise aileron; stations and ordinates in in. from airfoil L.E. and chord line, respectively]

Station	Ordinate		Station	Ordinate	
	Upper surface	Lower surface		Upper surface	Lower surface
0	-------	-------			
.03	0.11	-0.08	9.50	1.51	-0.91
.15	.27	-.17	10.10	1.47	-.90
.30	.42	-.23	10.69	1.43	-.88
.45	.56	-.28	11.38	1.34	-.83
.59	.67	-.32	13.07	1.23	-.78
.89	.86	-.38	14.26	1.10	-.70
1.19	1.00	-.43	15.45	.98	-.61
1.49	1.12	-.47	16.25	.88	-.55
1.78	1.22	-.51	16.63	.83	-.52
2.08	1.30	-.55	16.78	.82	-.49
2.38	1.37	-.59	16.93	.80	-.43
2.67	1.43	-.62	17.08	.78	-.20
2.97	1.47	-.66	17.23	.77	.04
3.27	1.51	-.69	17.38	.75	.20
3.56	1.54	-.71	17.52	.72	.31
4.16	1.59	-.77	17.67	.71	.39
4.75	1.62	-.82	17.82	.70	.44
5.35	1.63	-.85	17.97	.68	.48
5.94	1.64	-.89	18.12	.66	.50
6.53	1.63	-.90	18.27	.64	.53
7.13	1.62	-.91	18.42	.63	.55
7.72	1.60	-.92	18.56	.61	.56
8.32	1.57	-.91	18.71	.59	.56
8.91	1.54	-.91	18.76	.58	.58

L.E. radius: 0.18
Slope of radius through end of chord: 0.100
Shroud trailing-edge radius: 0.01

TABLE II

ORDINATES FOR AILERON ALONE

[24-in.-chord model of section of P-47B-3 wing taken through midsection of slotted Frise aileron; ordinates in in. from chord line]

Nosepiece				Tailpiece			
Station		Ordinate		Station		Ordinate	
(in. from airfoil L.E.)	(in. from aileron L.E.)	Upper surface	Lower surface	(in. from airfoil L.E.)	(in. from aileron L.E.)	Upper surface	Lower surface
17.54	0	-0.43	-0.43	19.75	2.21	0.48	-0.29
17.55	.01	-.40	-.45	19.90	2.36	.47	-.28
17.58	.04	-.36	-.45	20.05	2.51	.45	-.26
17.61	.07	-.33	-.45	20.20	2.66	.42	-.25
17.64	.10	-.30	-.45	20.50	2.96	.39	-.23
17.67	.13	-.26	-.45	20.79	3.25	.35	-.21
17.82	.28	-.13	-.44	21.09	3.55	.31	-.20
17.97	.43	-.02	-.43	21.39	3.85	.27	-.17
18.12	.58	.07	-.42	21.68	4.14	.23	-.15
18.27	.73	.16	-.41	21.98	4.44	.20	-.14
18.42	.88	.25	-.40	22.28	4.74	.17	-.12
18.56	1.02	.31	-.38	22.57	5.03	.13	-.10
18.71	1.17	.37	-.37	22.87	5.33	.10	-.08
18.86	1.32	.42	-.36	23.17	5.63	.07	-.06
19.01	1.47	.45	-.34	23.47	5.93	.05	-.04
19.16	1.62	.48	-.33	23.76	6.22	.02	-.02
19.31	1.77	.49	-.32	24.00	6.46	0	0
19.46	1.92	.50	-.31				
19.60	2.06	.50	-.30				
19.70	2.16	.49	-.29				

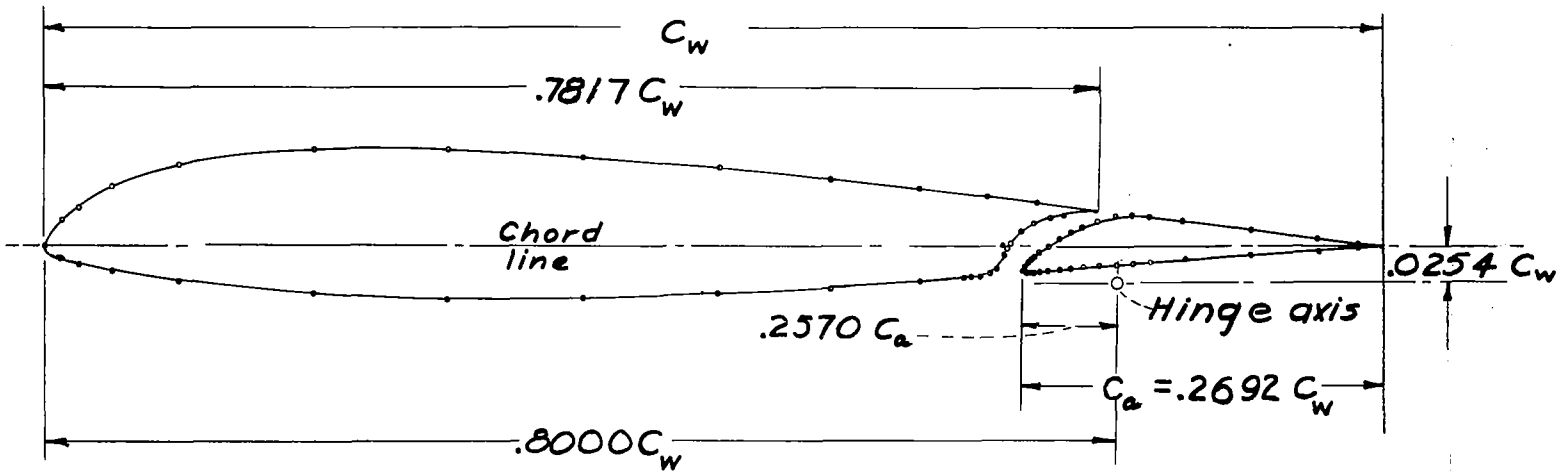

NATIONAL ADVISORY
COMMITTEE FOR AERONAUTICS.

Figure 1.- Cross section of model based on section of P-47B-3 wing taken through midsection of slotted Frise aileron.

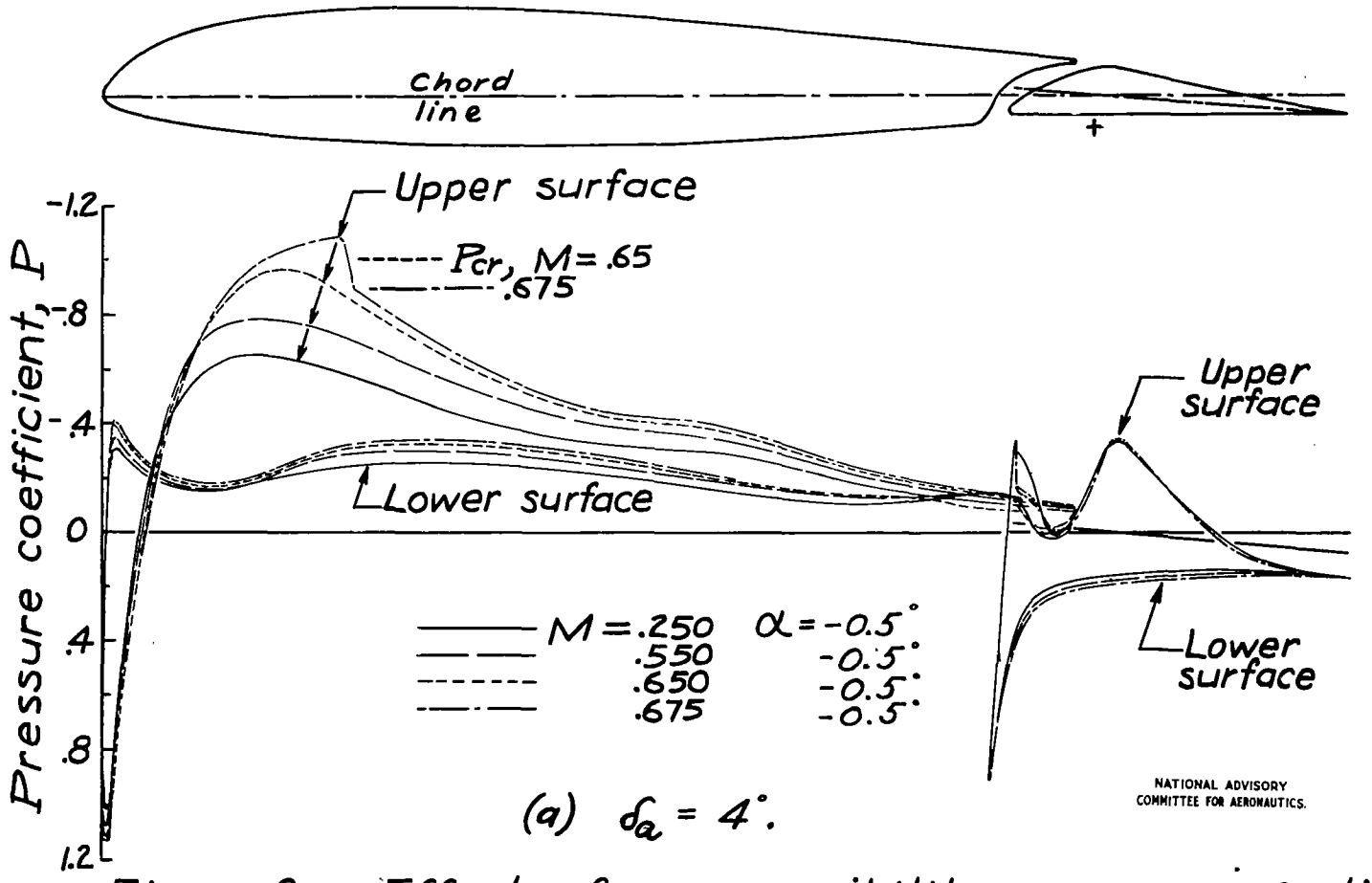

(a) $\delta_a = 4°$.

Figure 2.- Effect of compressibility on pressure distribution over airfoil with slotted Frise aileron.

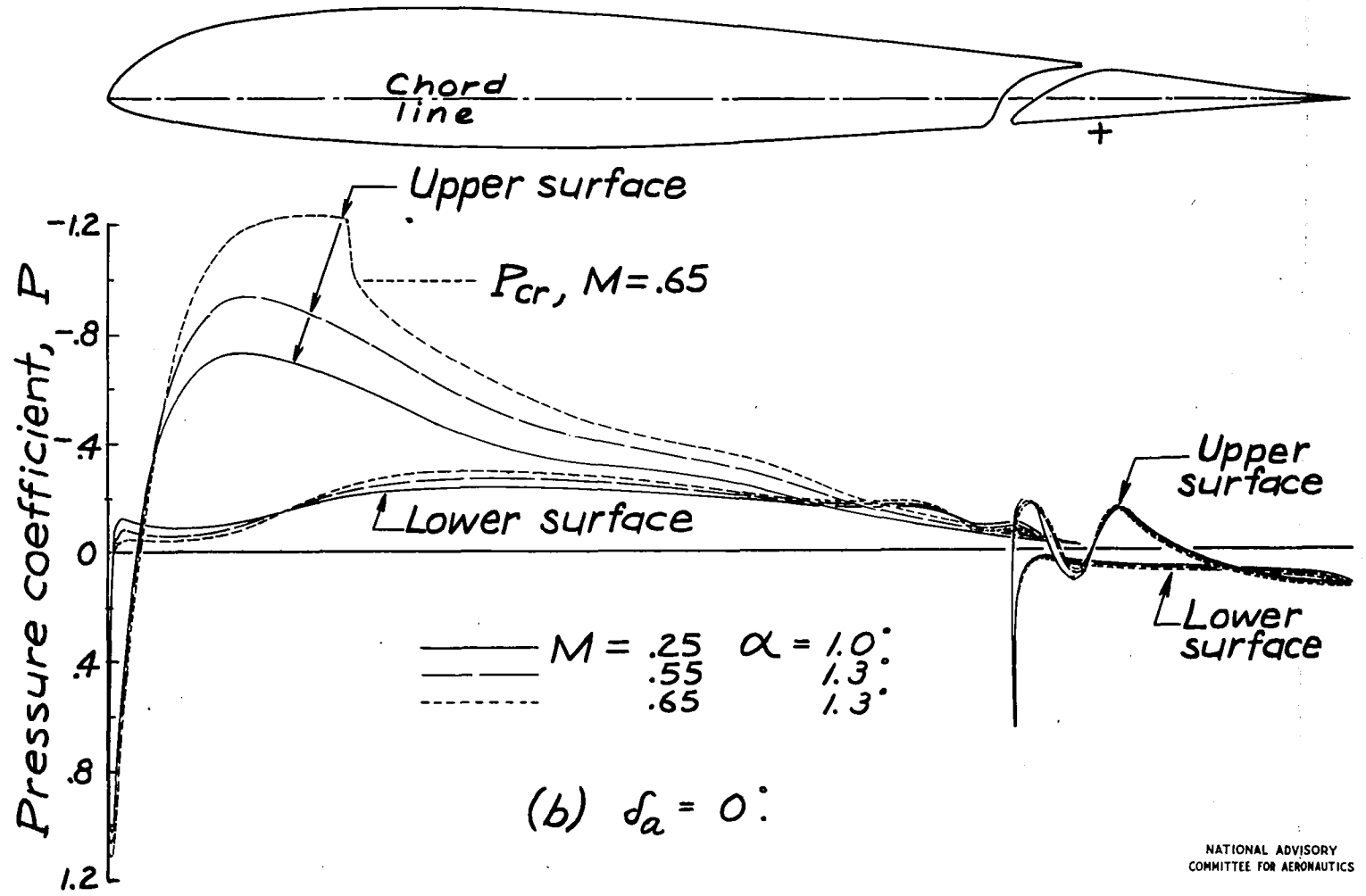

Figure 2.- Continued.

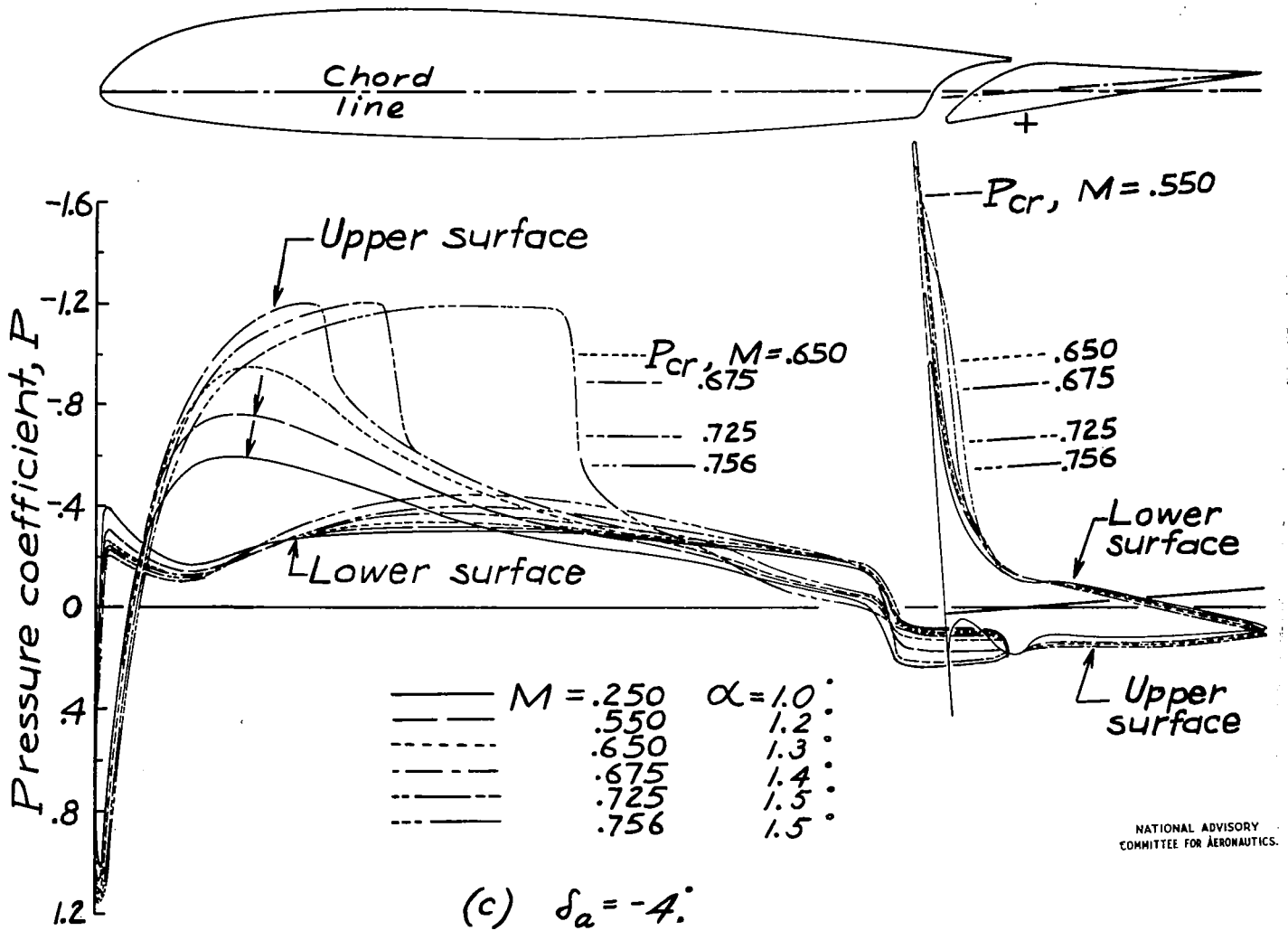

(c) $\delta_a = -4°$

Figure 2. – Concluded.

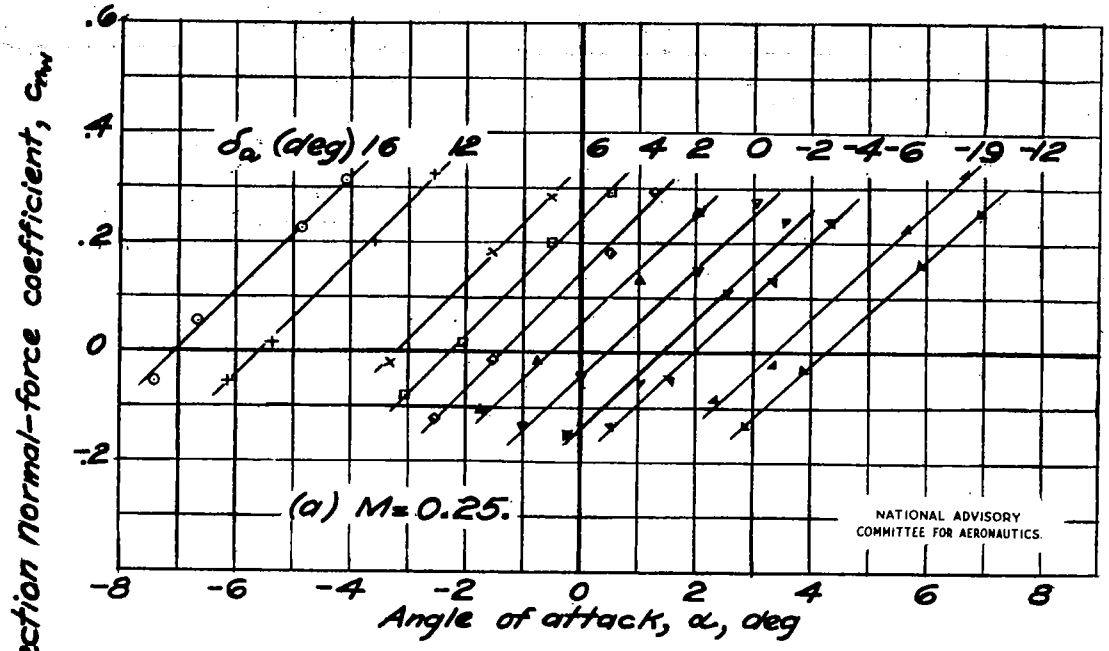

Figure 3.- Airfoil normal-force coefficient against angle of attack at various aileron deflections.

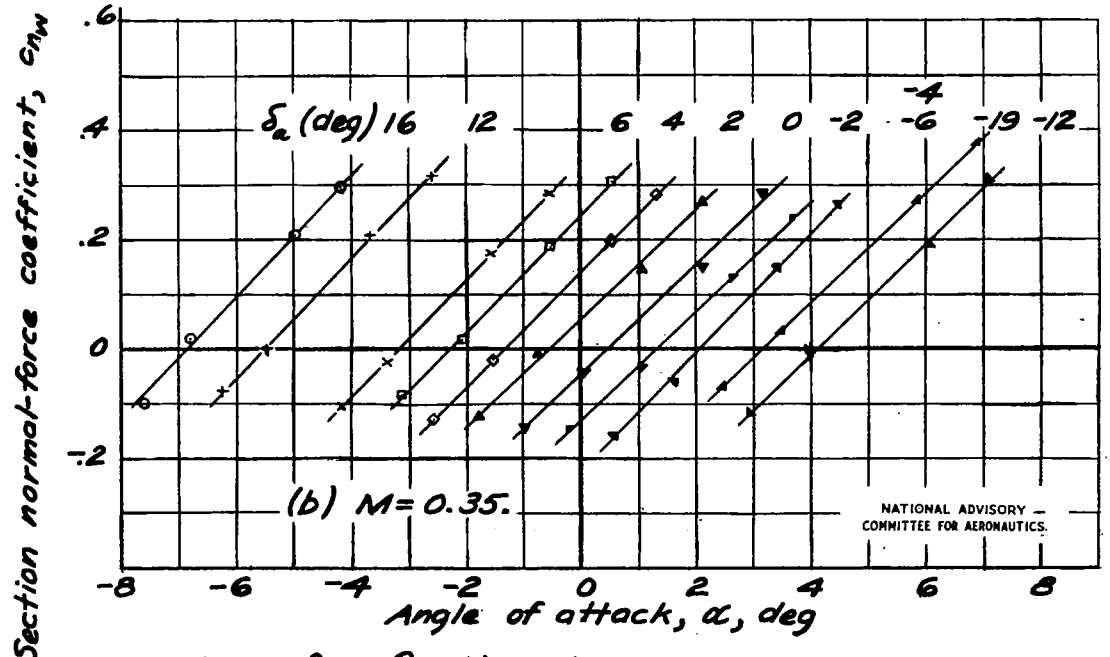

Figure 3.- Continued.

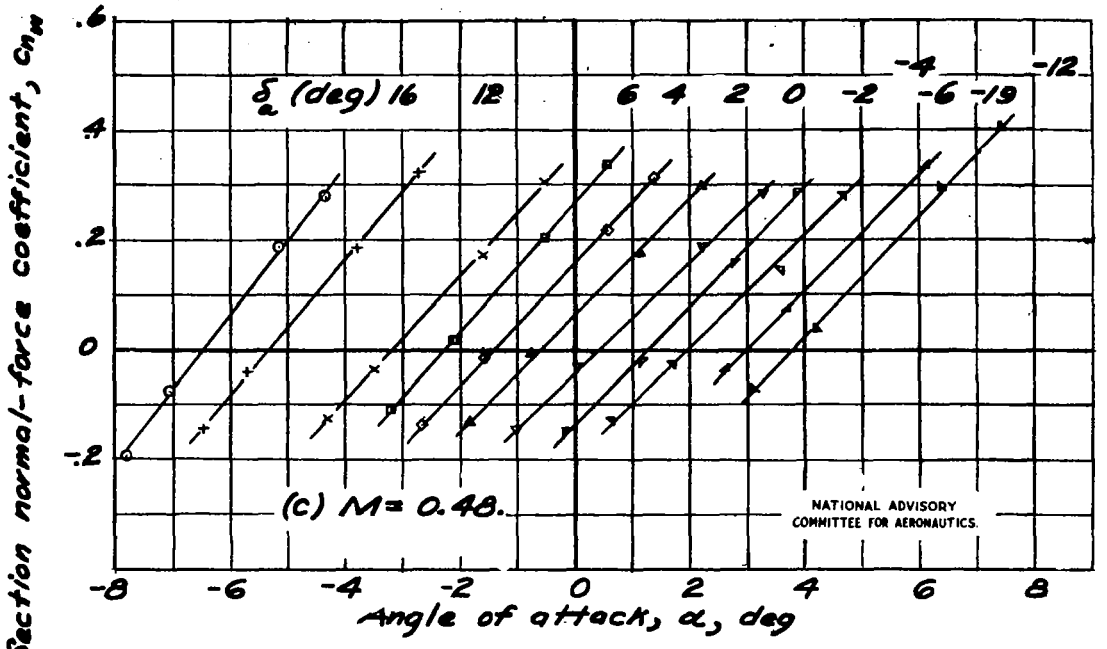

Figure 3.- Continued.

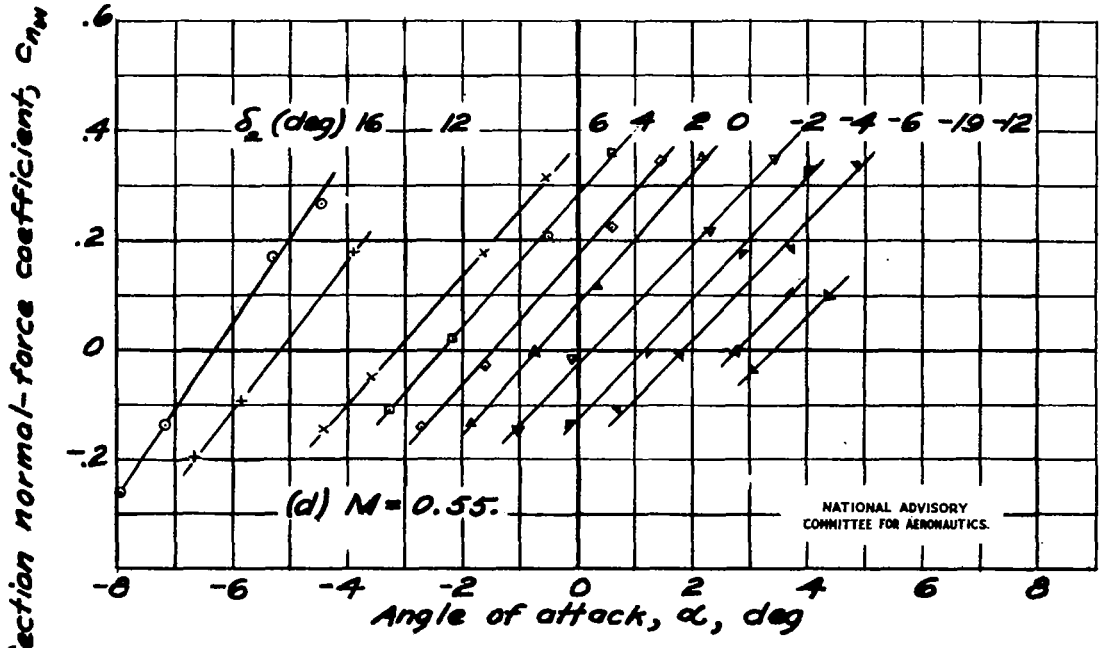

Figure 3.- Continued.

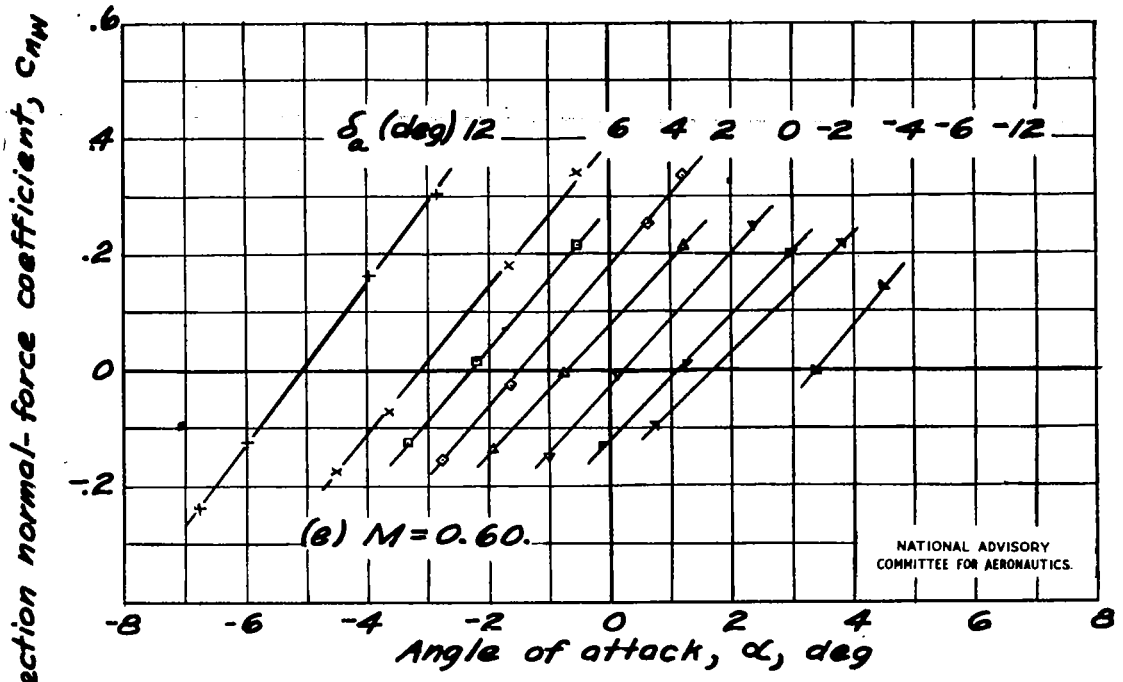

Figure 3.- Continued.

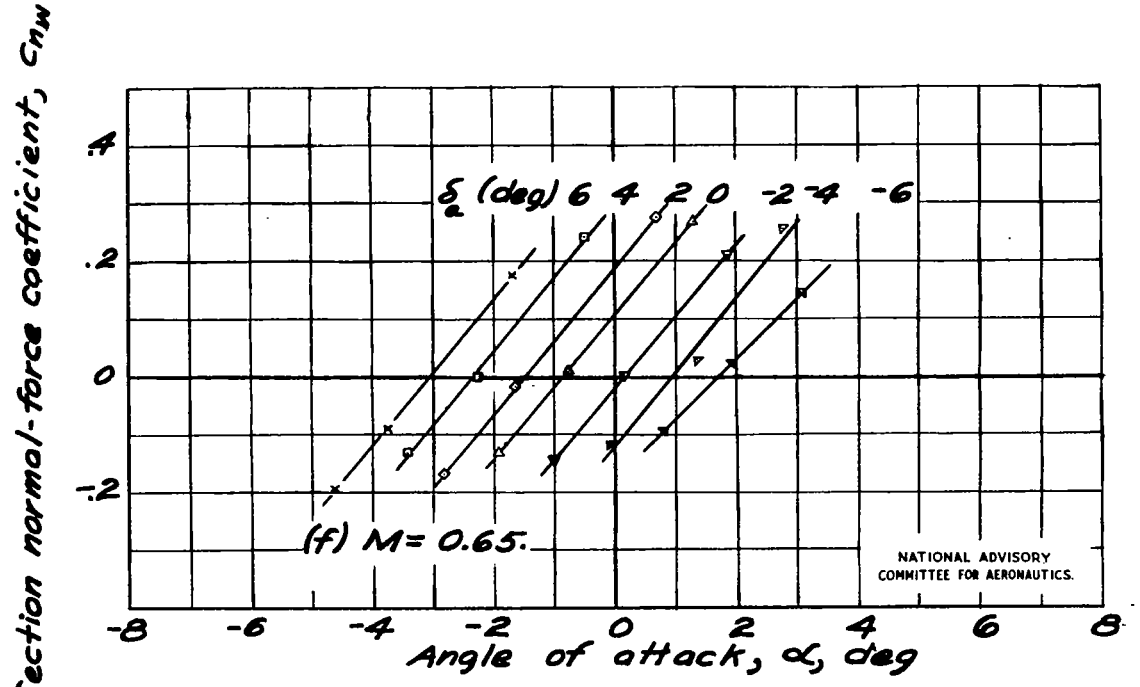

Figure 3.- Continued.

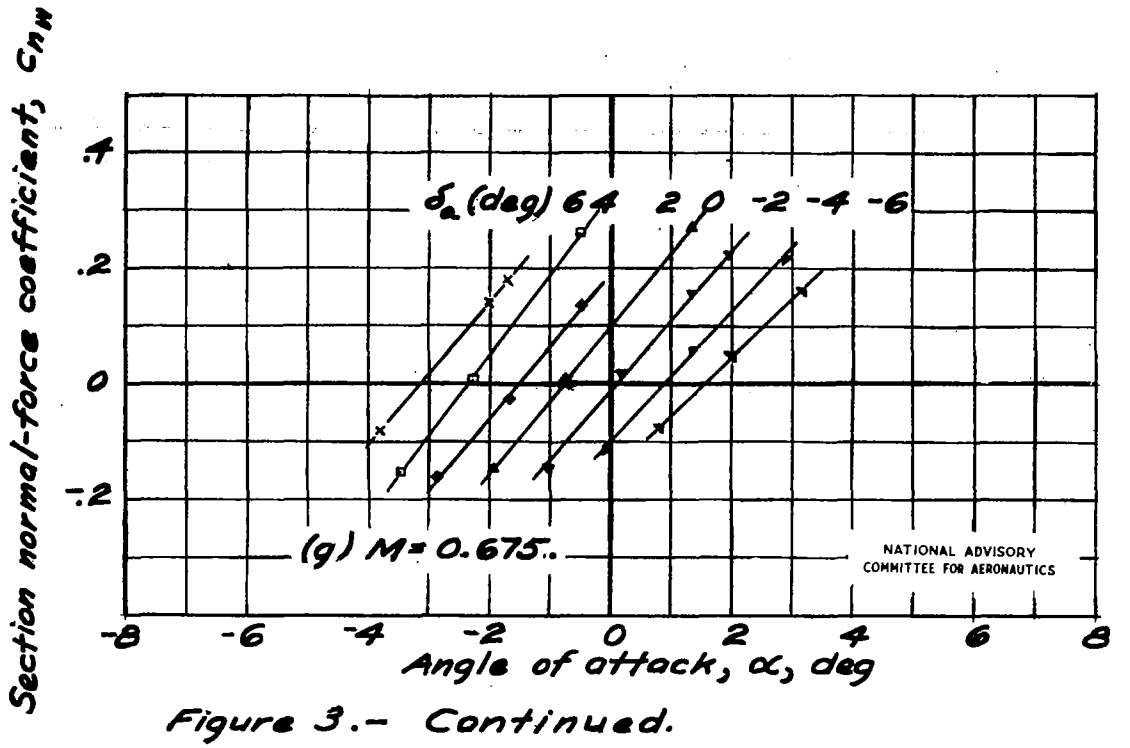

Figure 3.- Continued.

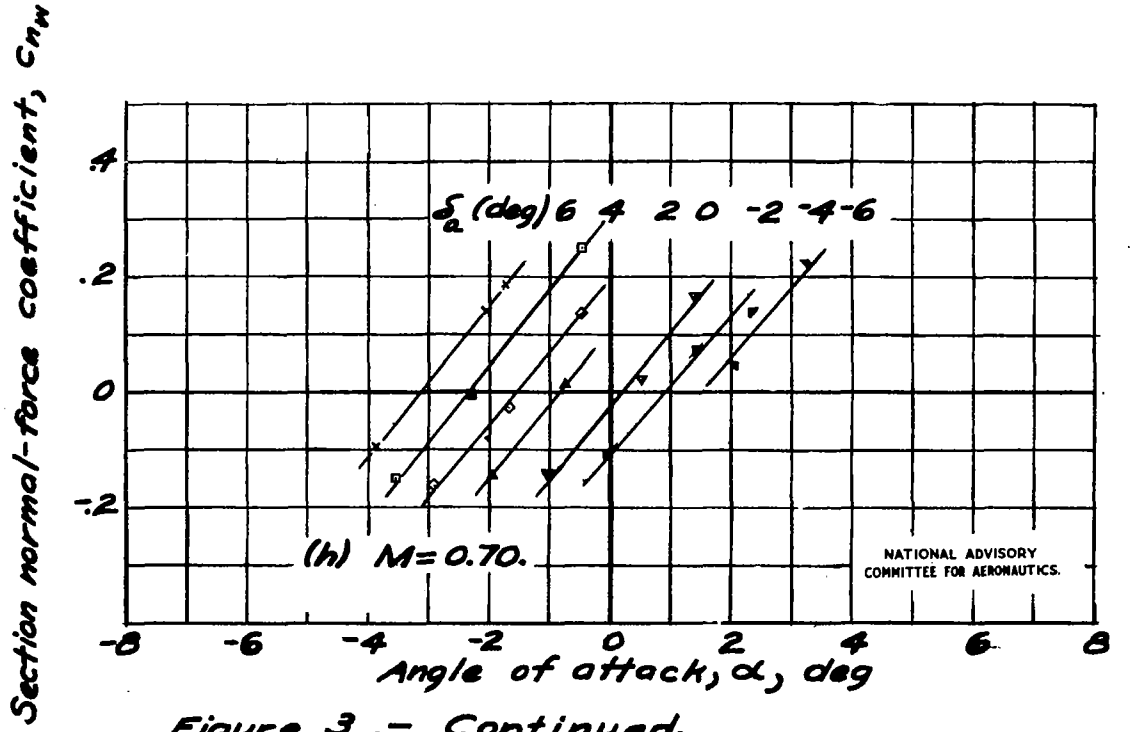

Figure 3.- Continued.

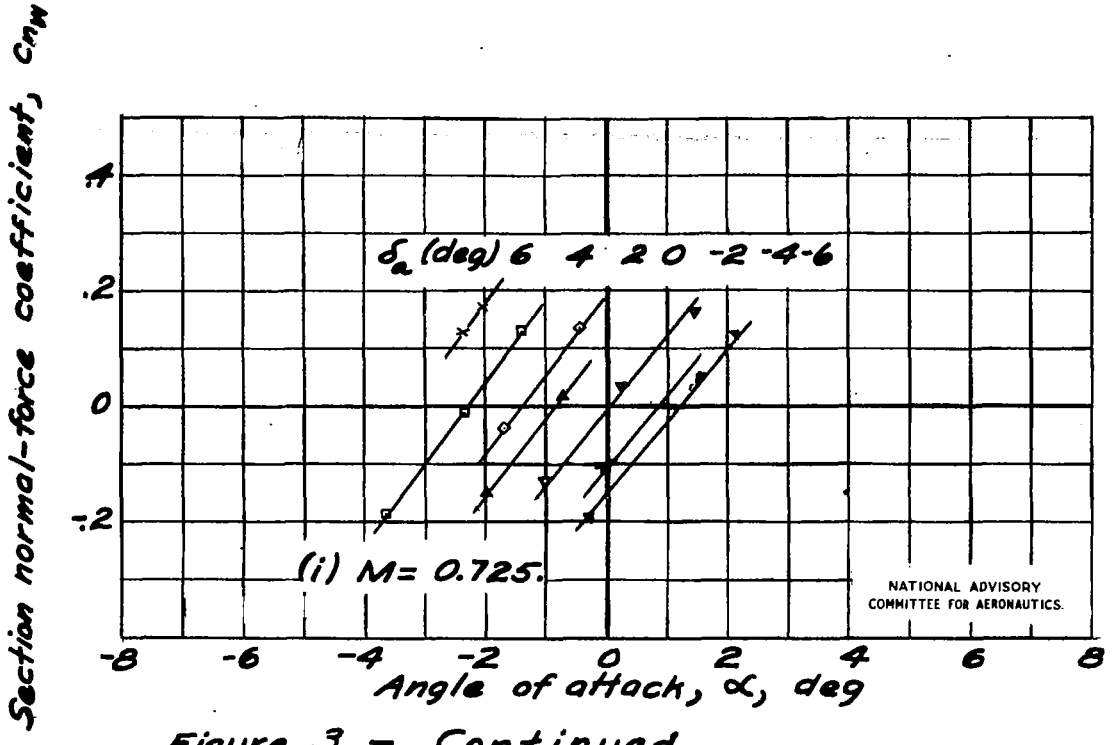

Figure 3.- Continued.

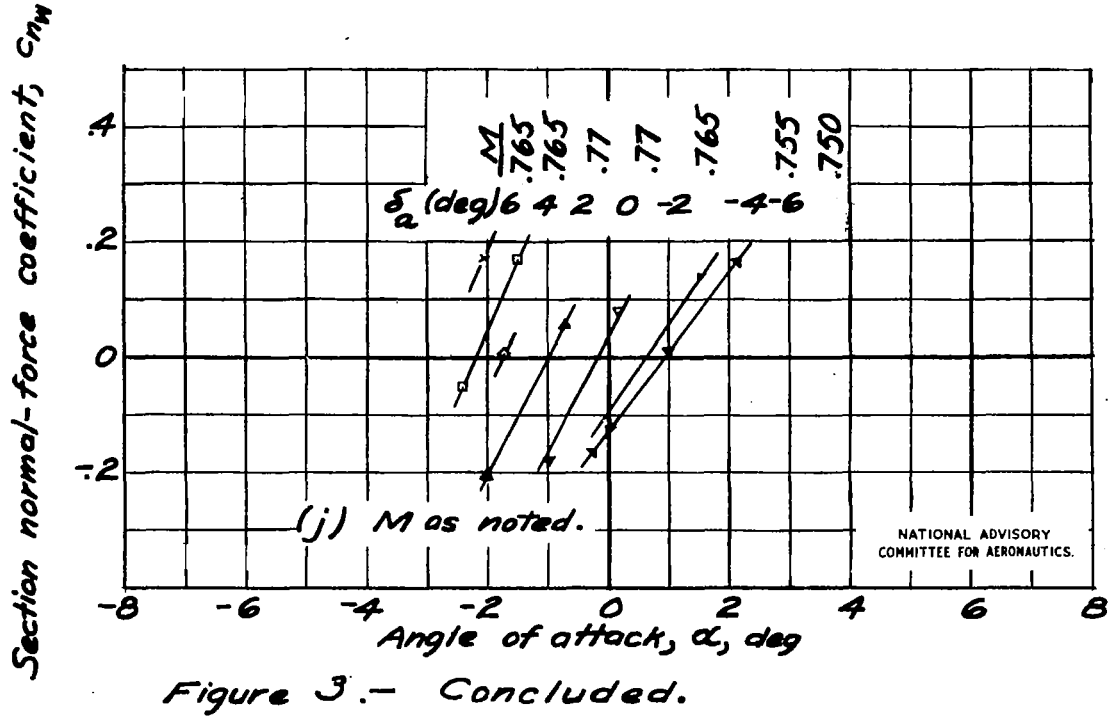

Figure 3.- Concluded.

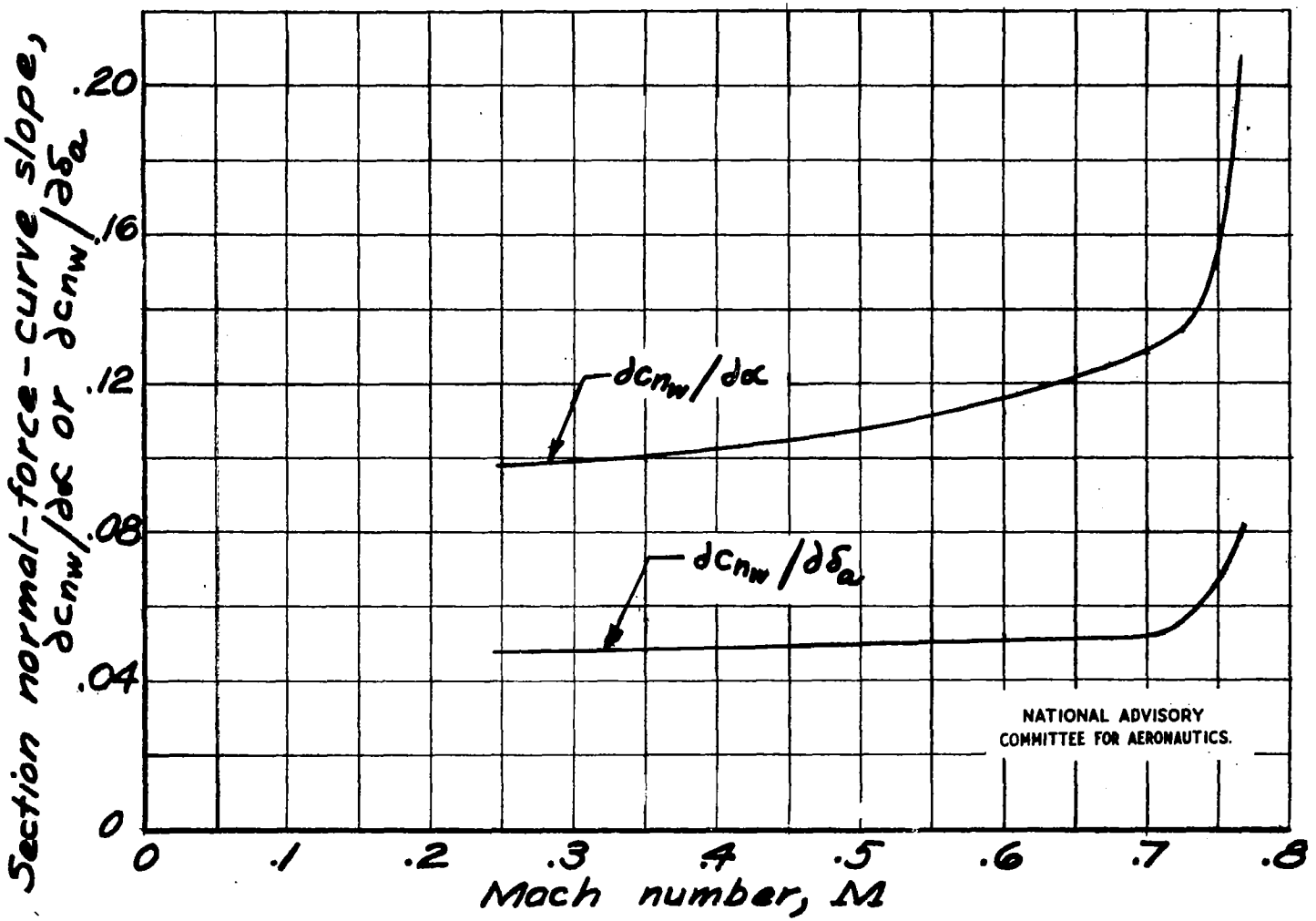

Figure 4 .- Effect of compressibility on normal-force-curve slope $dc_{n_w}/d\alpha$ at $\delta_a = 0°$ and $dc_{n_w}/d\delta_a$, at $\alpha = 0°$.

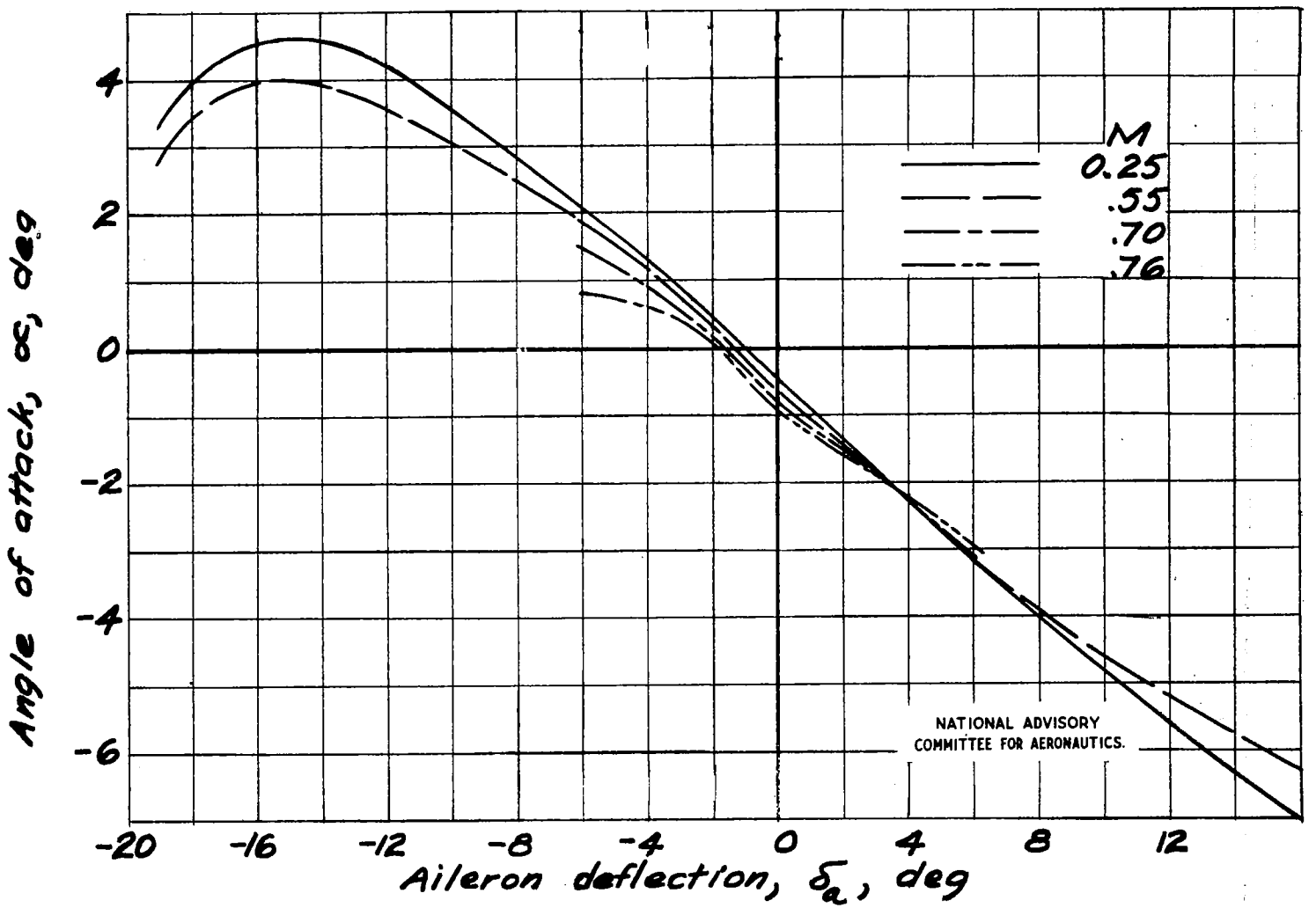

Figure 5.-Angle of attack for section airfoil normal-force coefficient of 0 against aileron deflection at various Mach numbers.

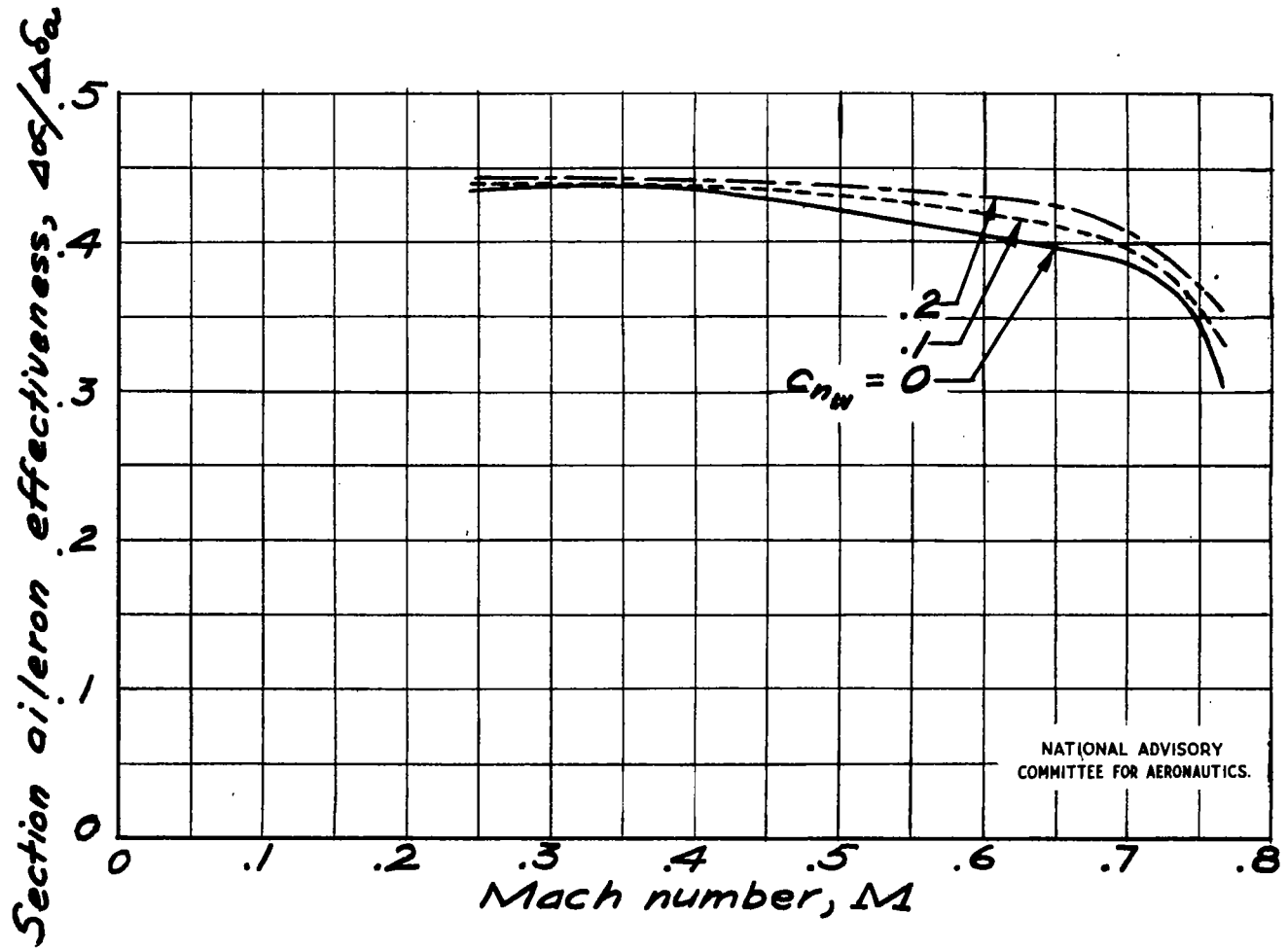

Figure 6.- Section average aileron effectiveness for aileron deflections from -6° to 6° at various section airfoil normal-force coefficients.

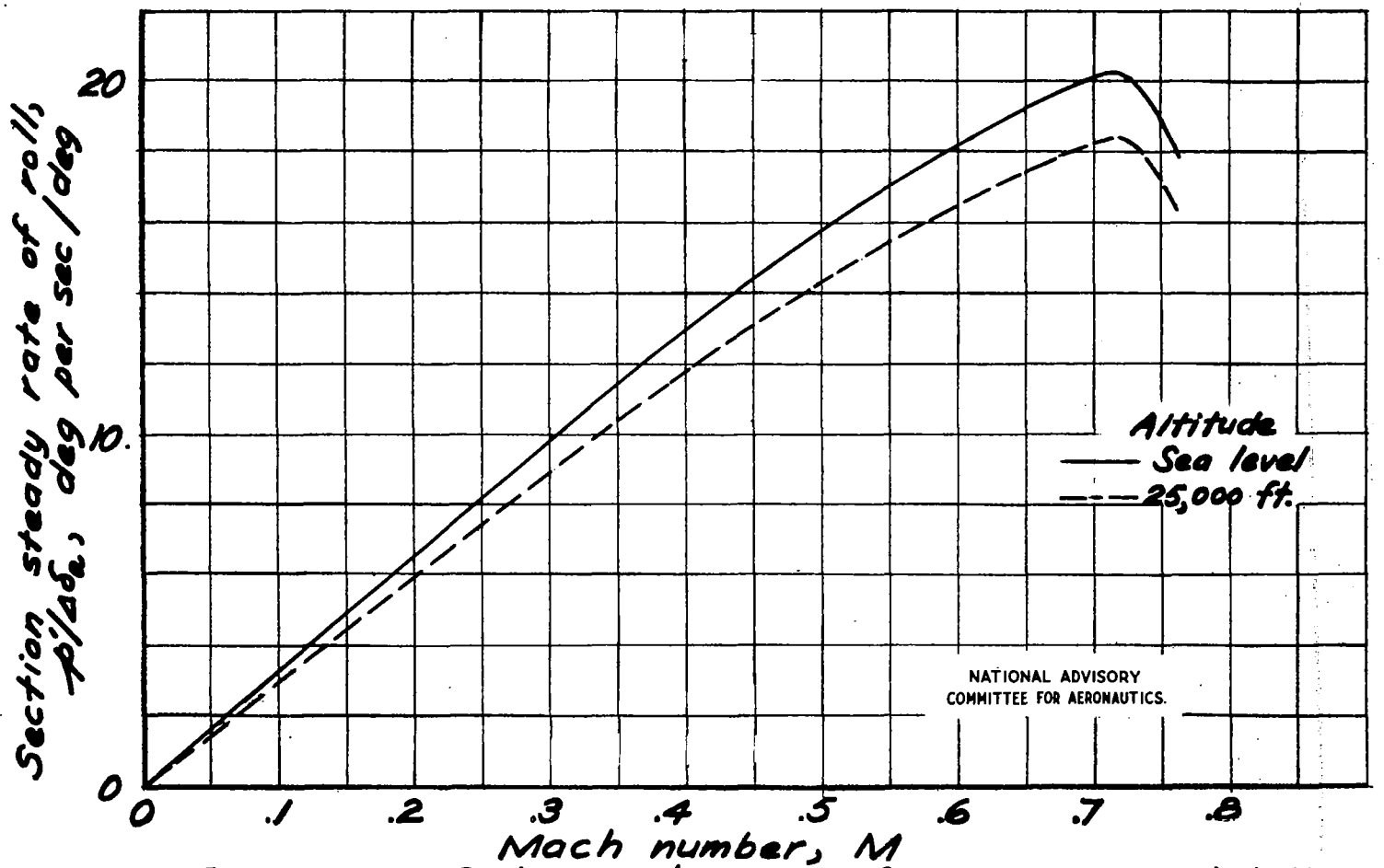

Figure 7.- Section steady rate of roll per degree deflection of single aileron against Mach number, $C_{n_w} = 0$.

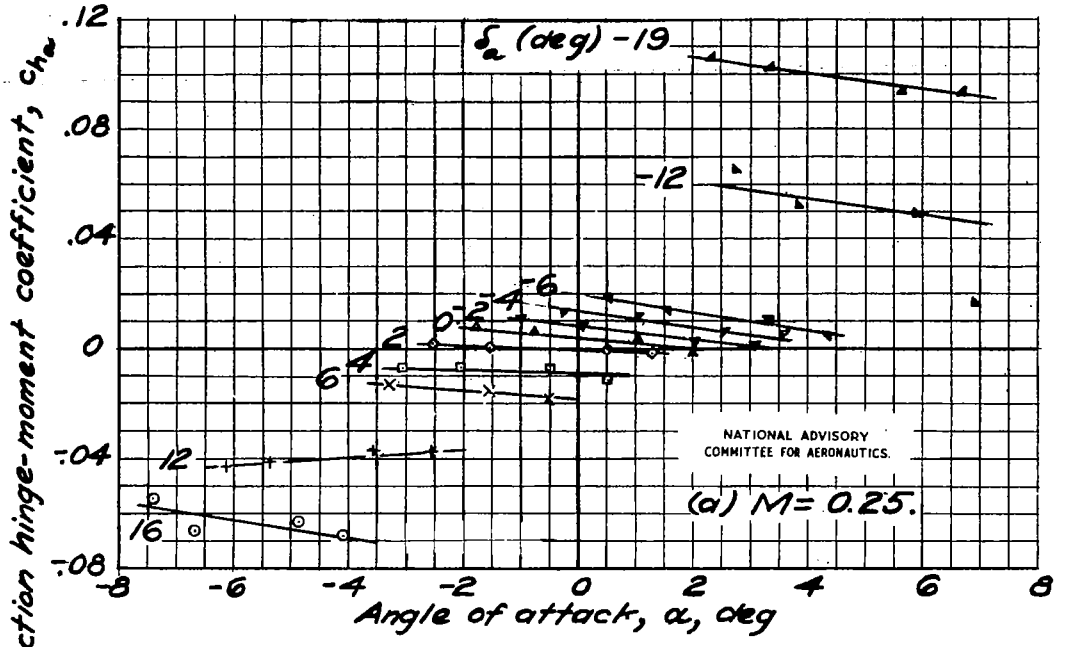

Figure 8.- Section aileron hinge-moment coefficient against angle of attack at various aileron deflections.

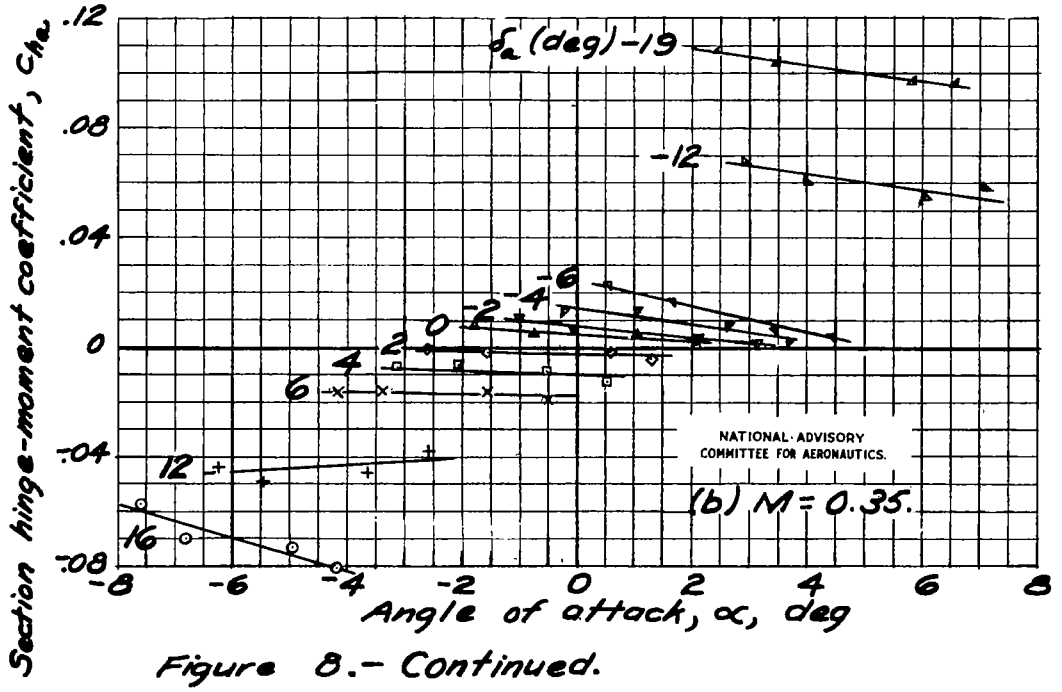

Figure 8.- Continued.

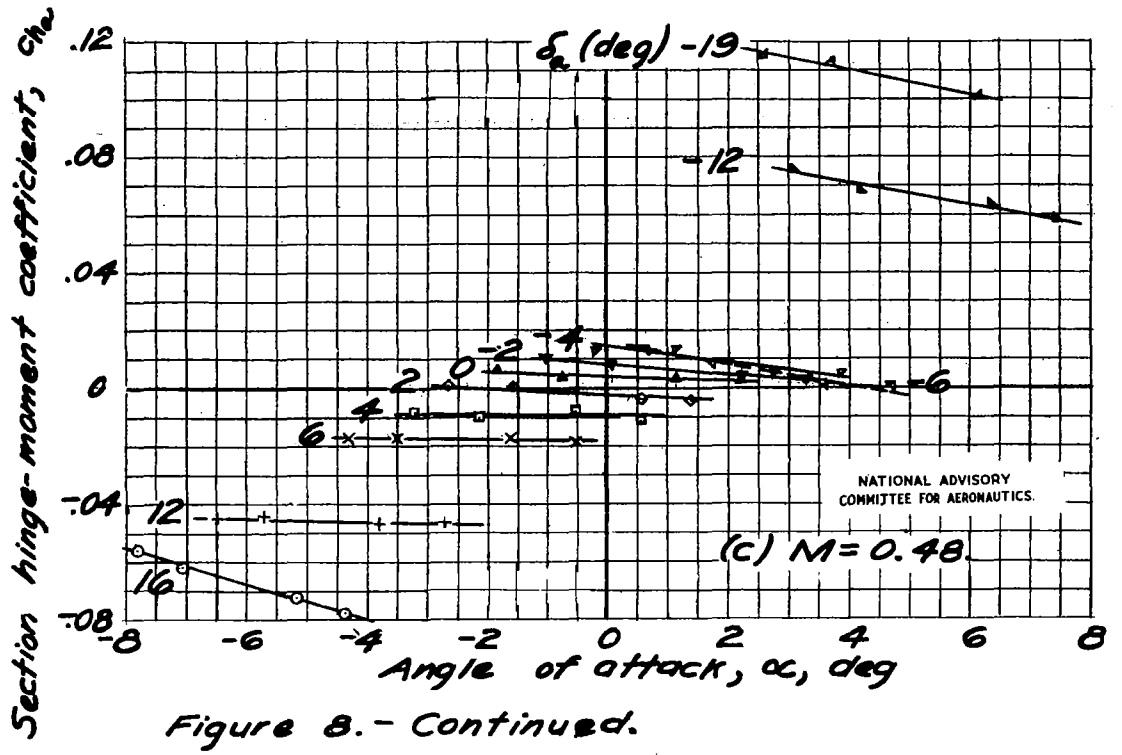

Figure 8.- Continued.

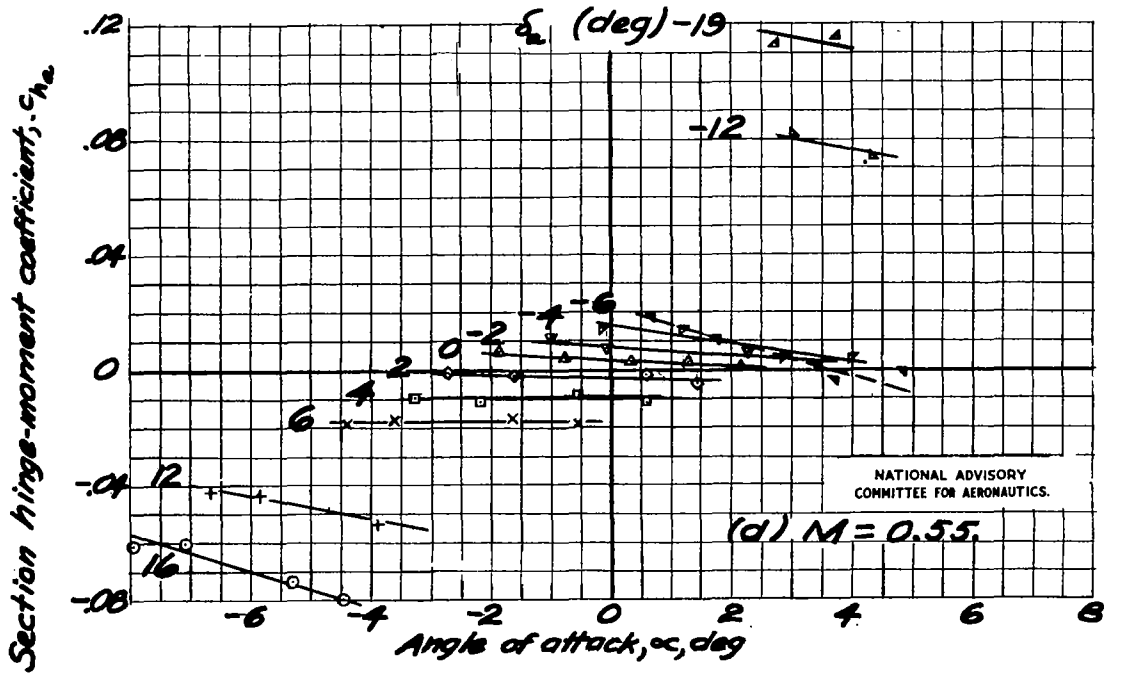

Figure 8.- Continued.

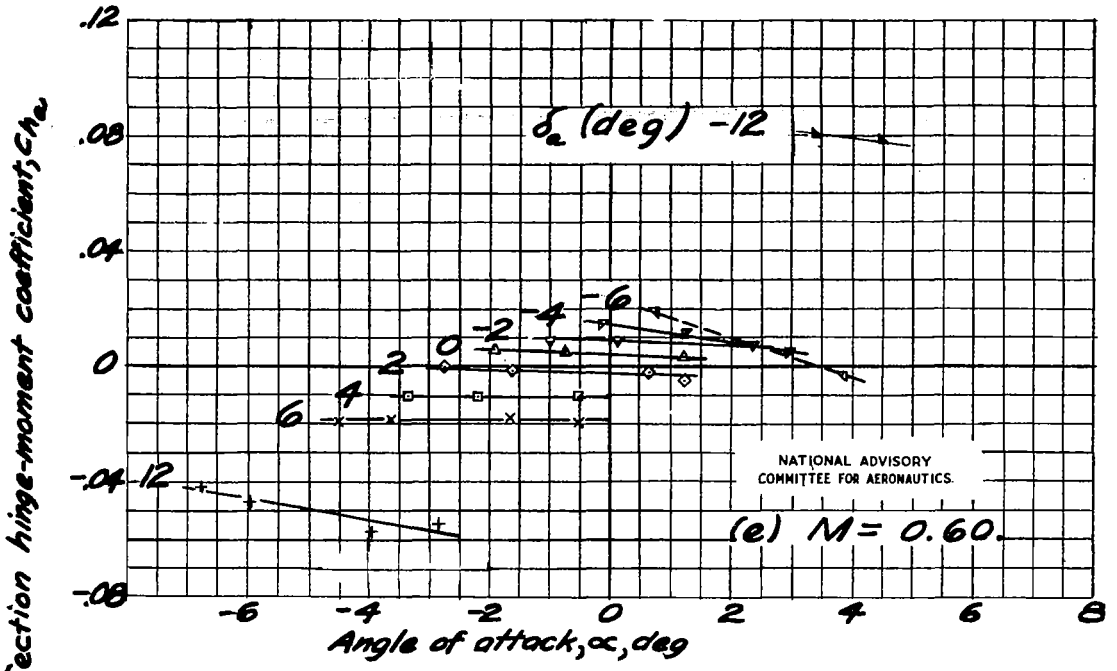

Figure 8.- Continued.

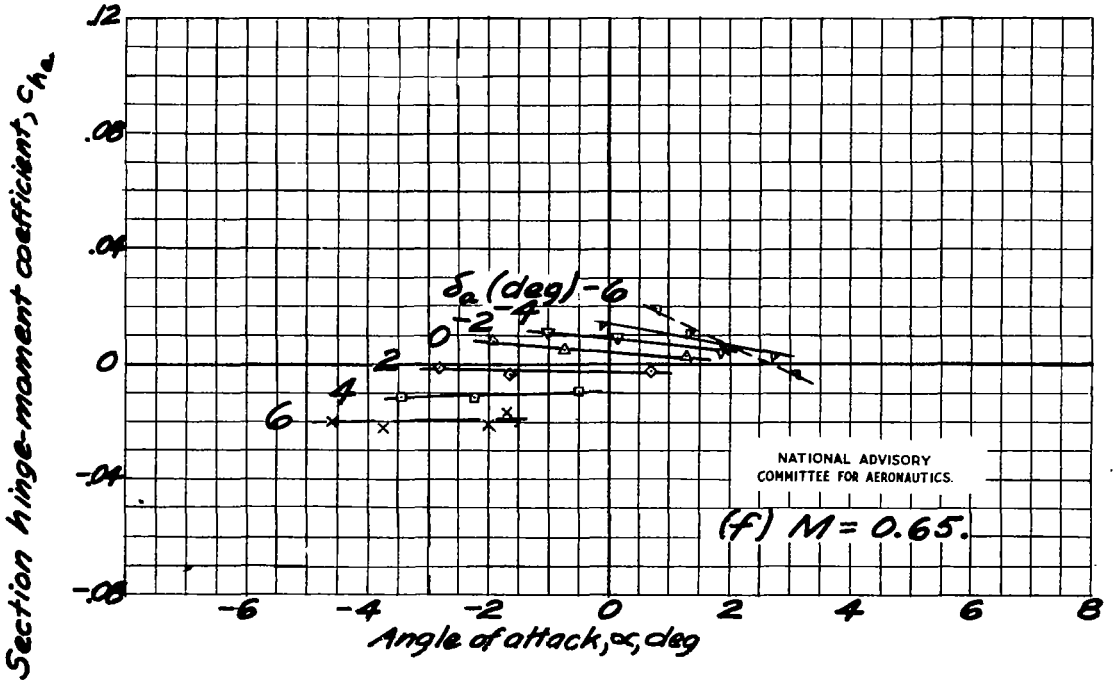

Figure 8.- Continued.

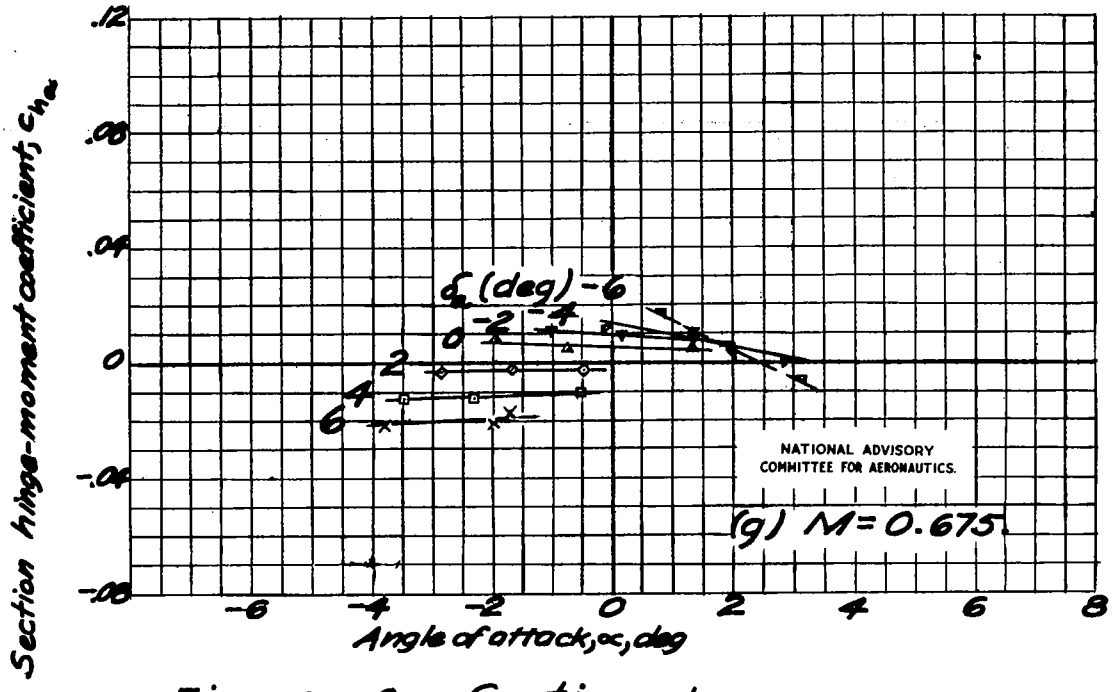

Figure 8.- Continued.

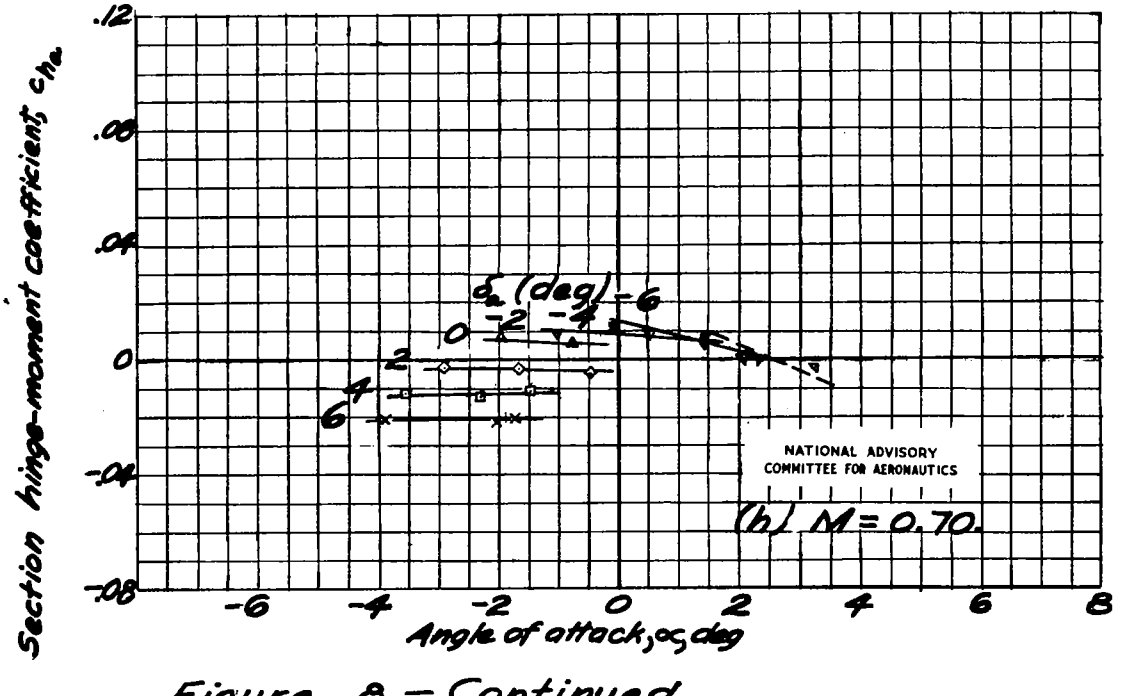

Figure 8.- Continued.

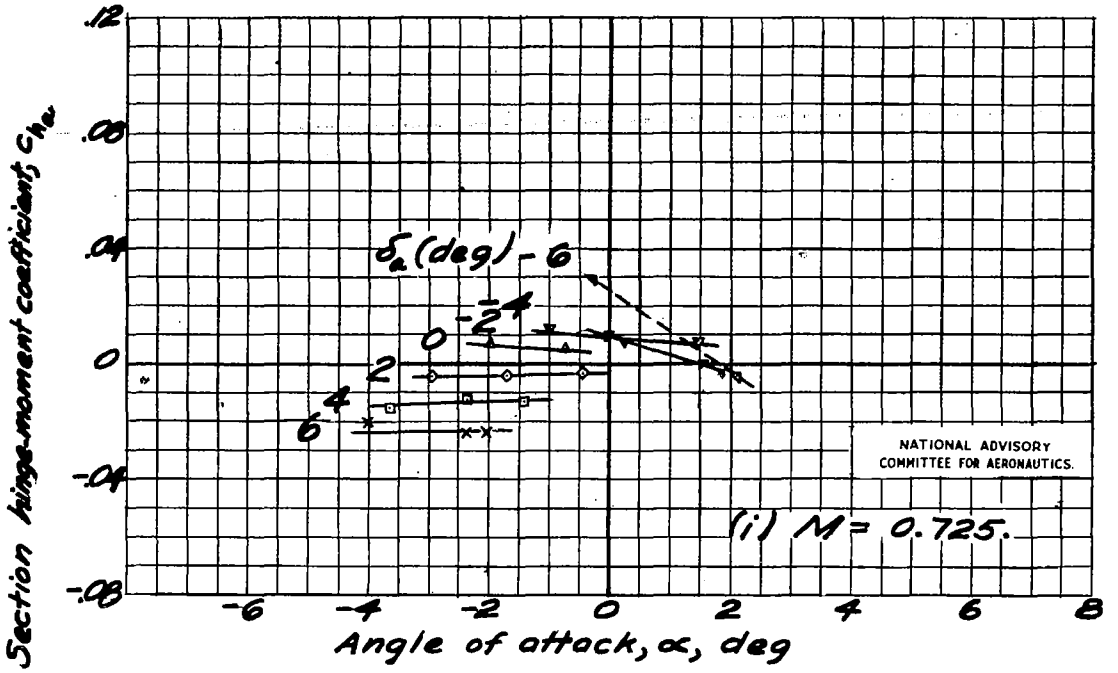

Figure 8.- Continued.

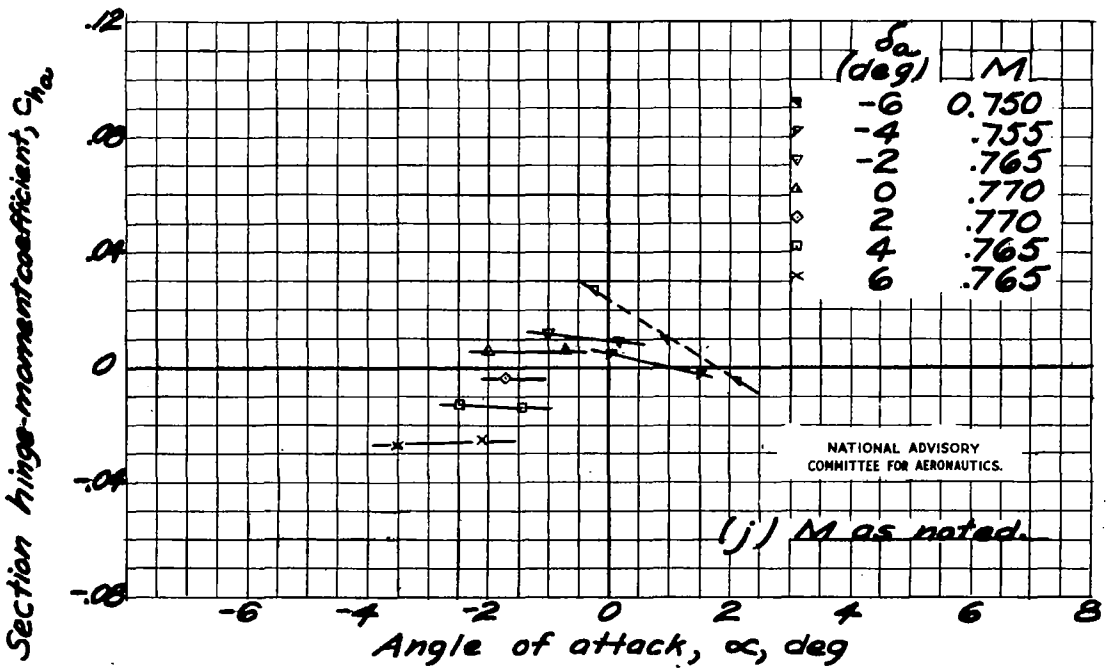

Figure 8.- Concluded.

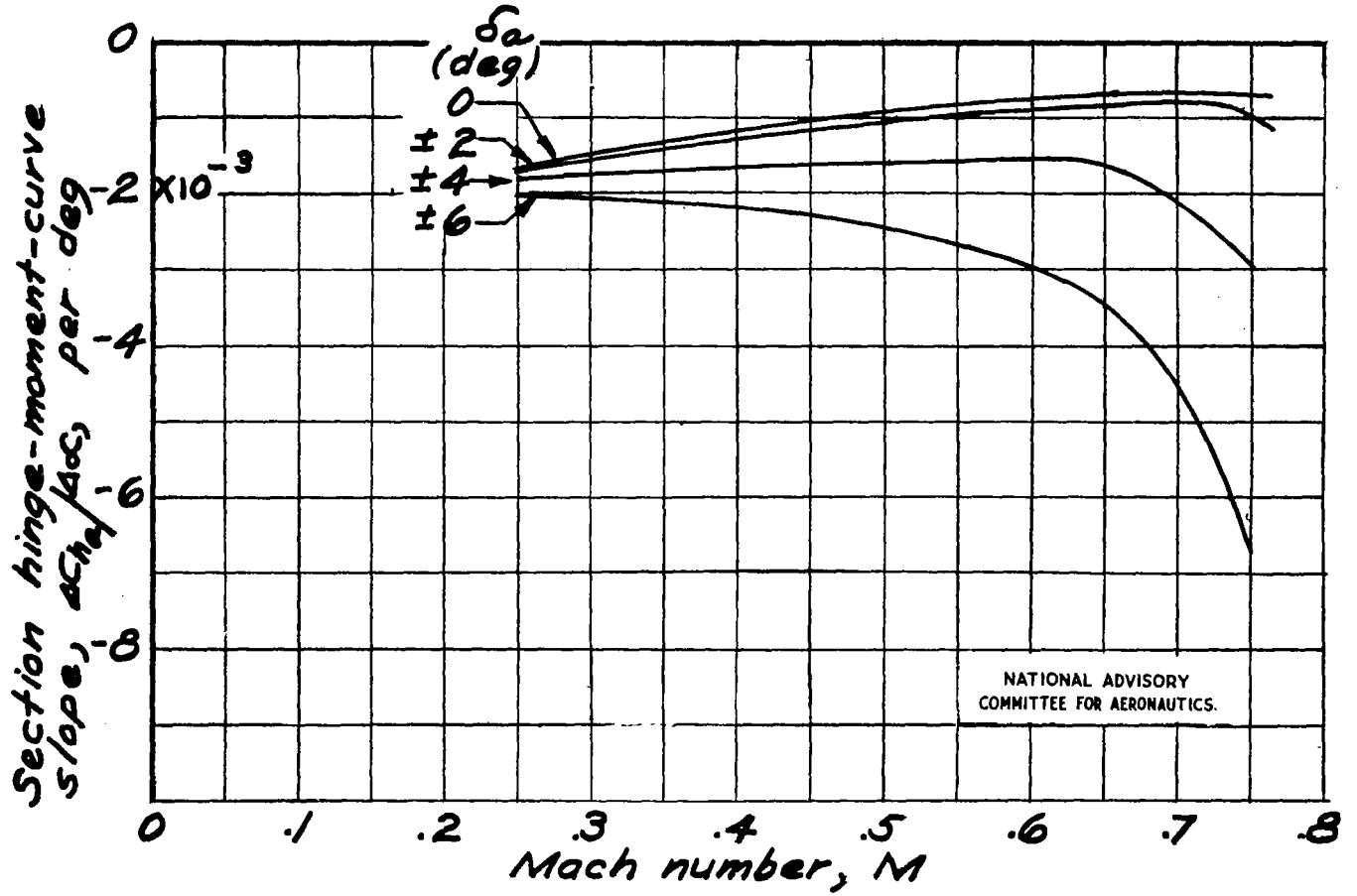

Figure 9.- Section average hinge-moment-curve slope $\Delta C_{h_\alpha}/\Delta\alpha$ for equal ± aileron deflections against Mach number for section airfoil normal-force coefficients from 0 to 0.2.

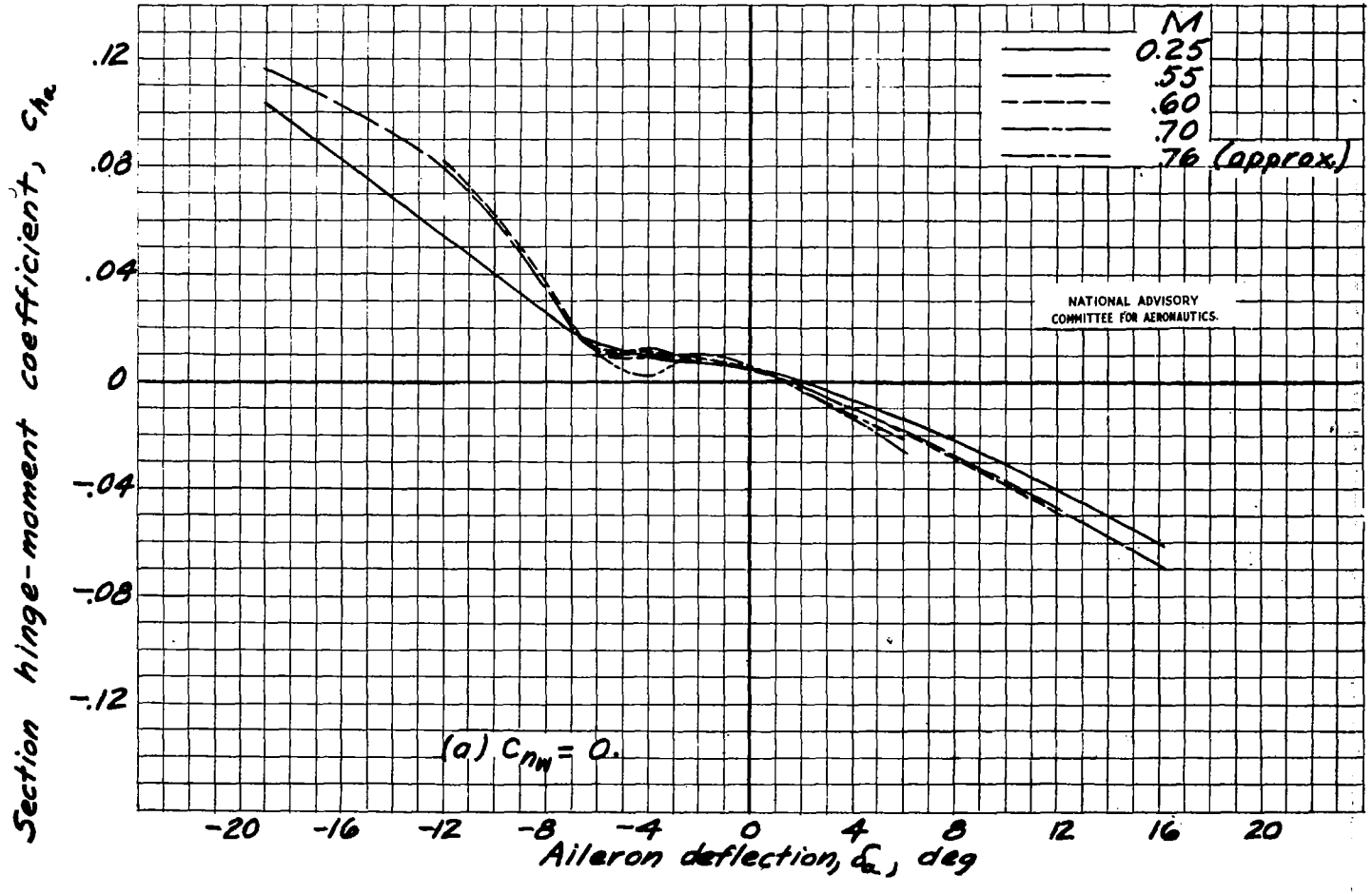

Figure 10.— Section aileron hinge-moment coefficient against aileron deflection at various Mach numbers.

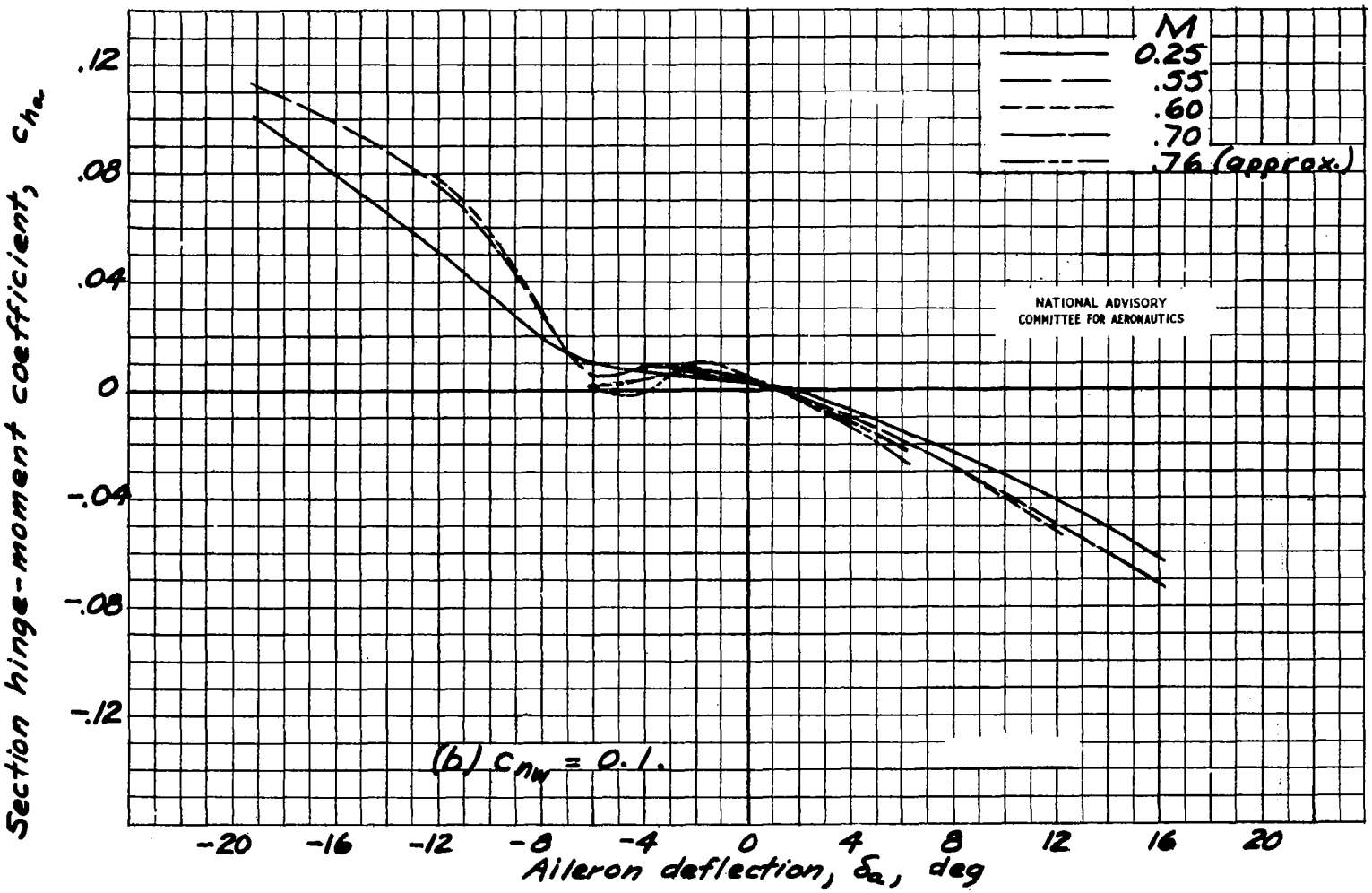

Figure 10.- Continued.

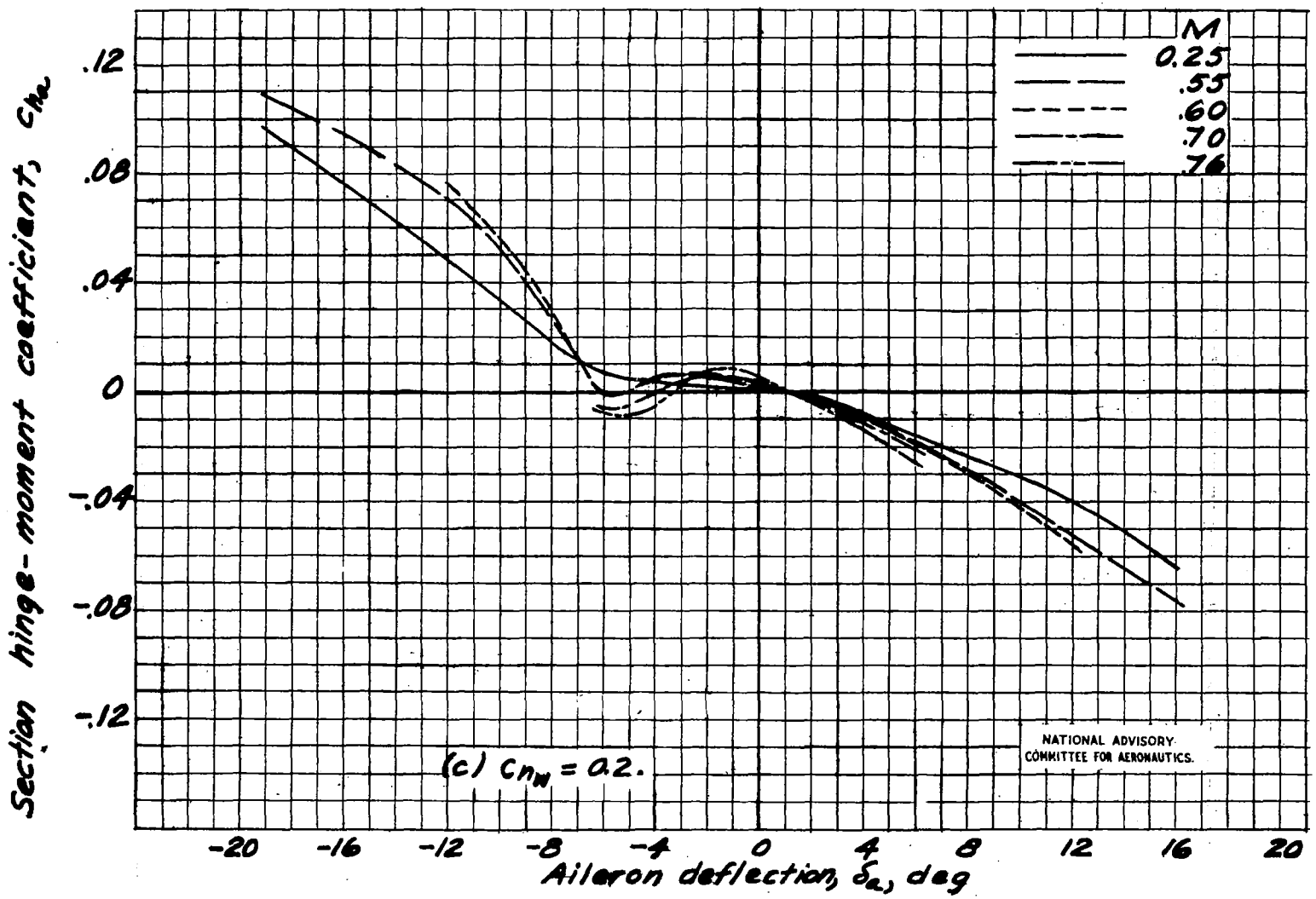

Figure 10.— Concluded.

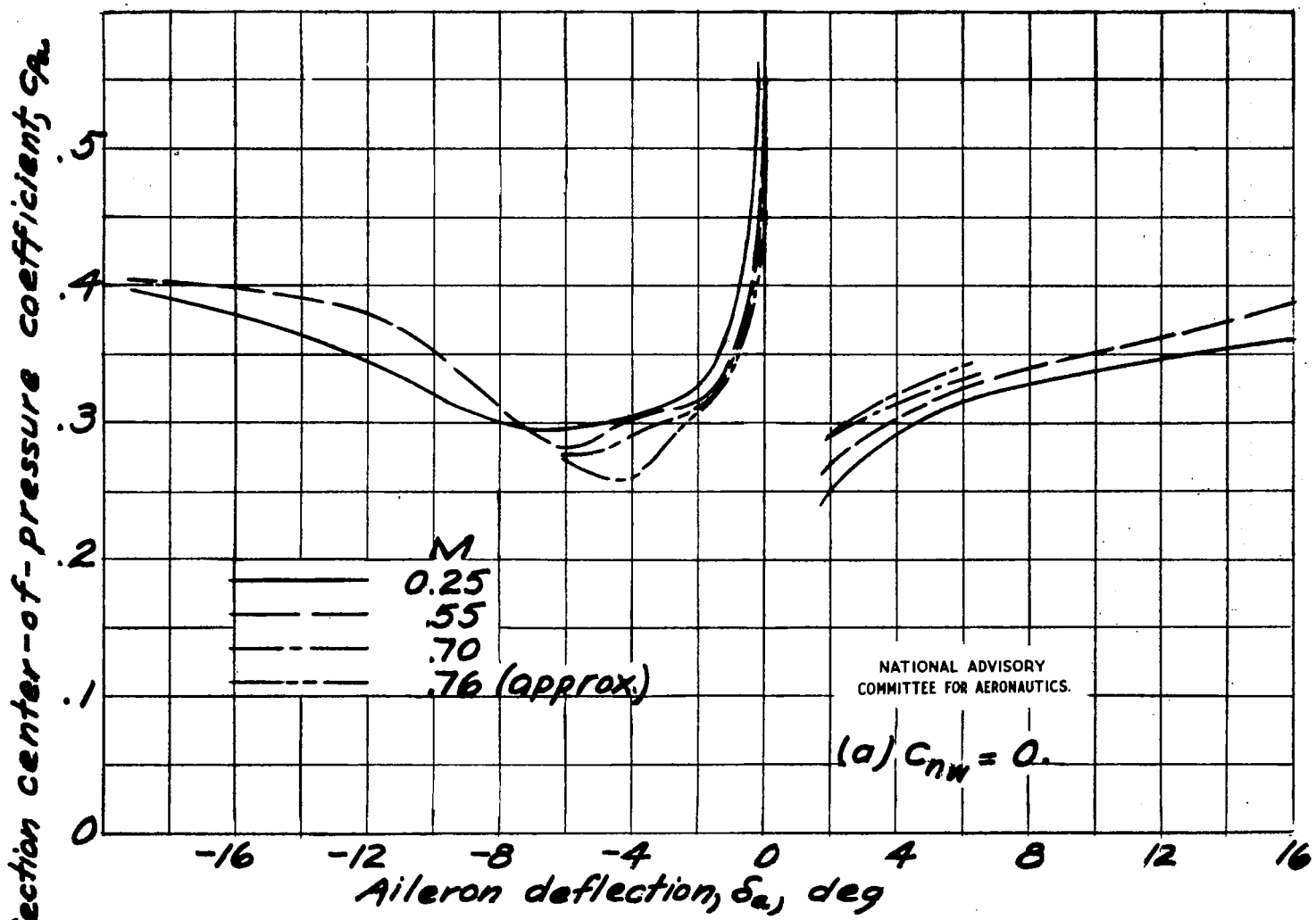

Figure 11.- Section aileron center-of-pressure coefficient against aileron deflection at various Mach numbers.

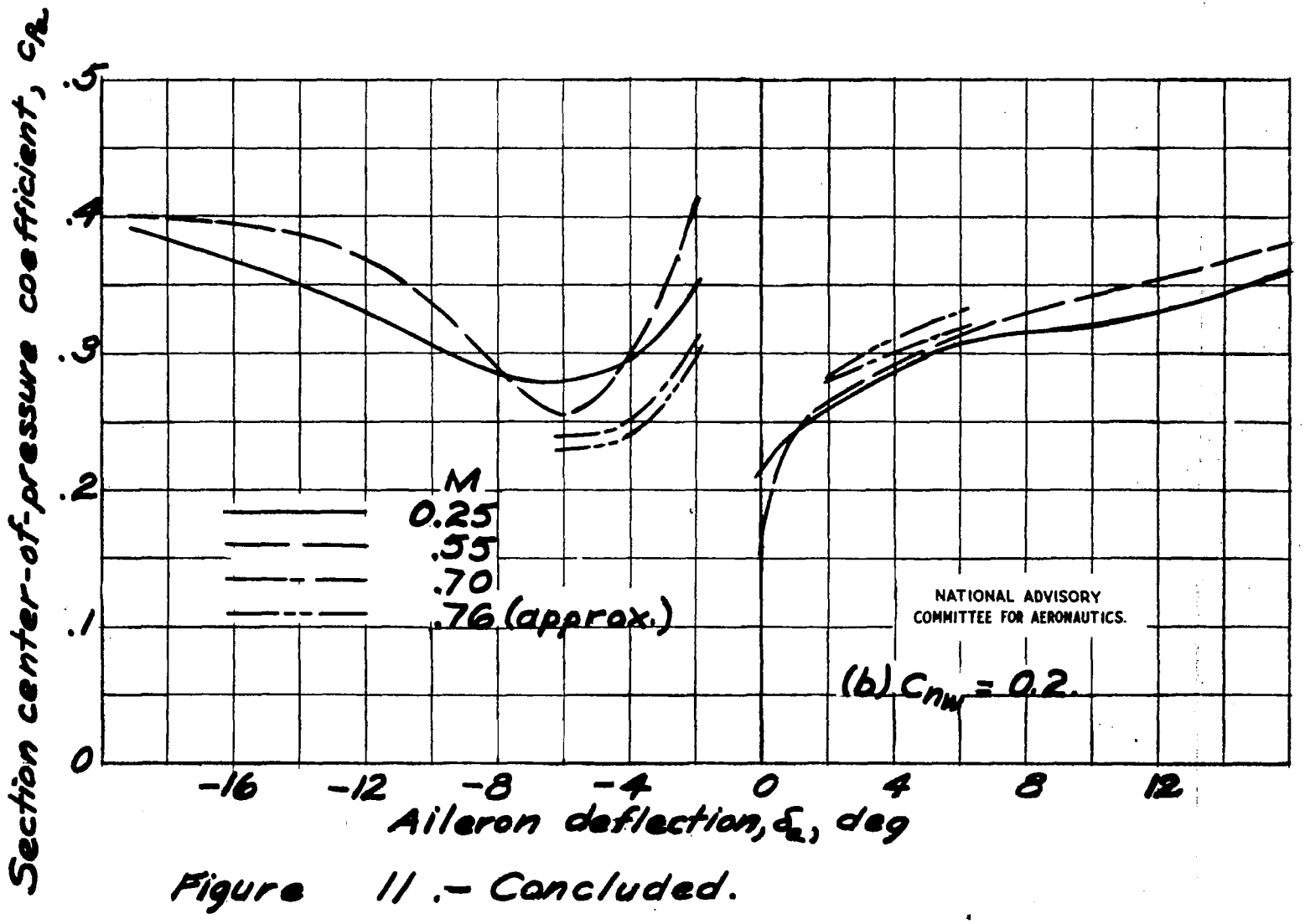

Figure 11.- Concluded.

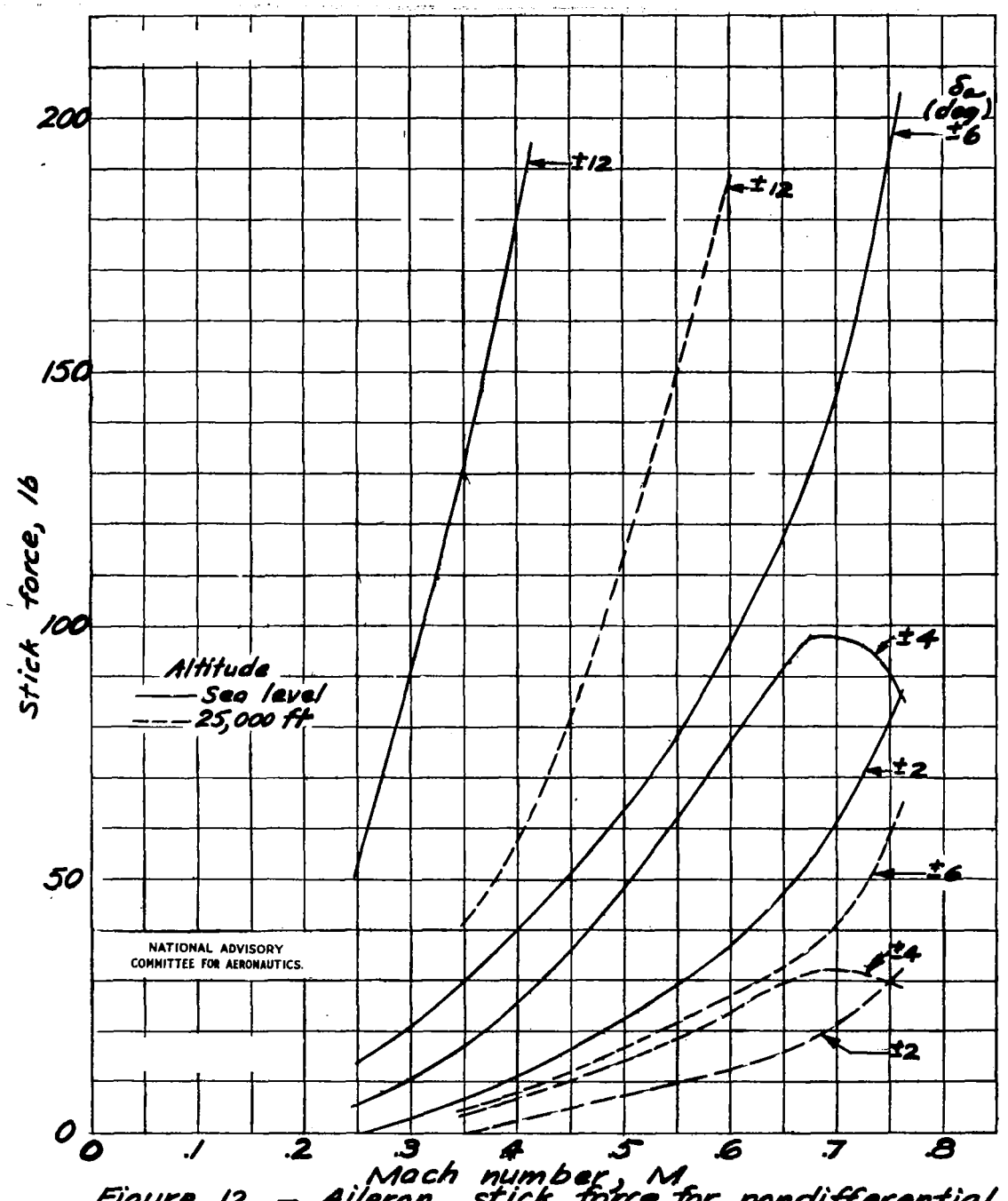

Figure 12.- Aileron stick force for nondifferential aileron deflections and steady rate of roll at two altitudes.

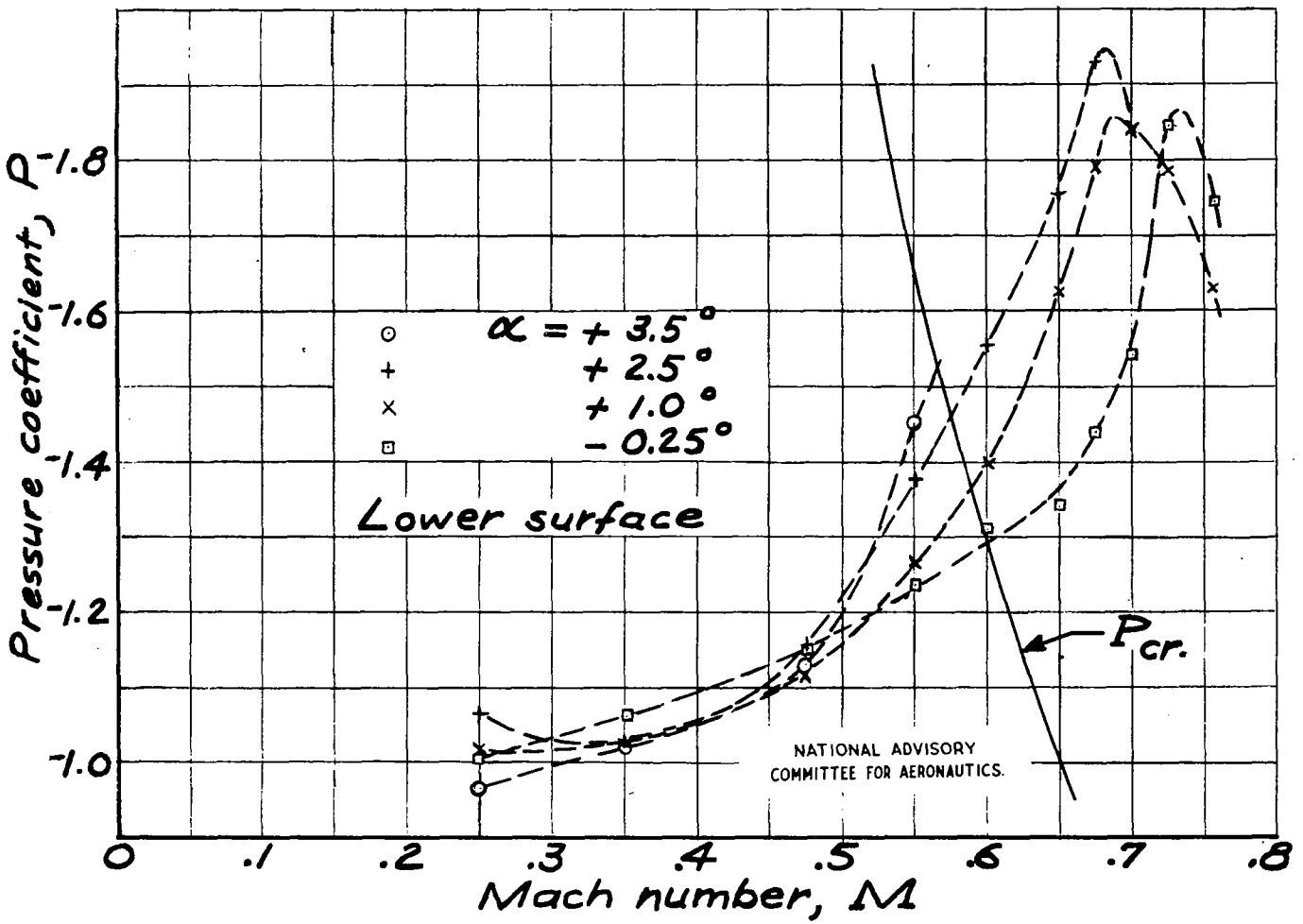

Figure 13.— Effect of compressibility on peak negative pressure coefficient of aileron. $\delta_a = -4°$.

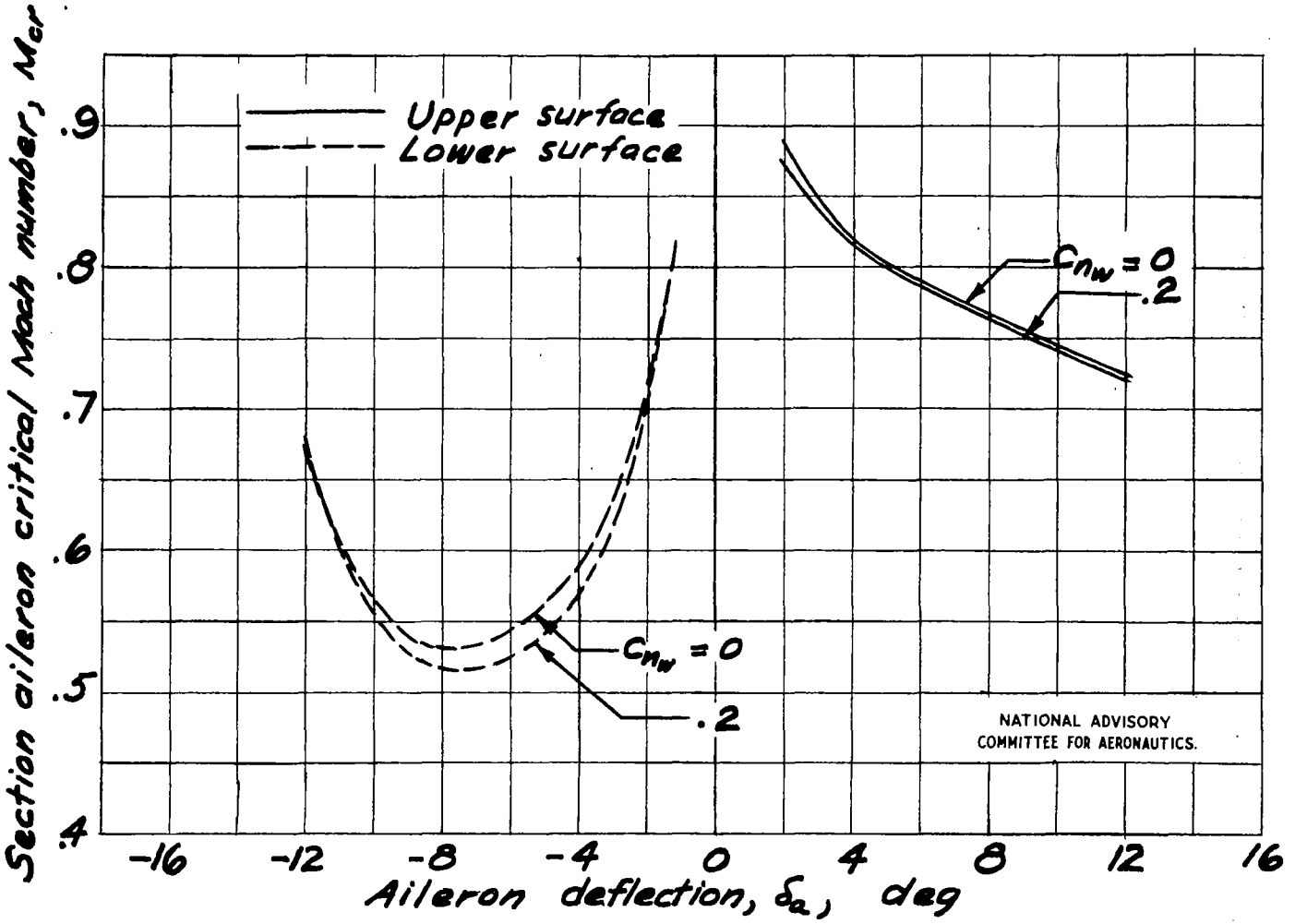

Figure 14.—Section critical Mach number of aileron against aileron deflection at various section airfoil normal-force coefficients.

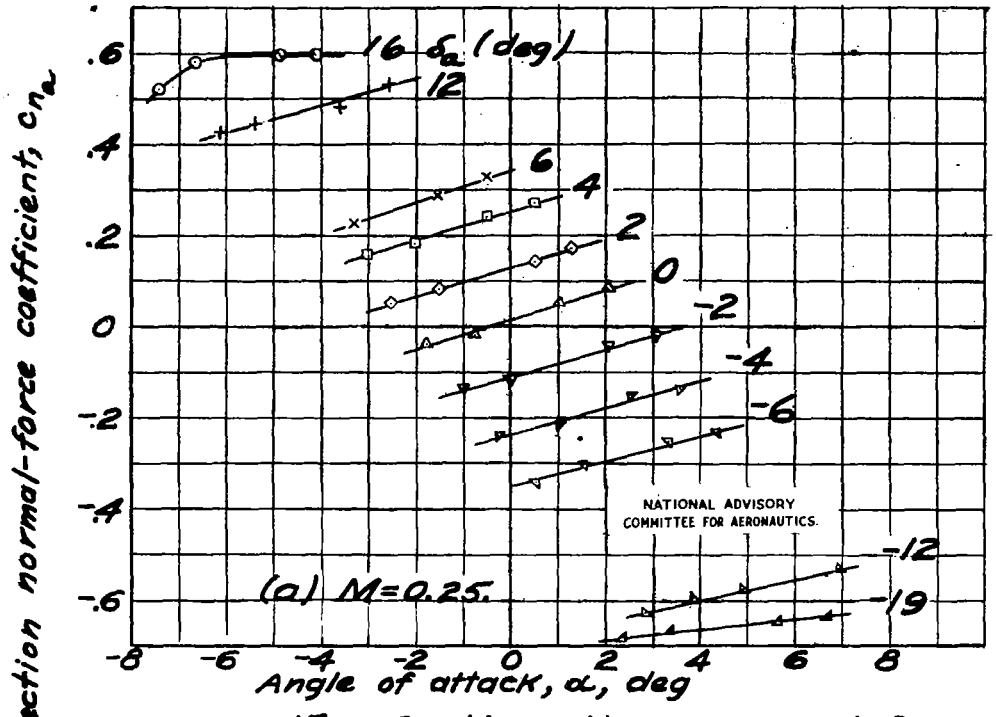

Figure 15.- Section aileron normal-force coefficient against angle of attack at various aileron deflections.

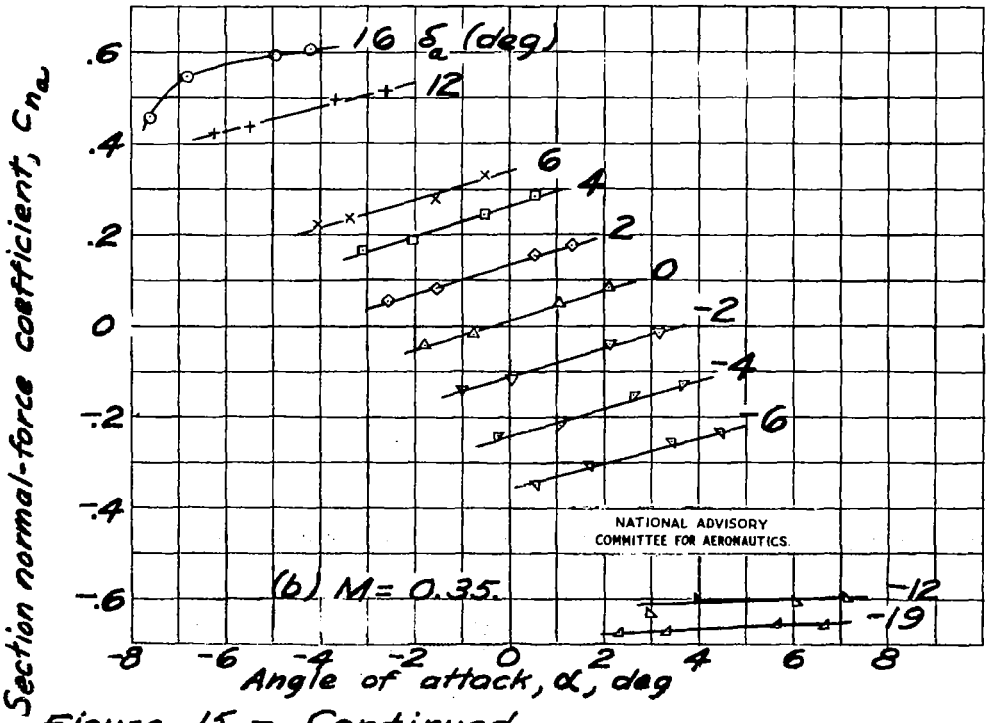

Figure 15.- Continued.

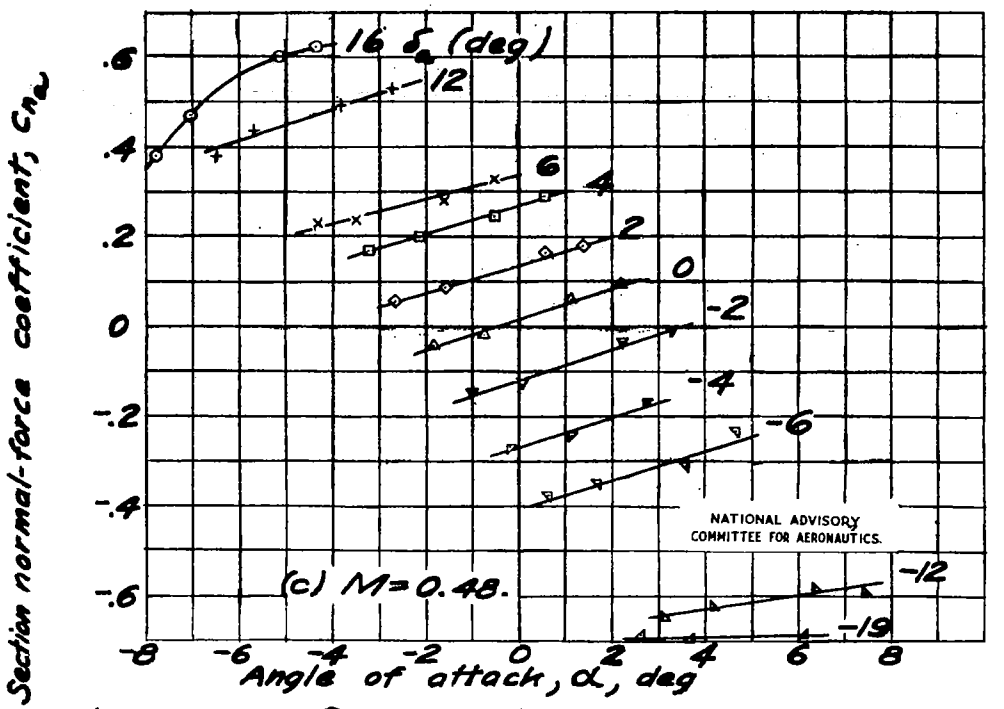

Figure 15.- Continued.

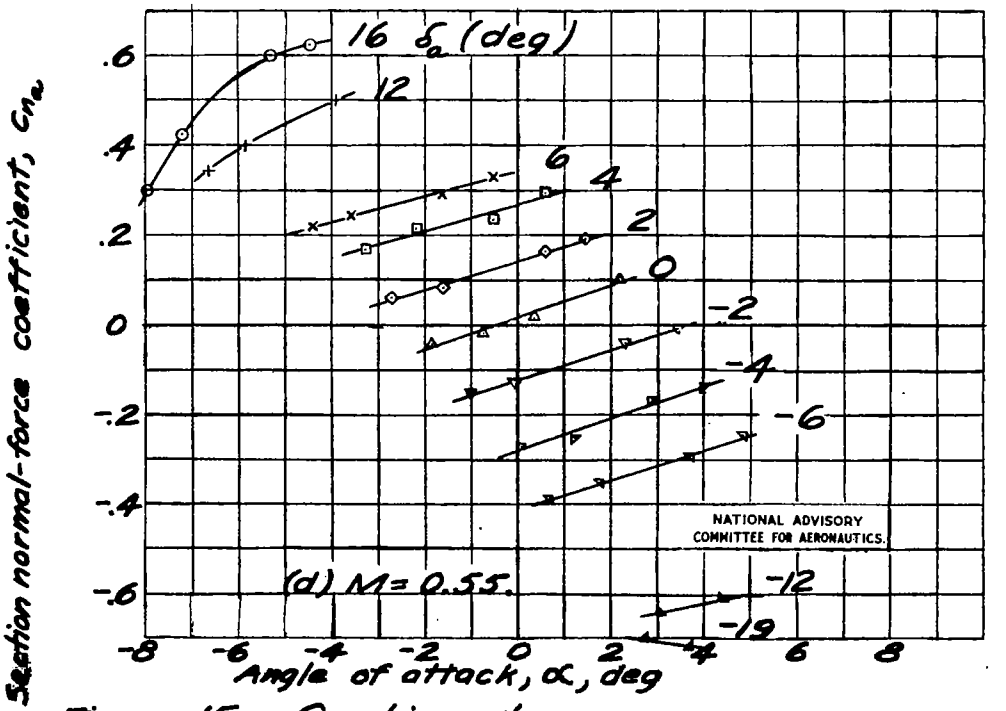

Figure 15.- Continued.

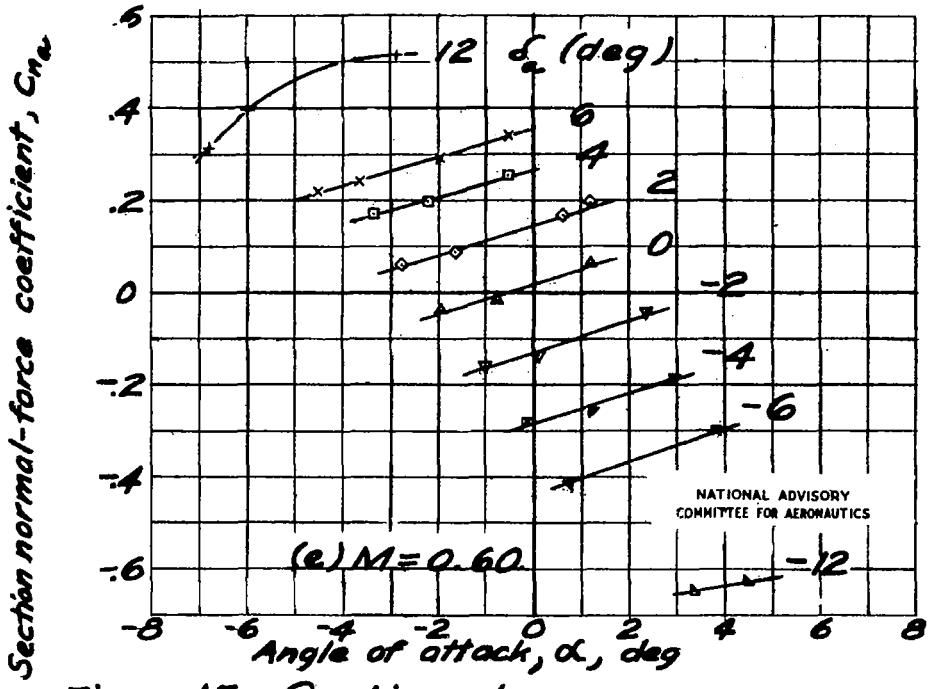

Figure 15.- Continued.

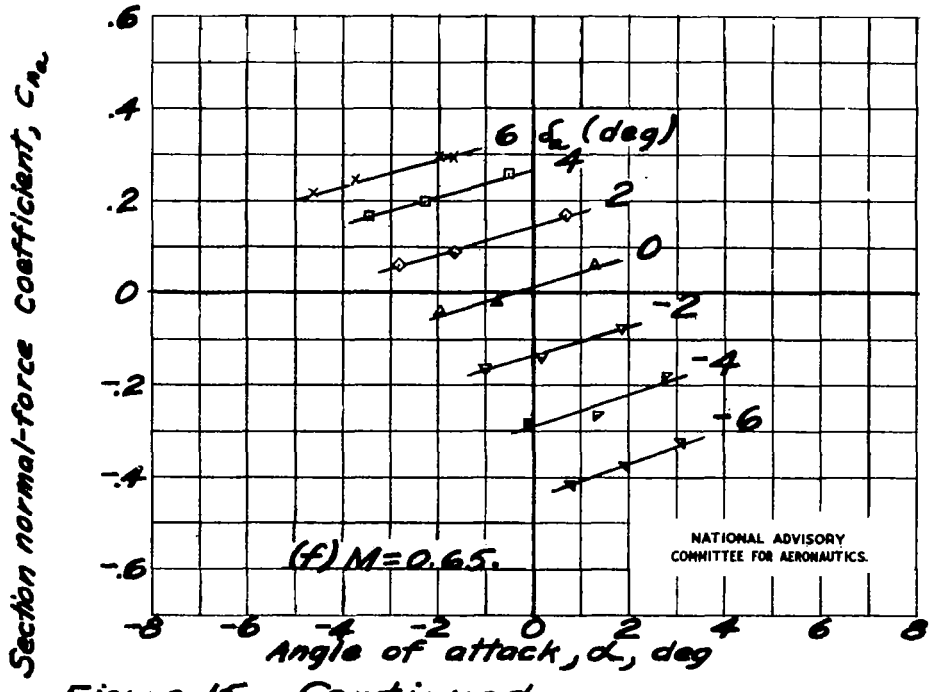

Figure 15.- Continued.

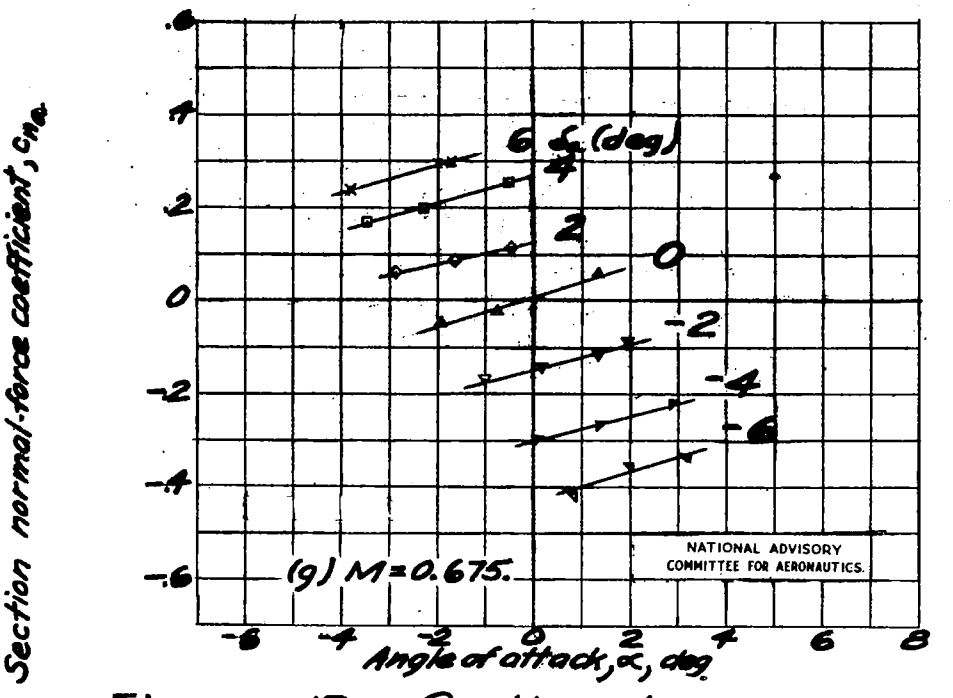

Figure 15.- Continued.

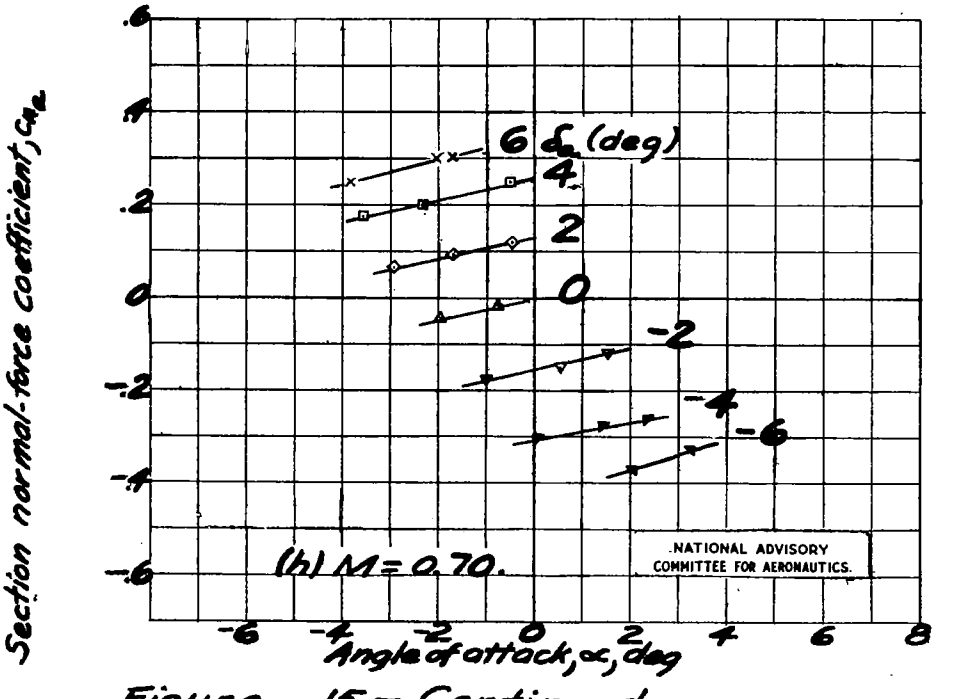

Figure 15.- Continued.

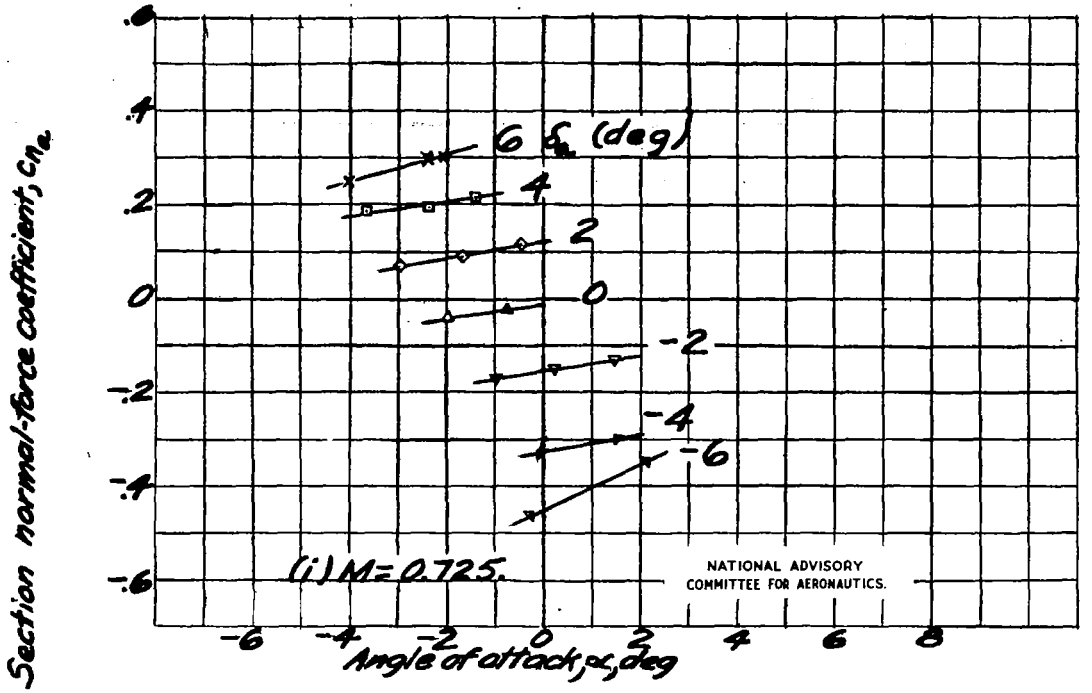

Figure 15.- Continued.

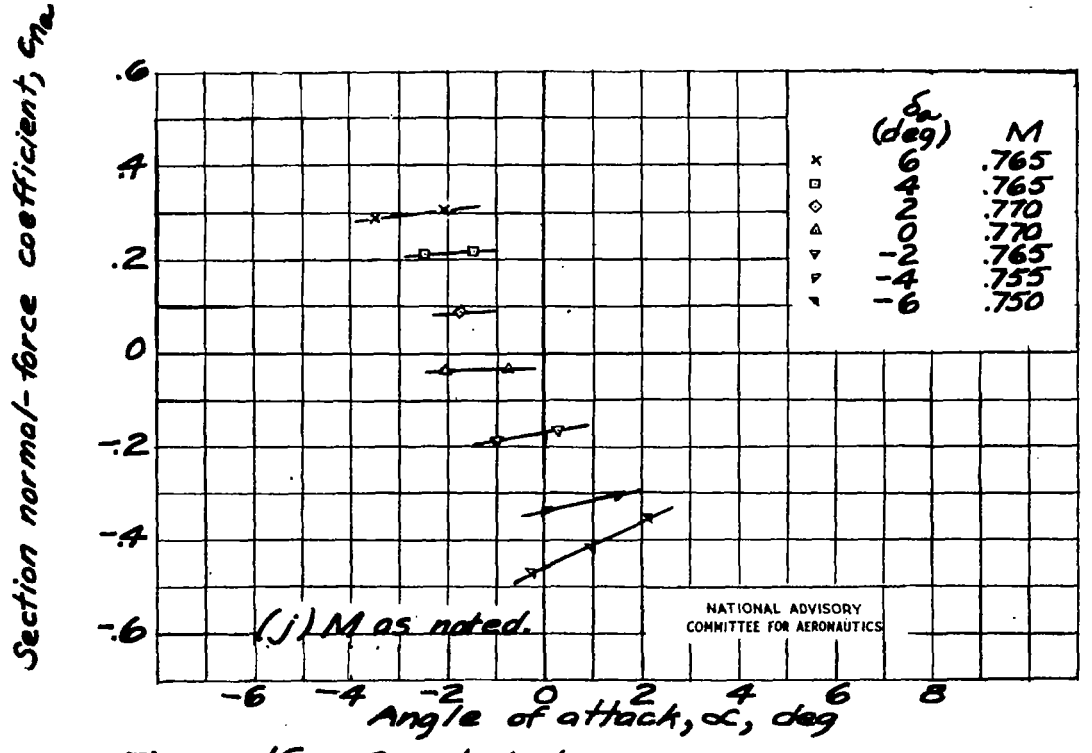

Figure 15.- Concluded.

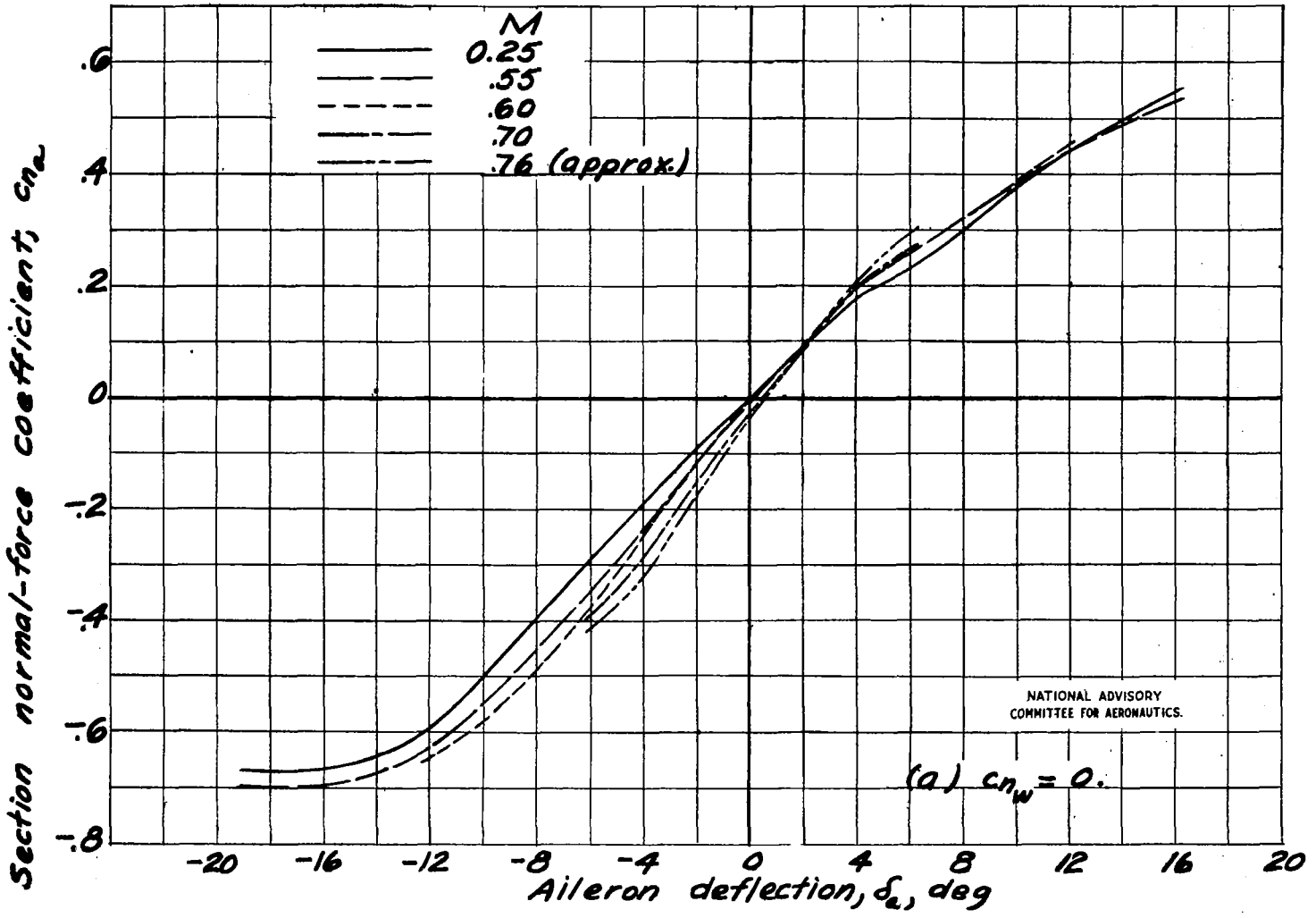

Figure 16.- Section aileron normal-force coefficient against aileron deflection at various Mach numbers.

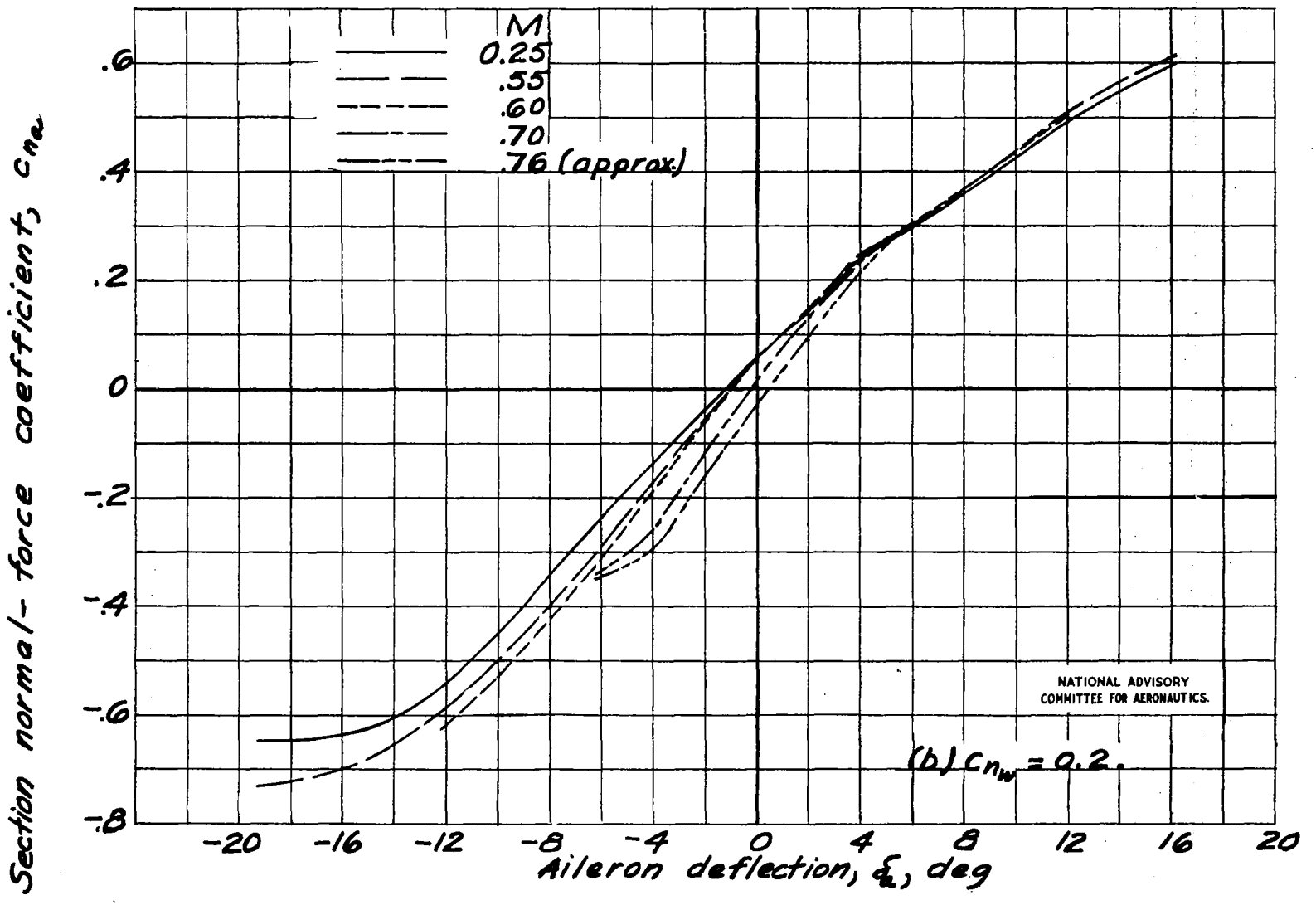

Figure 16.- Concluded.

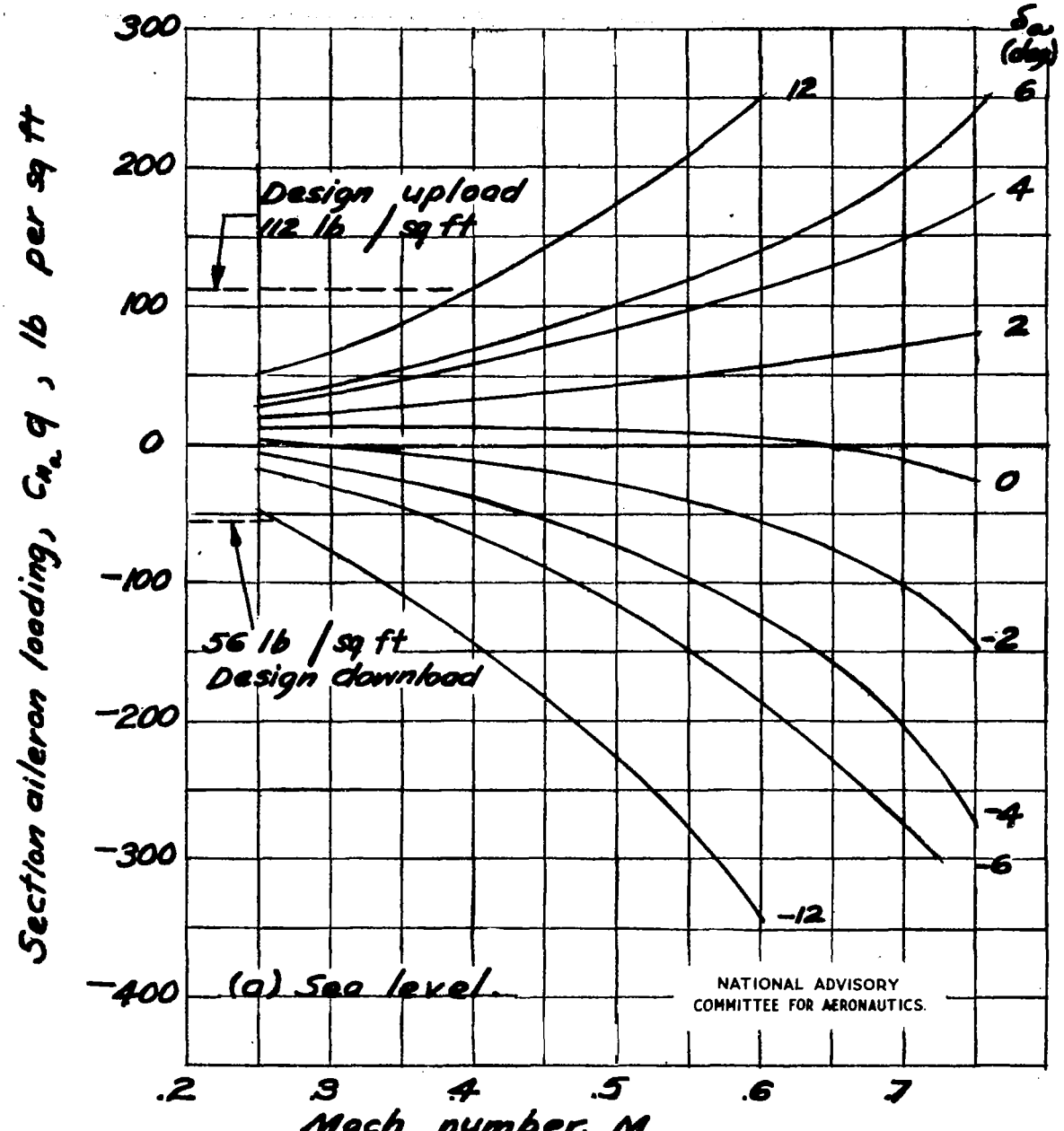

Figure 17.- Section aileron loading at various aileron deflections for steady rate of roll.

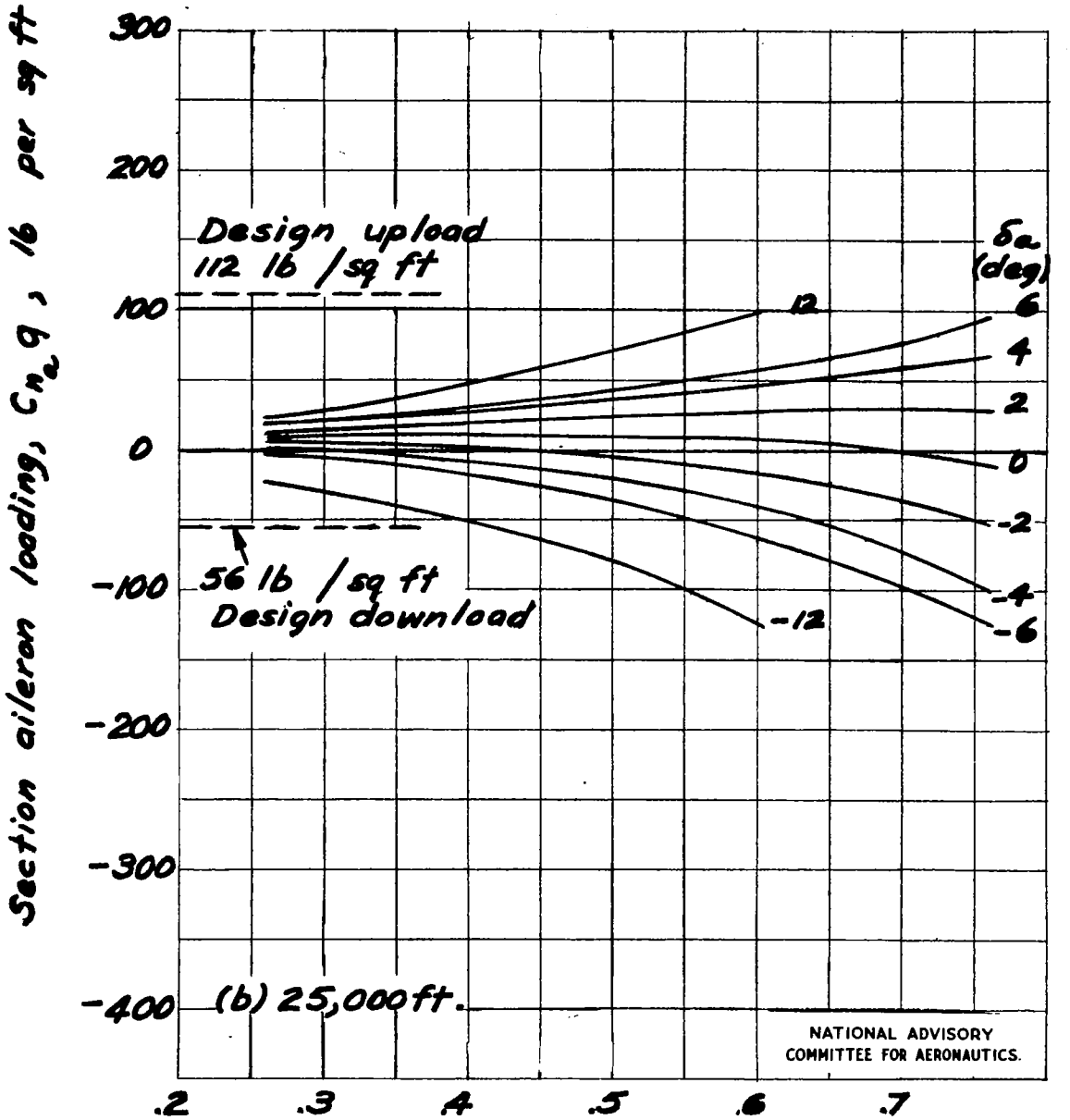

Figure 17.- Concluded.

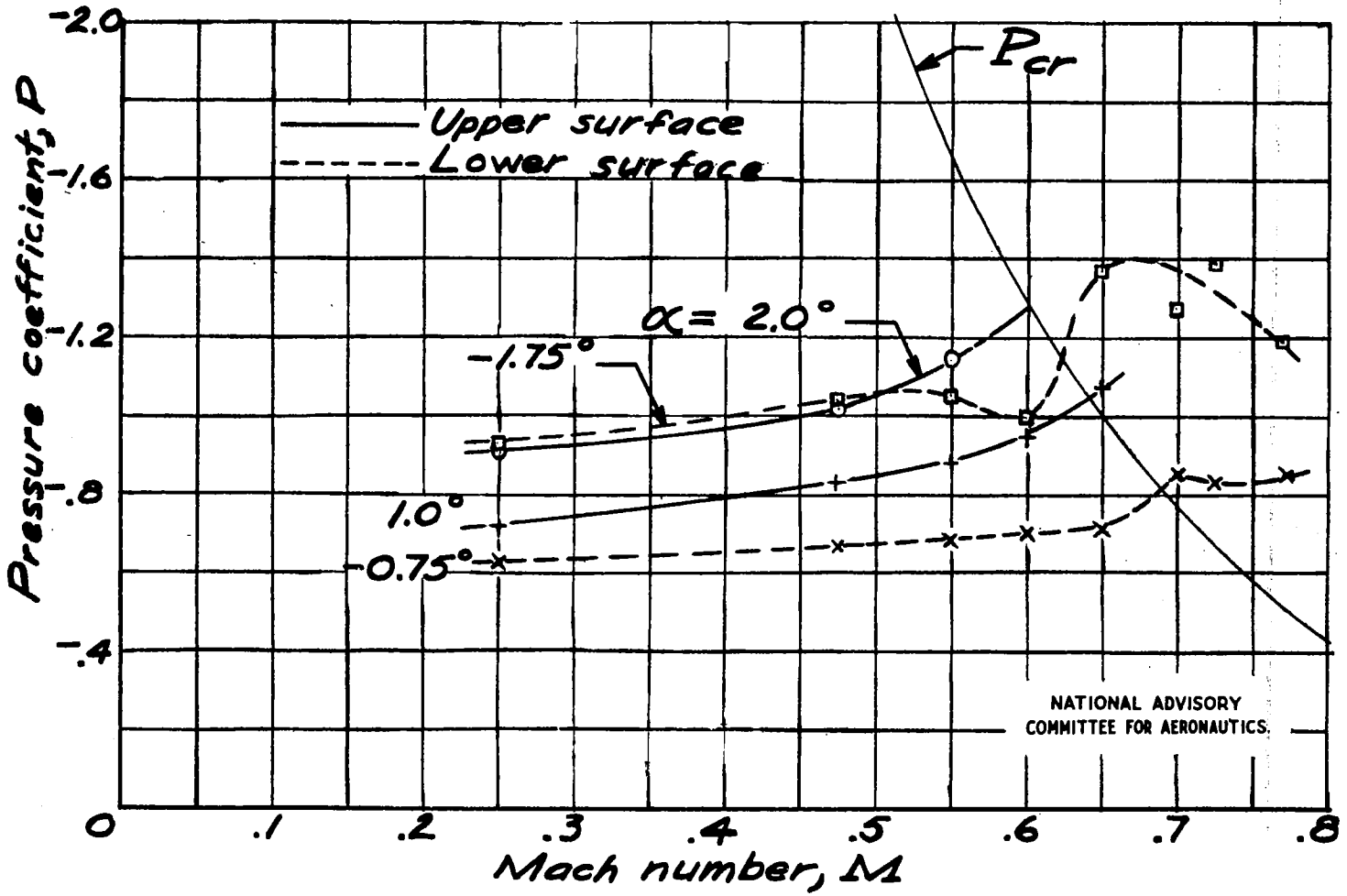

Figure 18.— Effect of compressibility on peak negative pressure coefficient of main portion of airfoil. $\delta_a = 0°$.

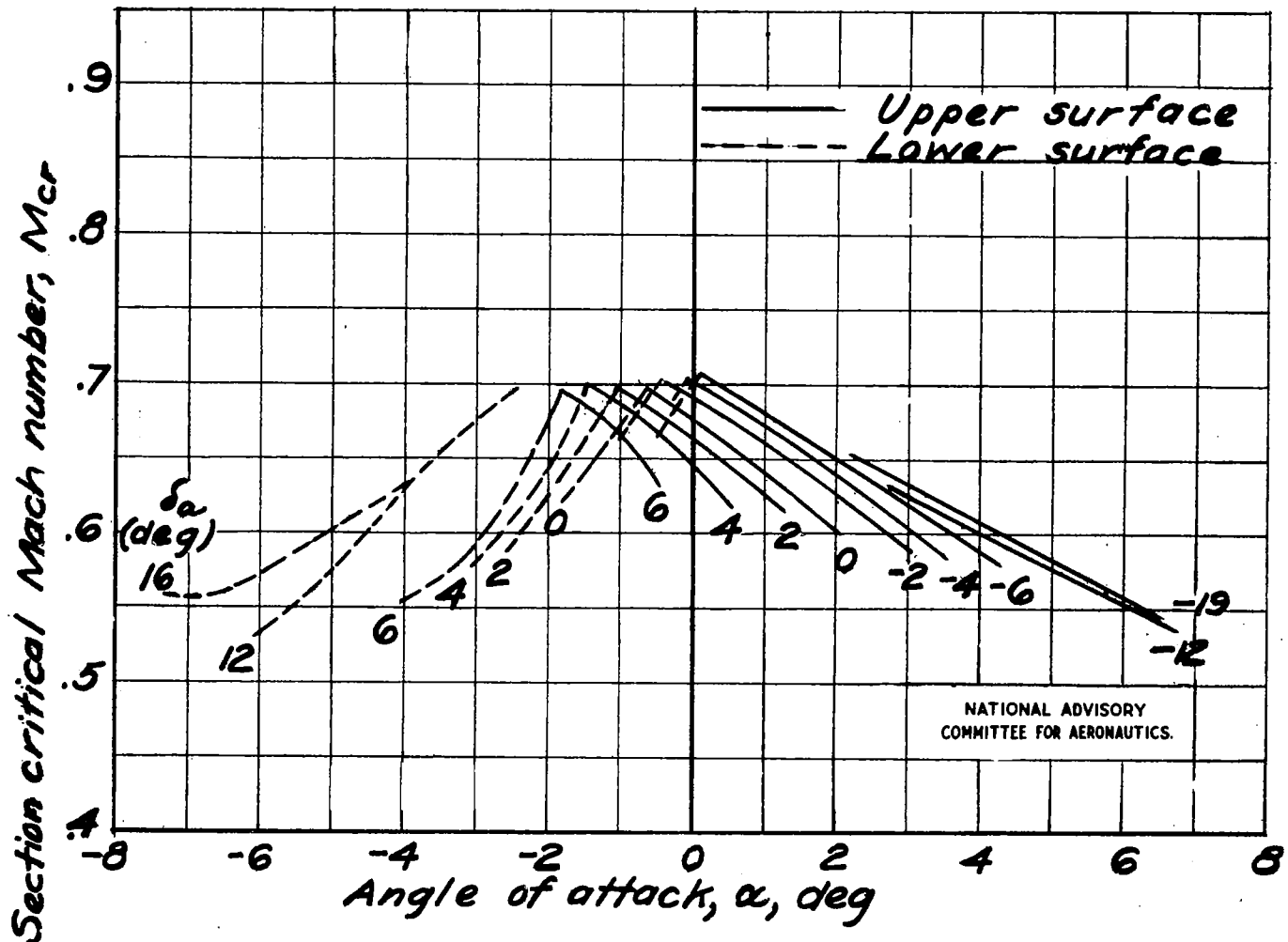

Figure 19.- Section critical Mach number of main portion of airfoil against angle of attack at various aileron deflections.

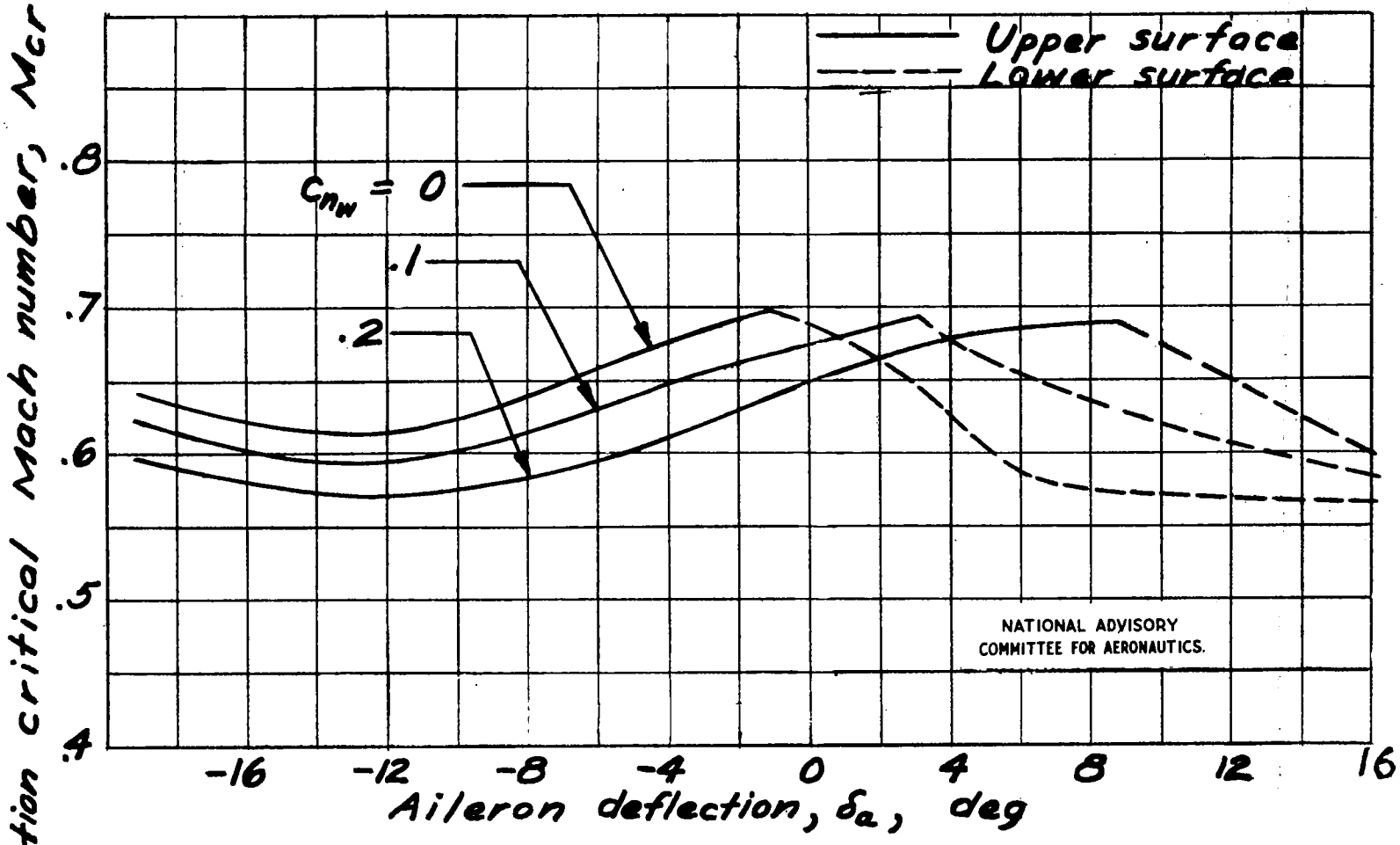

Figure 20.- Section critical Mach number of main portion of airfoil against aileron deflection at various section airfoil normal-force coefficients.

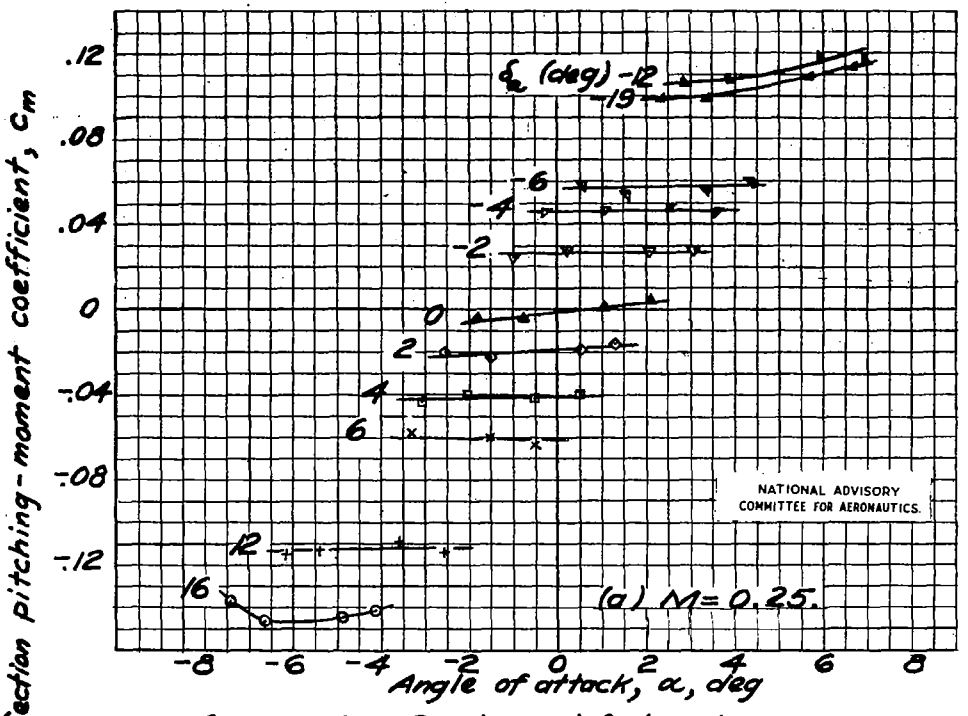

Figure 21.- Section airfoil pitching-moment coefficient against angle of attack at various aileron deflections.

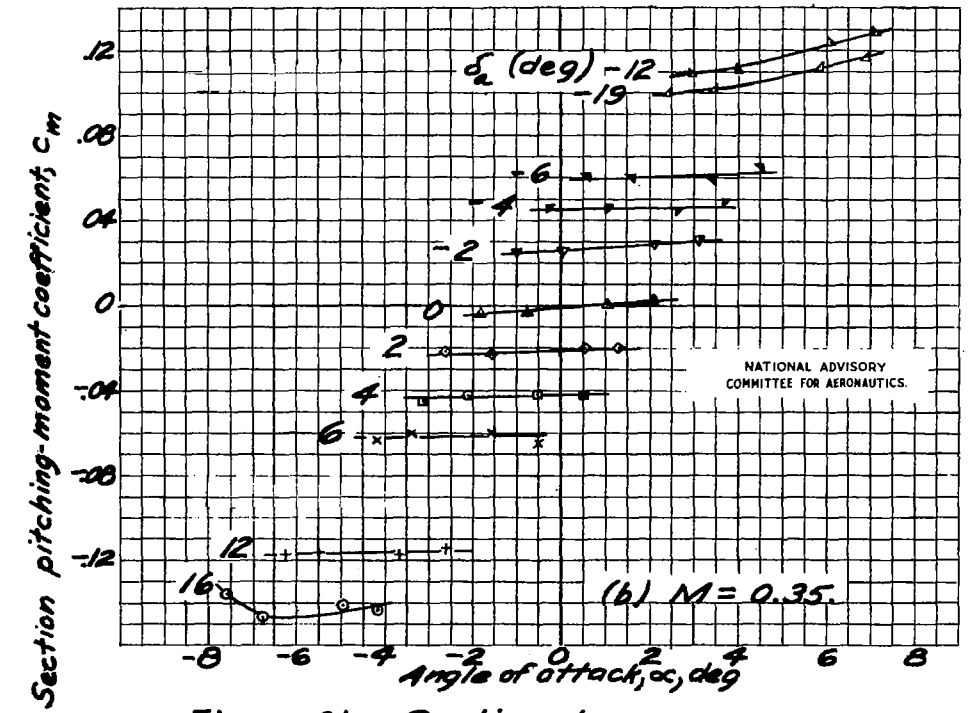

Figure 21.- Continued.

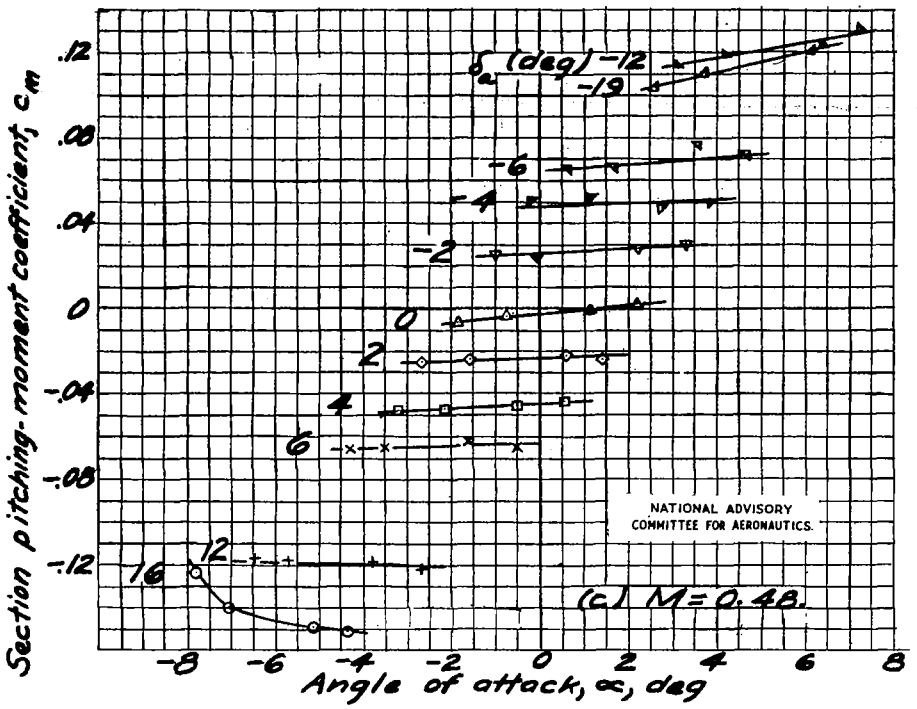

Figure 21.- Continued.

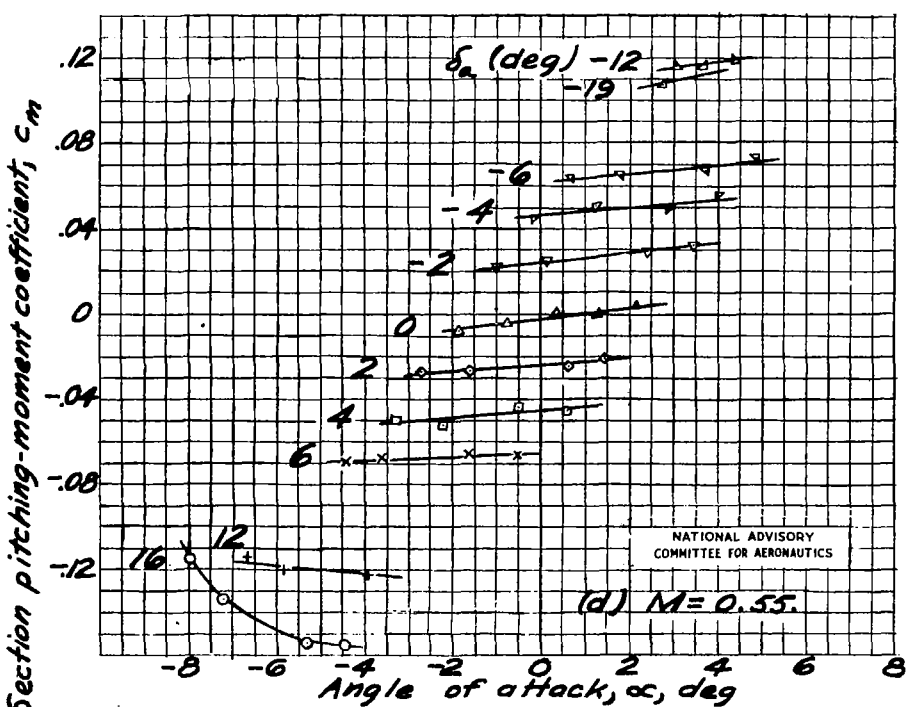

Figure 21.- Continued.

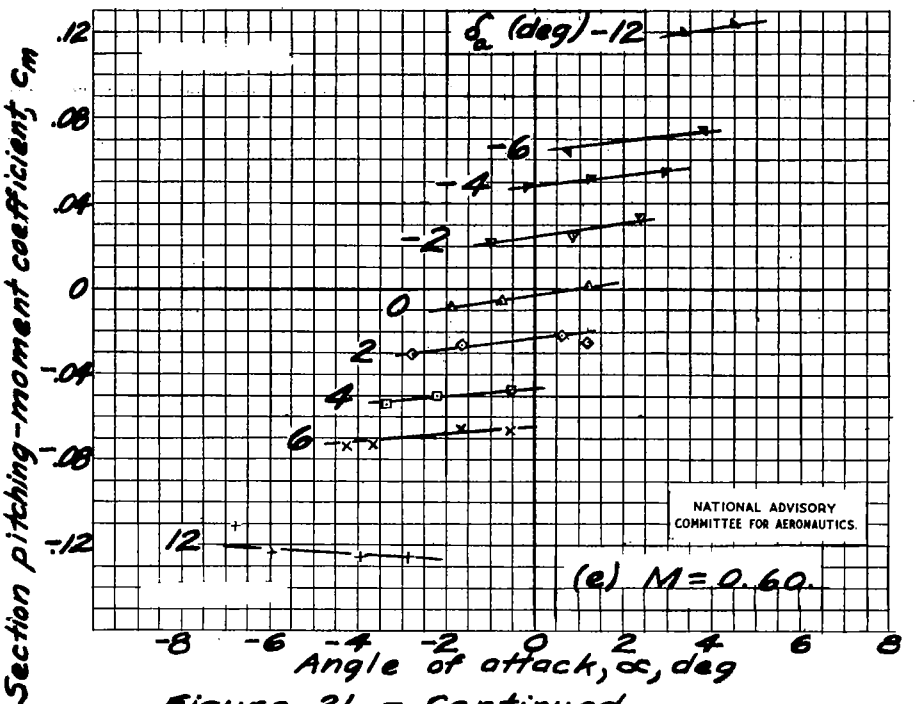

Figure 21. - Continued.

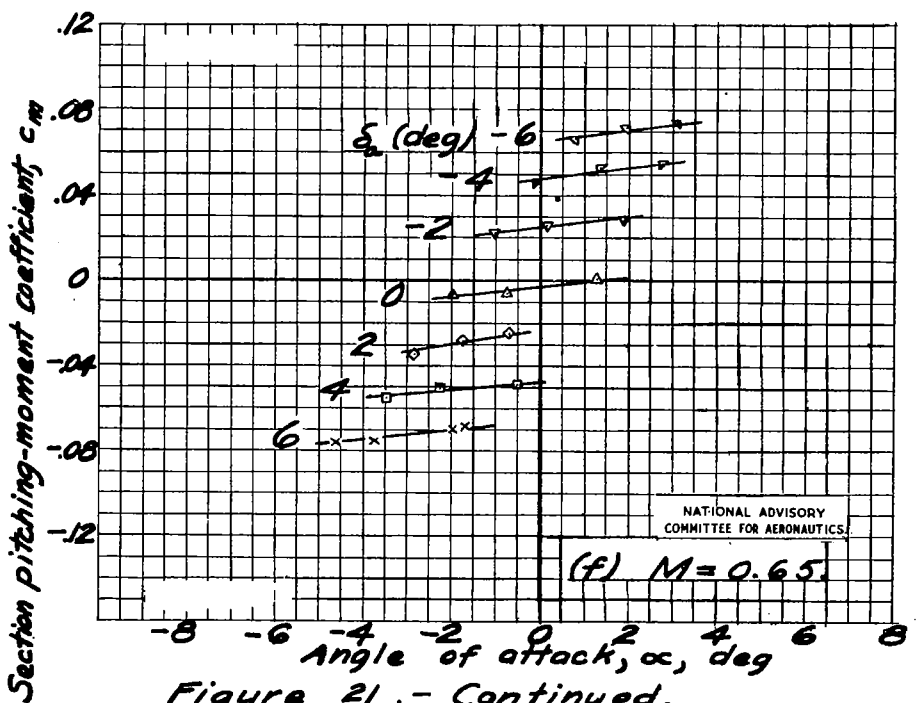

Figure 21 .- Continued.

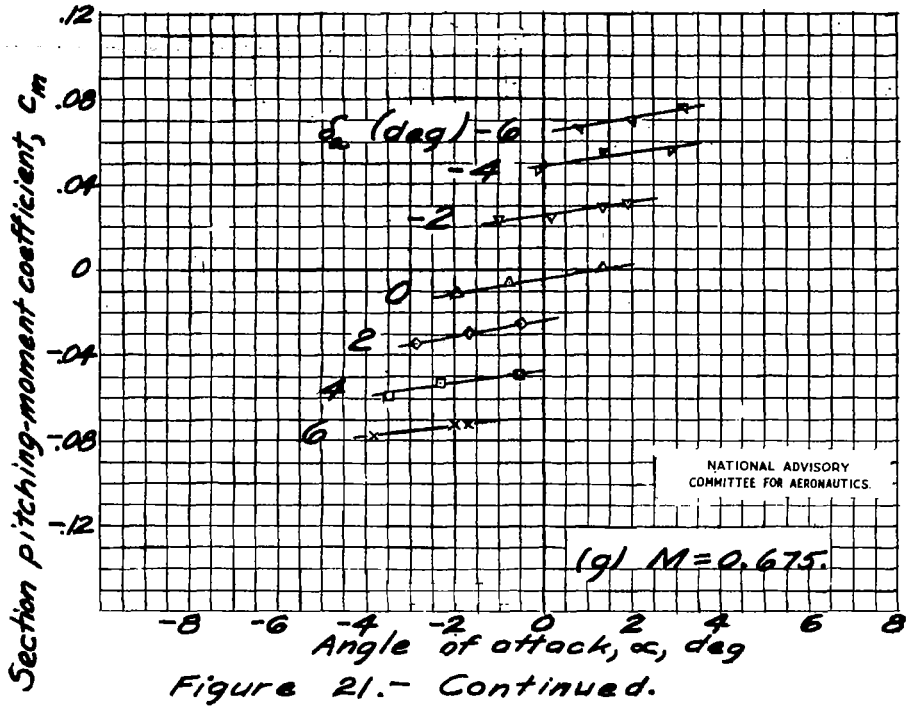

Figure 21.- Continued.

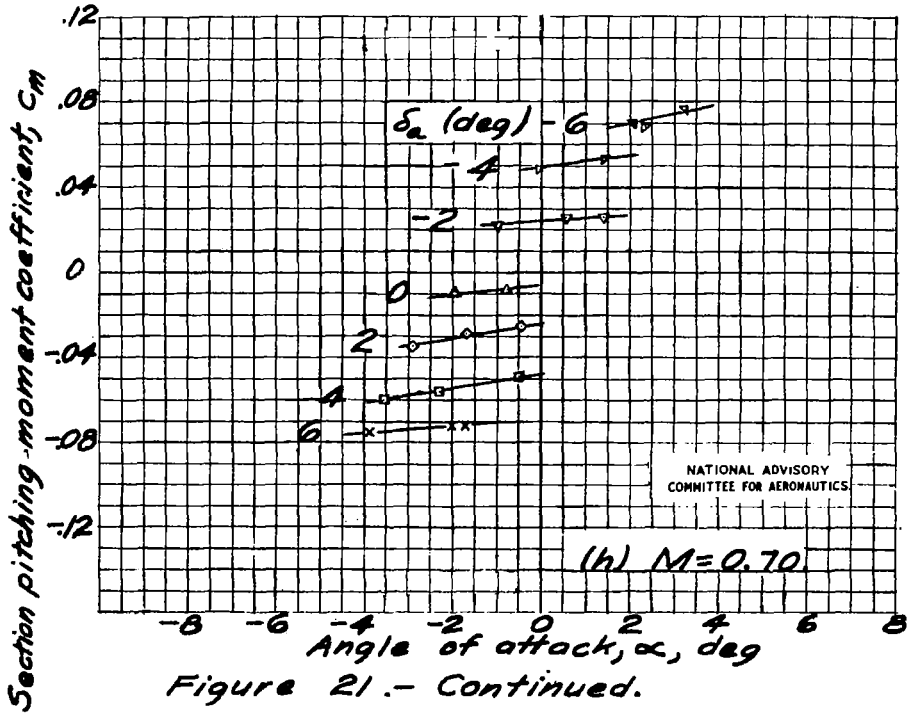

Figure 21.- Continued.

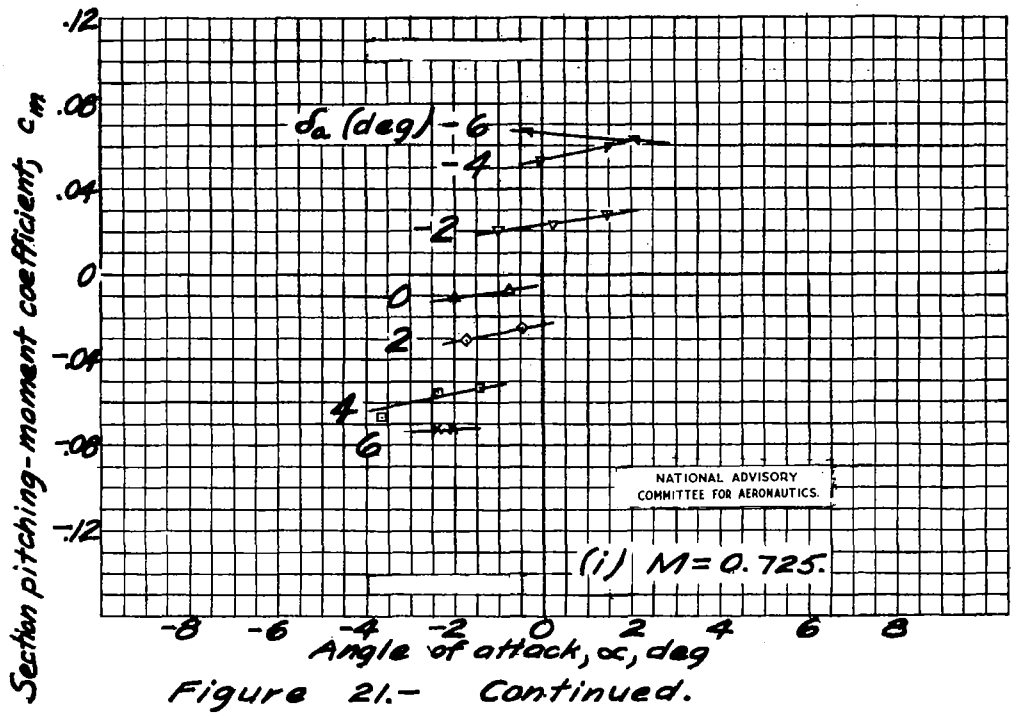

Figure 21.- Continued.

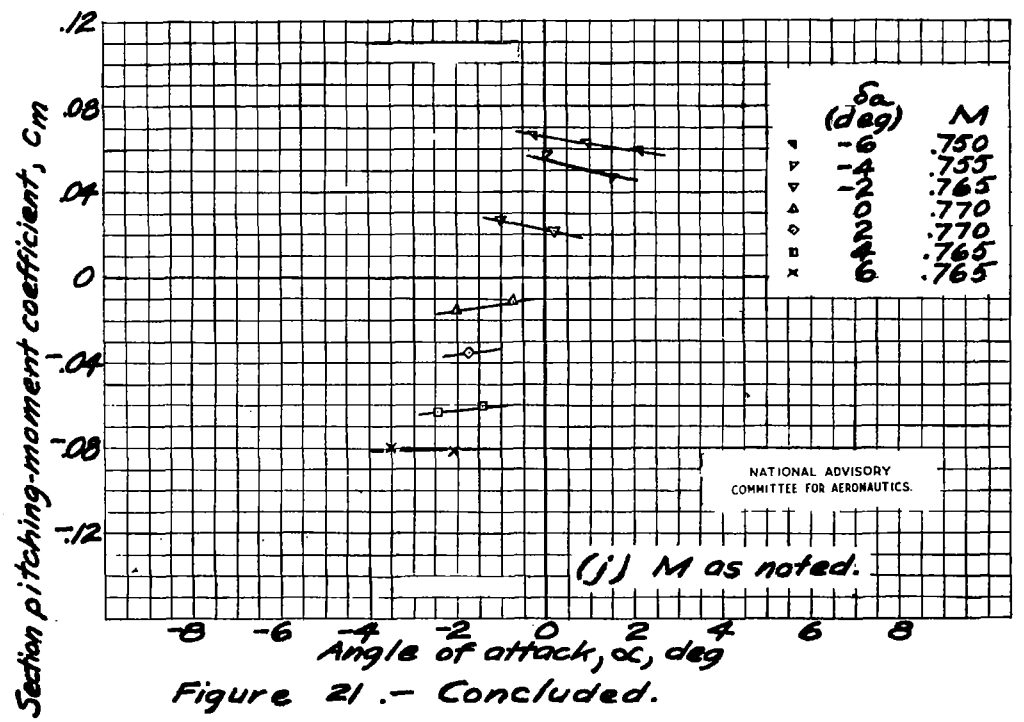

Figure 21.- Concluded.

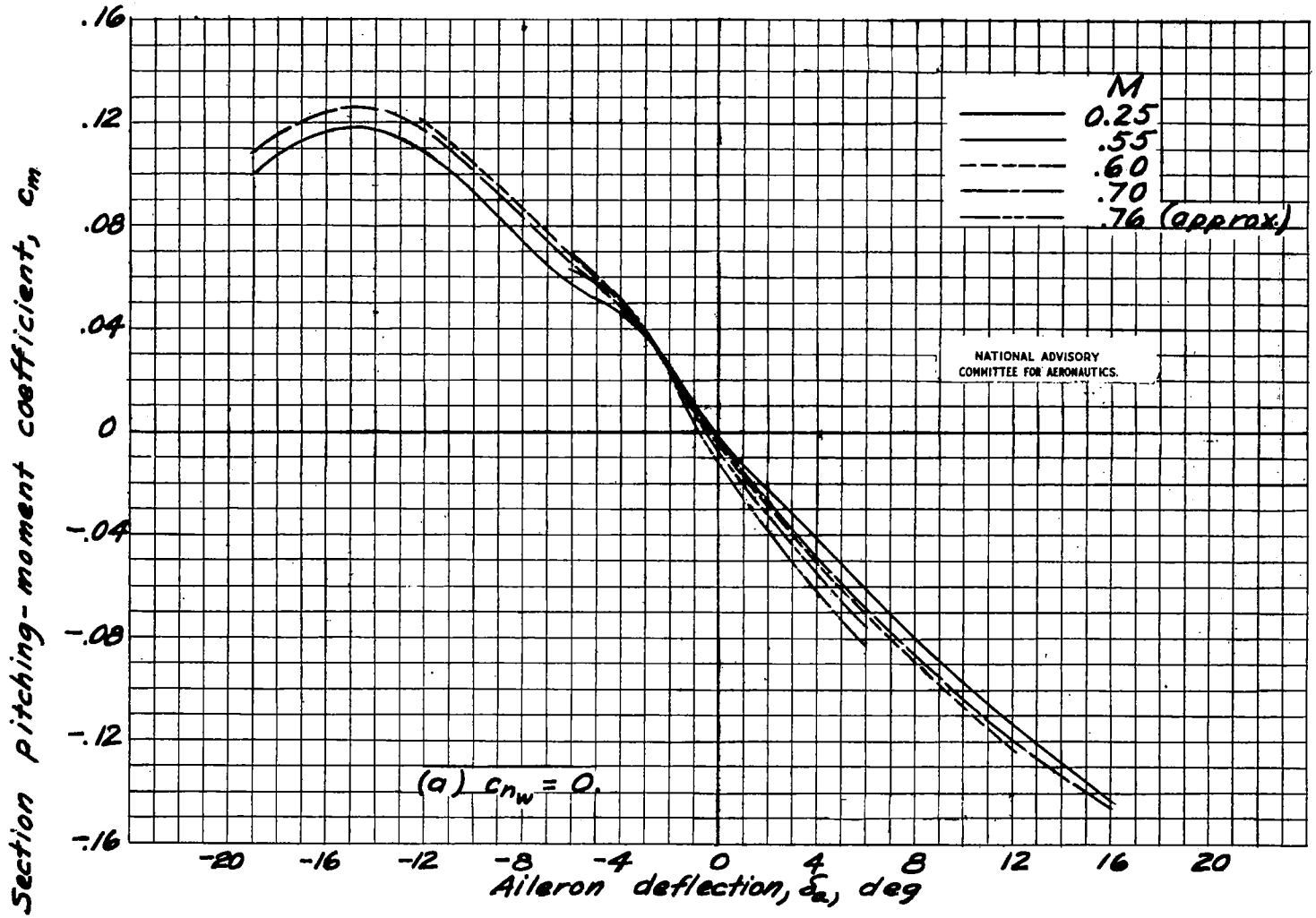

Figure 22.—Section airfoil pitching-moment coefficient against aileron deflection at various Mach numbers.

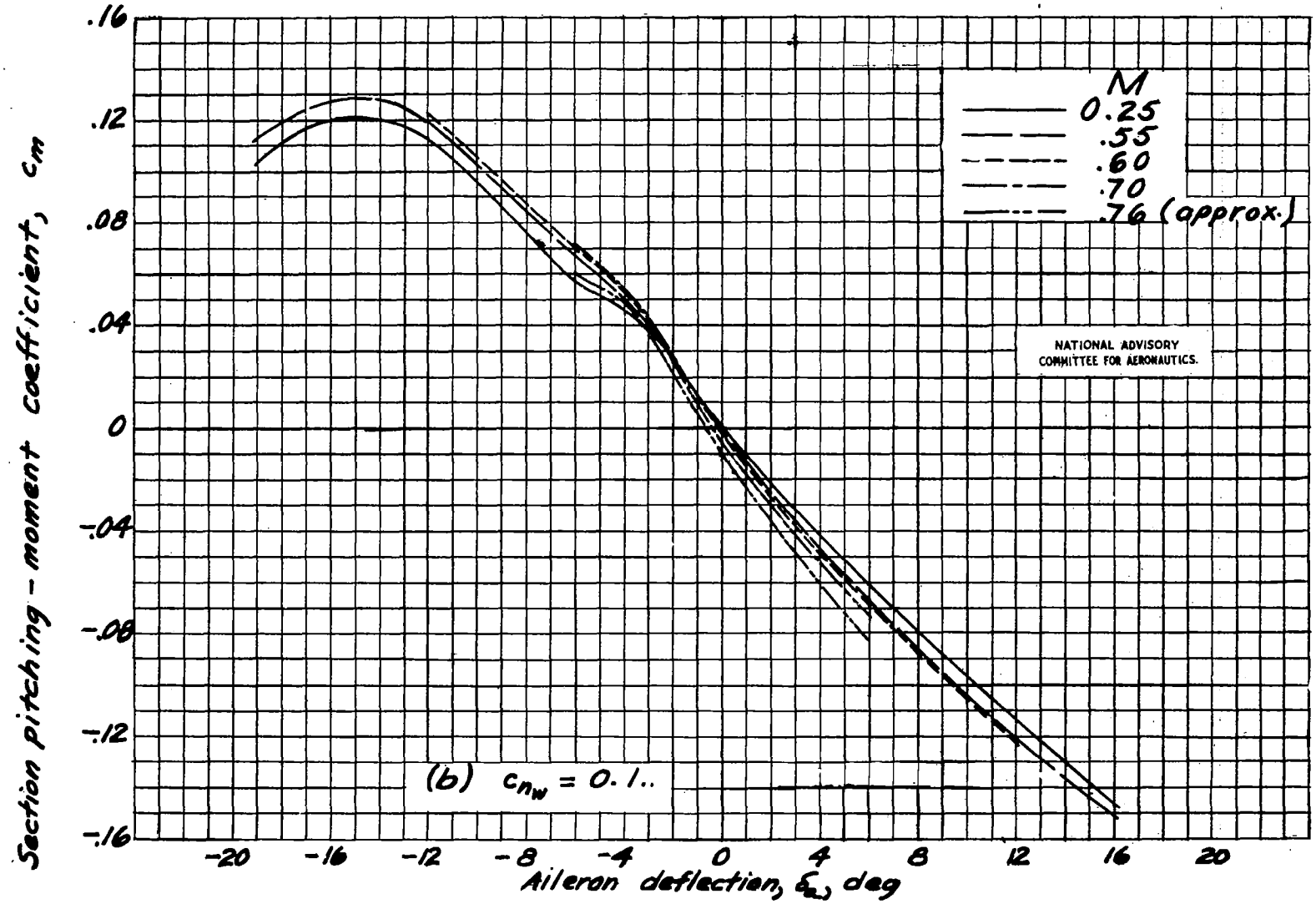

Figure 22.- Continued.

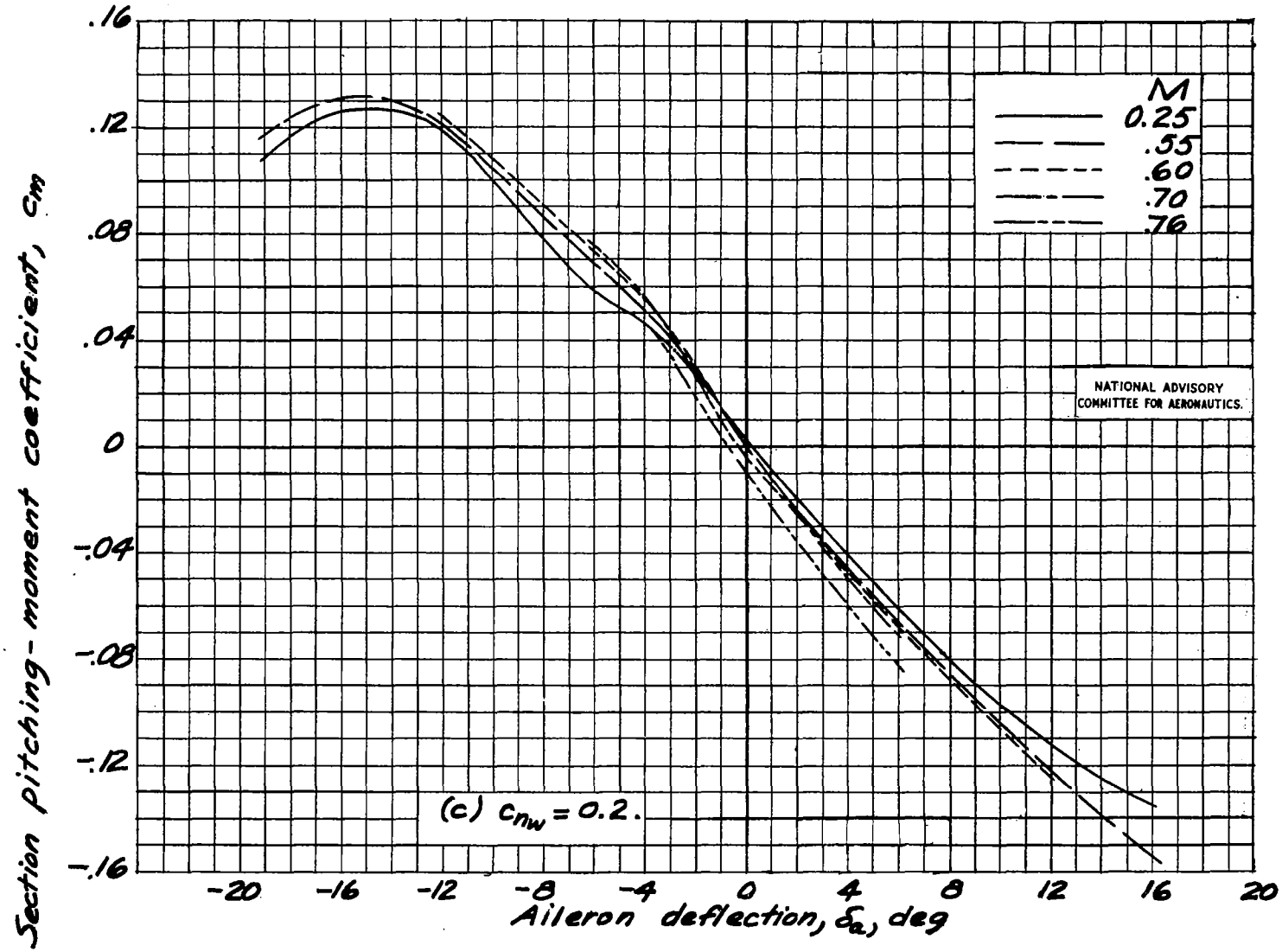

Figure 22.- Concluded.

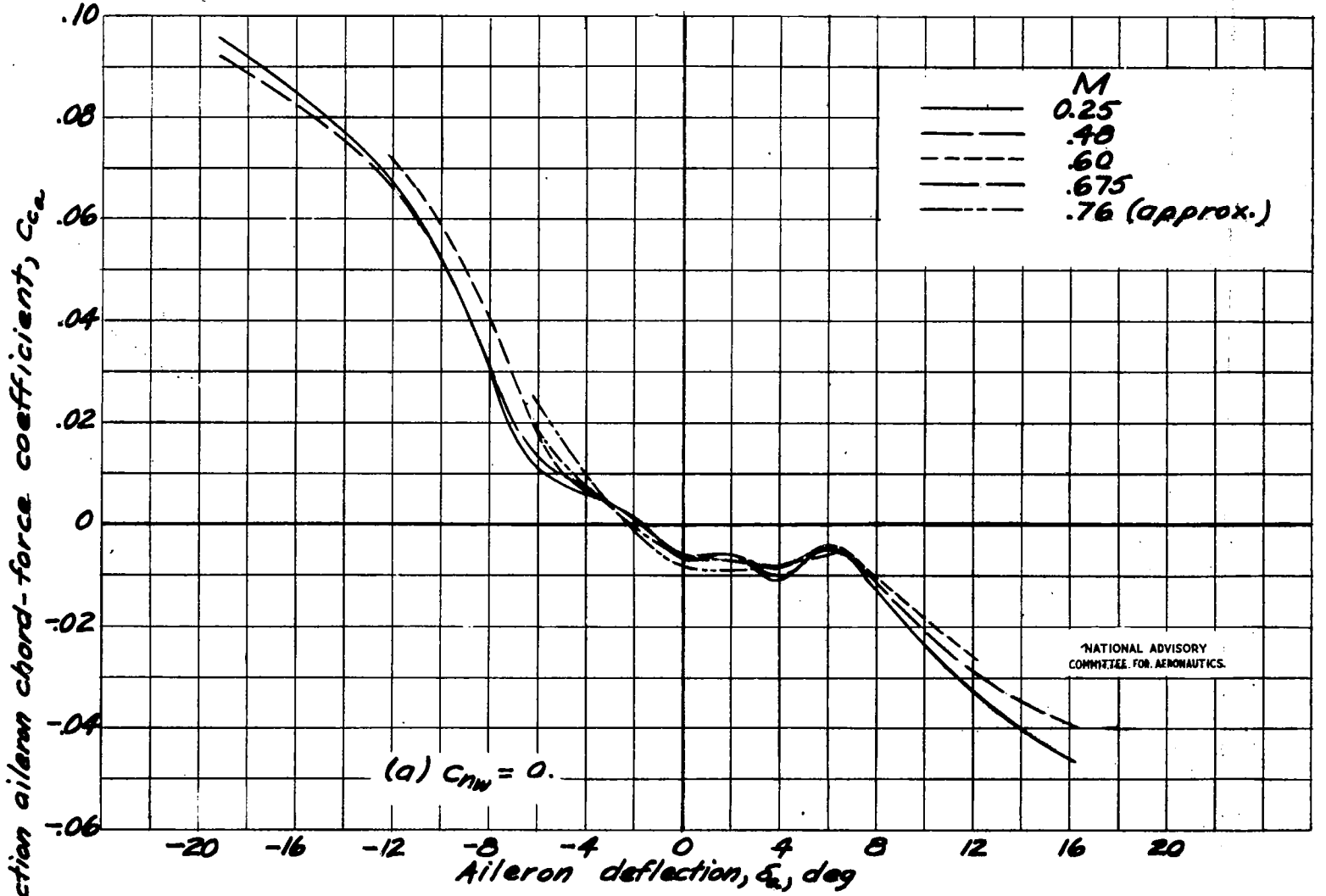

Figure 23.- Section aileron chord-force coefficient against aileron deflection at various Mach numbers.

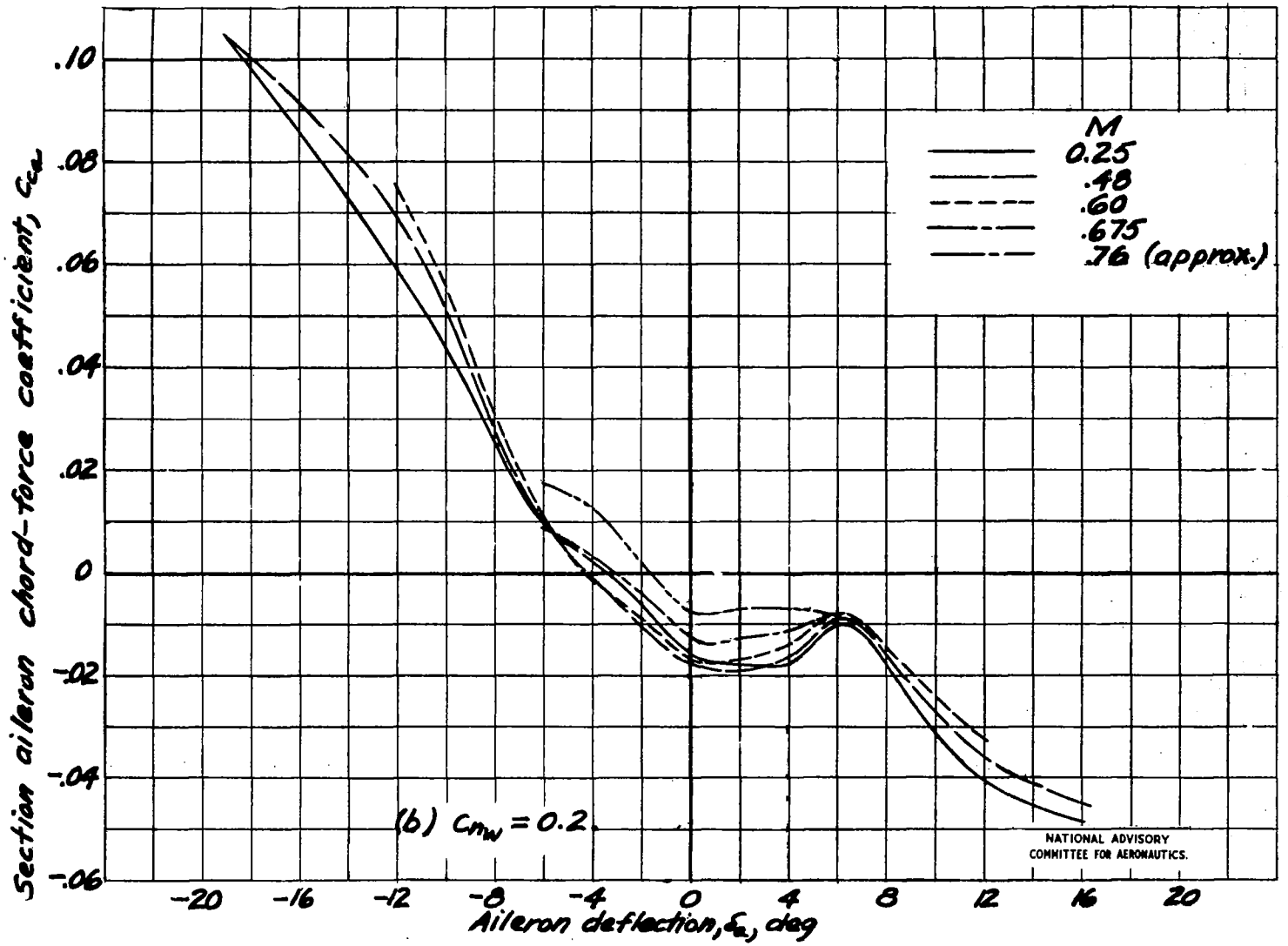

Figure 23.- Concluded.